

MODELING SIMULATION AND PRELIMINARY EXPERIMENTATION OF
TOWED TETHER SYSTEM

Except where reference is made to the work of others, the work described in this thesis is my own or was done in collaboration with my advisory committee. This thesis does not include proprietary or classified information.

Pradeep Chowdary Kolla

Certificate of Approval:

P. K. Raju
Thomas Walter Professor
Mechanical Engineering

David G Beale, Chair
Professor
Mechanical Engineering

Dan Marghitu
Professor
Mechanical Engineering

George T. Flowers
Interim Dean
Graduate School

MODELING SIMULATION AND PRELIMINARY EXPERIMENTATION ON
TOWED TETHER SYSTEM

Pradeep Chowdary Kolla

A thesis

Submitted to

the Graduate Faculty of

Auburn University

in Partial Fulfillment of the

Requirements for the

Degree of

Master of Science

Auburn, Alabama
December 17, 2007

MODELING SIMULATION AND PRELIMINARY EXPERIMENTATION ON
TOWED TETHER SYSTEM

Pradeep Chowdary Kolla

Permission is granted to Auburn University to make copies of this thesis at its discretion, upon the request of individuals or institutions and at their expense. The author reserves all publication rights.

Signature of Author

Date of Graduation

VITA

Pradeep Chowdary Kolla, son of Sri. Ashok Kumar Kolla and Smt. Usha Rani Kolla, was born on Dec 7th, 1983, in Chirala, Andhra Pradesh, India. He graduated with a Bachelor's Degree in Mechanical Engineering from Anna University, Chennai, India in June, 2005. He joined the Department of Mechanical Engineering at Auburn University in August 2005 for pursuing his graduate studies. His research interests include modeling and simulation of systems, processes and production flow.

THESIS ABSTRACT
MODELING SIMULATION AND PRELIMINARY EXPERIMENTATION ON
TOWED TETHER SYSTEM

Pradeep Chowdary Kolla

Master of Science, December 17, 2007
(B.E Anna University, 2005)

146 Typed Pages

Directed by David G Beale

Aero-dynamic drag forces and their effect on the path taken by a cable in a towed system are studied with the aid of an advanced computational software packages. A piece of rope (tether) is towed at the top end in a circular pattern and a body of known mass has been attached at the other end of the rope. Based on many computer simulations, observations have been made on the path traveled by the attached body at the lower end of the tether, for various angular velocities. The effect of certain factors such as internal damping, stiffness, mass-ratio and tow radii for increasing angular velocities, on the path traveled by the attached body have been studied, by modeling and simulations. Generally the tip radius and verticality of the lower end of the tether increases with increase in angular velocity, reaching a maximum value prior to a jump. The jump angular velocity range shifts towards higher velocities when parameters such as mass ratio, tow radius and bushings stiffness and damping are increased. Superposition plots have been obtained to visualize the envelope of space within which the tether can be

found at any given angular velocity (within the range of angular velocities considered), showing the formation of a node for angular velocities higher than jump velocity. An experiment was performed to validate simulated results, using a $3.285\text{E-}5$ lb/ft, 58" long, Spider Wire as the tether. Based on drag coefficient parameter values that best fit the experimental data, simulated shapes matched experimental results, as did verticality, with maximum 33% error over a speed range of 12-25 radians/second. The use of material with unknown damping/stiffness and the use of inexpensive and imprecise equipment may have caused the variations between the simulated results and the experimental results, but nevertheless did bolster confidence in the simulated results.

ACKNOWLEDGMENTS

I would like to thank my advisor, Dr. David G Beale for guiding me through the various stages of this work. His confidence and support, in every aspect of my research helped me complete this work as planned. I would like to thank Dr. P.K. Raju for his support and guidance. I would also like to thank Dr. Dan Marghitu for serving on my committee and also for his support during my course work.

Special thanks are due to Jake Miller, Dr. Mark Clark and Dr. Henry Burdg of Auburn Technical Assistance Center (ATAC) for their guidance and support while working on various simulation projects.

I would like to thank David J Banscomb, Yogesh R Kondareddy, Anil Nelaturi and Sai Siddharth Kumar Dantu for their help during the final stage of this work. I would also like to thank Ramsis Fargag, Lab manager Textile Engineering, for his guidance in determining initial material required for the experiment.

I would like to show my deepest gratitude to my parents, without whose support I would not have reached this far. Everything achieved by me, is a result of their support. I would also like to thank my brothers Sandeep and Gautham for their love and affection.

Special thanks are due to my friends Akhila Avirneni, Ramraj Gottiparthi, Jyothi Swaroop Gandikota, Pallavi Chitta and Dr. Mukund Karanjikar for their help and encouragement during my graduate studies.

Style manual or journal used: Guide to Preparation and Submission of Theses and
Dissertations.

Computer Software used: ADAMS 2005 R2 and Microsoft Office 2003.

TABLE OF CONTENTS

LIST OF FIGURES	xiii
LIST OF TABLES.....	xvii
INTRODUCTION	1
1.1 Past and Present Research.....	2
1.2 ADAMS	14
1.3 Scope of Work	15
FUNDAMENTAL MODEL.....	16
2.1 Design of Model/System.....	17
2.2 Calculations.....	26
MODELING, SIMULATION AND BENCHMARKING.....	28
3.1 Assumptions made in Modeling	28
3.2 Modeling.....	28
3.2.1 Tow Link.....	31
3.2.2 Cylinder.....	31
3.2.3 Sphere	32
3.2.4 Spherical Joints	32
3.2.5 Revolute Joint	33
3.2.6 Motion Statement.....	33
3.2.7 Drag Forces.....	35

3.3	Simulation for Preliminary Model Validation/Correlation.....	37
3.3.1	Tip Radius and Angular Velocity	38
3.3.2	Comparison of the ADAMS Model Response with Published Data	39
3.4	Superposition in ADAMS Model	42
NUMERICAL RESULTS		47
4.1	Simulation Parameters	47
4.1.1	Damping/Stiffness.....	48
4.1.2	Mass of Drogue.....	50
4.1.3	No of Segments.....	50
4.1.4	Tow radius	51
4.2	Simulation Results	51
4.2.1	Effect of Damping / Stiffness	52
4.2.1.1	Effect of Zero Stiffness-Varying Damping.....	52
4.2.1.1.1	Effect of Damping on Verticality	53
4.2.1.1.2	Effect of Damping on Tip Radius.....	54
4.2.1.2	Effect of Varying Stiffness-Constant Damping.....	55
4.2.1.2.1	Effect of Varying Stiffness-Constant Damping on Verticality.....	56
4.2.1.2.2	Effect of Varying Stiffness-Constant Damping on Tip Radius	57
4.2.1.3	Effect of Varying Stiffness and Damping.....	58
4.2.1.3.1	Effect of Damping/Stiffness on Verticality	59
4.2.1.3.2	Effect of Damping on the Tip Radius	61
4.2.2	Effect of End Mass.....	63
4.2.2.1	Effect of End Mass on the Tip Radius	64

4.2.2.2	Effect of End body Mass on Verticality	70
4.2.3	Effect of Tow Radius	71
4.2.3.1	Effect of Tow Radius on Verticality	72
4.2.3.2	Effect of Tow Radius on Tip Radius	73
4.2.4	Time Response Plot	77
Investigations into an Experimental System for Validation with Application to Realistic		
Tether Materials		
5.1	Experimental Setup	81
5.1.1	Table Top	82
5.1.2	DC Motor	82
5.1.3	DC Motor Speed Controller	83
5.1.4	Aluminum Beam	84
5.1.5	Tachometer	85
5.1.6	Digital Cameras	88
5.1.7	Tether	88
5.1.7.1	Weight method	88
5.1.7.2	Microscopic Method	89
5.2	Operation Procedure and Measurements	94
5.3	Limitations in Experimental Validation Procedure	97
5.4	ADAMS Modeling Based on Experimental Setup	98
5.5	Comparison of ADAMS Simulation with Experimental Data	101
5.5.1	Correlation Based on Verticality Data Plots	101
5.5.1.1	Effect of Co-Efficient of Drag on Verticality (ADAMS Results)	104

5.5.2	Correlation Based on Snap Shots and Superposition Pattern for Verticality	104
5.5.3	Correlation Based on Snap Shots and Superposition Pattern for Tip Radius	106
CONCLUSIONS		108
6.1	Future Work	109
REFERENCES		111
APPENDIX –A.....		114
	Tables – ADAMS Simulation data and Published data [8]	114
APPENDIX-B.....		117
ADAMS/SOLVER DATA SET		117

LIST OF FIGURES

Figure 2.1: Simple Tether Mass System.....	17
Figure 2.2: Hoerner’s Cross-Flow Principle.....	19
Figure 2.3: Resolution of Forces.....	21
Figure 2.4: Original Model and Discretized Model at Stationary Position	23
Figure 2.5: Differences between Types of Modeling	23
Figure 2.6: Views of the Model	25
Figure 3.1: Discretized ADAMS Model.....	30
Figure 3.2: Step Function Curve.....	34
Figure 3.3: System at Stationary Position.....	37
Figure 3.4: Tip Radius Vs Angular Velocity Curve generated by ADAMS	39
Figure 4.1: Screen-Shot showing Bushing Element	48
Figure 4.2: Verticality Vs Angular Velocity: Varying Damping-Zero Stiffness.....	54
Figure 4.3: Tip Radius Vs Angular Velocity: Varying Damping-Zero Stiffness	55
Figure 4.4: Verticality Vs Angular Velocity: Varying Stiffness - Constant Damping	57
Figure 4.5: Tip Radius Vs Angular Velocity: Varying Stiffness-Constant Damping	58
Figure 4.6: Plot of Verticality Vs Angular Velocity: Various Damping and Stiffness Values	60
Figure 4.7: Plot of Tip Radius Vs Angular Velocity: Various Damping and Stiffness Values	62

Figure 4.8: Path Taken by End Mass: Angular Velocities less than 0.225 rad/s.....	62
Figure 4.9: Path Taken by End Mass: Angular Velocities less than 8.30-8.34 rad/s-No Damping.....	63
Figure 4.10: Tip Radius Vs Angular Velocity: Effect of Mass Ratio.....	65
Figure 4.11: Path Taken by End Mass: Mass Ratio - 0.5, Angular Velocity 3.00-3.5 rad/s	66
Figure 4.12: Path Taken by End Mass: Mass Ratio - 0.5, Angular Velocity 8.30-8.35 rad/s.....	66
Figure 4.13: Path Taken by End mass: Mass Ratio - 0.75, Angular Velocities 8.3-8.35 rad/s.....	67
Figure 4.14: Path Taken by End mass: Mass Ratio - 0.75, Angular Velocities 3.0-3.5 rad/s.....	67
Figure 4.15: Path Taken by End Mass: Mass Ratio - 1.023, Angular Velocities 3.0-3.04 rad/s.....	68
Figure 4.16: Path Taken by End mass, Mass Ratio - 1.023, Angular Velocities 8.3-8.34 rad/s.....	68
Figure 4.17: Path Traveled by End Mass: Mass Ratio - 1.1, Angular Velocity 3.0-3.5 rad/s.....	69
Figure 4.18: Path Traveled by End Mass: Mass Ratio - 1.1, Angular Velocity 8.3-8.45 rad/s.....	70
Figure 4.19: Verticality Vs Angular Velocity: Mass Ratio (Mm) from 0.50 – 1.1	71
Figure 4.20: Effect of Tow Radius: Verticality Vs Angular Velocity.....	72
Figure 4.21: Effect of Tow Radius: Tip Radius Vs Angular Velocity	74

Figure 4.22: Path Traveled by End Mass: Tow Radius- 7 inch,	75
Angular Velocity 12-12.50 rad/s.....	75
Figure 4.23: Path Traveled by End Mass: Tow Radius 8 inch,	75
Angular Velocity 12.0-12.5 rad/s.....	75
Figure 4.24: Path Traveled by End Mass: Tow Radius-9 inch,	76
Angular Velocity 12.0-12.50 rad/s.....	76
Figure 4.25: Path Traveled by End Mass: Tow Radius- 10 inch,	76
Angular Velocity 12.0-12.5 rad/s.....	76
Figure 4.26: Path Traveled by End Mass: Tow Radius- 11 inch,	77
Angular Velocity 12.0-12.50 rad/s.....	77
Figure 4.27: Time Response Plot: Tip Radius Vs Time (No Jump).....	78
Figure 4.28: Time Response Plot: X-Position Vs Time (No Jump)	78
Figure 4.29: Time Response Plot: Tip Radius Vs Time (Jump).....	79
Figure 4.30: Time Response Plot: X Position Vs Time (Jump)	80
Figure 5.1: DC Motor	82
Figure 5.2: DC Motor Speed Controller	84
Figure 5.3: Bottom view of the Setup with Aluminum Beam (Tow Link) and Thread (Tether)	85
Figure 5.4: DC Motor, Speed Controller and Tachometer	87
Figure 5.5: Snapshot-1 of a Multi-Strand Braided Material (Spider Wire-fishing line) using a Microscope	90
Figure 5.6: Snapshot-1 of a Multi-Strand Braided Material (Spider Wire-fishing line) using a Microscope	91

Figure 5.7: Experimental Setup- Front View.....	92
Figure 5.8: Experimental Setup Bottom View.....	93
Figure 5.9: Snap Shot to Measure Elevation of the End of the Tether	94
Figure 5.10: Bottom View of the System; Shape of the Tether.....	96
Figure 5.11: ADAMS Model based on the Experimental Setup	98
Figure 5.12: Verticality Vs Angular Velocity - ADAMS Model for Experiment Validation- Varying Speed	100
Figure 5.13: Tip Radius Vs Angular Velocity - ADAMS Model- Experimental Validation-Varying Speed	100
Figure 5.14: Path Taken by Tether- ADAMS Model- Experimental Validation- Varying Speed.....	101
Figure 5.15: Comparison of Experimental and Simulation Data: Verticality Vs Angular Velocity.....	102
Figure 5.16 Snap Shot of ADAMS Model- Experimentation Model	104
Figure 5.17: Snap Shot of Experimental Model	105
Figure 5.18: Super Position Screen Shot: ADAMS Model based on Experimentation..	105
Figure 5.19: Screen Shot of Pattern of the Tether	106
Figure 5.20: Snap Shot of the Experiment: Bottom View	107

LIST OF TABLES

Table 4.1: Damping Values-Zero Stiffness	53
Table 4.2: Stiffness Values-Constant Damping.....	56
Table 4.3: Damping Values-Zero Stiffness	59

CHAPTER 1

INTRODUCTION

The concept/operation of a simple pendulum has been studied for ages. Theoretically speaking a simple pendulum, once set in motion, never comes to a stop in presence of vacuum. One of the factors that slows down and eventually gets a simple pendulum to a stop in presence of air is the resistance offered by the air. This resistance in other terms is also known as “drag” and the forces causing this resistance are called “drag forces”. The magnitude and direction of drag forces are dependent to a certain extent on various parameters such as the type of material (co-efficient of drag) and geometry of the object. The drag forces on any system can be easily resolved into forces along the three dimensional axes for easy computations. One can approximate the drag forces acting on standard shaped bodies from published data without any difficulty. In the present day with the advancement of technology and the availability of computational and analysis software packages, the study of drag forces or “aero-dynamic drag forces” and in turn their effect on the path taken by a cable in a towed system, can be easily performed. In this work a study has been performed on a towed-tether (cable) system. A piece of rope (tether) is towed at the top end in a circular pattern and a body of known mass has been attached at the other end of this rope. One can expect drag forces, inertia forces and gravity to be acting on this system. Interesting observations have been made in

terms of the path traveled by the attached body at the lower end of the tether, for various angular velocities. The primary objective of this work is to identify and study the effect of certain factors on the path traveled by the attached body by modeling and simulations.

1.1 Past and Present Research

Towed cable systems have been studied for several years because of the possible applications they offer such as delivery and pickup of loads from remote locations. The following describes/reviews some of the related literature.

The method of exchange of goods between a moving aircraft and people on the ground was first patented by Chilowsky, [1] in the year 1931. This was the first documented method to provide a means of communication between a moving aircraft and the ground. A similar method with a detailed approach has been patented by Smith, [2] in the year 1939 with the development of a hopper attached with a parachute for lowering it in an upright position. Anderson [3] in 1942 patented his practical method and apparatus for delivery and pickup of load by an aircraft in flight in a pre-determined path. Apart from the characteristics of the load, various parameters such as drag, gravity, inertia, speed, altitude, differences in tension cable were taken into account to determine the path that needs to be followed. Nate Saint, a missionary pilot to Ecuador, was one of the first persons to practically apply the concept behind “towed cable systems” to delivery gifts to the people of Ecuador [4].

Research has been done for several years considering the various aspects of the towed cable concept. A brief summary of part of the research that has been done is written in the following paragraphs.

Genin and Citron [5] studied the degree of coupling between longitudinal and transverse modes of motion using a non-linear mathematical model of an extensible (flexible) cable in a uniform flow field. The systems of equations used were hyperbolic and the method of characteristics aided in obtaining the solutions for the system of equations. The degree of coupling between the two modes of motion was evaluated by examining and altering the associated coupling terms in the system of equations. The longitudinal motion seems to be uncoupled from the transverse motion. The transverse dynamic motion creates centripetal acceleration. The increase in centripetal acceleration increases the magnitude of the longitudinal motion thereby stabilizing the system. The effect of coupling, between the transverse and longitudinal modes of motion, caused by tension was also studied. The authors suggested that the coupling effect of the tension can be studied/ evaluated by examining the transverse motion without considering the effect of centripetal acceleration. The authors also identified the presence of a closed loop effect wherein the transverse motion affects the centripetal acceleration through the tension which in turn affects the transverse motion.

Winget and Huston [6] discussed a three-dimensional non-linear finite element dynamic model of a tether (cable/chain). The cable was divided into segments made up of a series of links connected by ball and socket joints. The properties of each segment of the cable such as size, shape, mass and also the number of segments chosen are arbitrary. This model is assumed to have $3N+3$ number of degrees of freedom where N indicates the number of links. The authors, based on the governing equations of motion which were numerically integrated using a fourth order Runge-Kutta method, developed a computer code, which when provided with the required input data such as the number of links, masses etc. In order to validate the accuracy of the developed code, a sample example of an off-shore oil rig configuration has been simulated.

Russell and Anderson [7] studied a lumped mass model having two degrees of freedom to understand the equilibrium and stability of a circularly towed cable. The model consisted of an inextensible mass-less rod with a lumped mass attached to the end. The model has also been evaluated to examine the effect of various types of drags such as viscous drag and viscous drag with a cross-wind. To evaluate the effect of crosswinds having a constant magnitude on the motion of the system, a linearized model has been used. When the case of “no-drag” was considered, all the drag-dependent terms were set to zero and as a result the “stiffness” and “damping” matrix became symmetric and purely gyroscopic respectively. When the gyroscopic effects were considered, a stabilizing effect on the lower branch of the tip radius curve was seen and the instabilities present prior to considering this effect changed forms from static to dynamic. For the

“viscous drag” effect, the appropriate system of equations chosen were called as coupled transcendental equations and were in general difficult to solve. When the co-efficient of viscous drag (non-dimensional co-efficient) was close to the critical co-efficient there was a possibility of three non-linear jumps two of which occur when the 1) system jumps from larger tip radius to smaller tip radius when the angular frequency was increased 2) system jumps from a smaller tip radius to a larger tip radius when the angular frequency was decreased and 3) the system jumps from a larger tip radius to a smaller one when the angular frequency is decreased while the bar segment is assumed to be on the upper portion of the stable curve.

Russell and Anderson [8] studied the equilibrium and stability of an elastic cable whose top/upper end was towed in a horizontal plane at a constant velocity in a circular path by using a finite element approach. The fluid/aerodynamic drag was mainly composed of the tangential component and the normal component which are directly proportional to the square of the respective velocity components. Newton-Raphson method was used to solve the non-linear algebraic equations of motion. The major assumptions made by the authors are that the co-efficient of drags in the normal and tangential directions, density of the material and the diameter of the segment remain constant over the entire length of each segment. The stability analysis was performed based on the assumption of an infinitesimal motion about a given nonlinear equilibrium position. The theoretical data obtained were in good agreement with that of the

experimental data. Per the authors a jump from one configuration to the other were typically observed in non-linear spring-mass systems.

Leonard and Nath [9] studied the various differences/similarities between the finite element methods and the lumped parameters method in regard to oceanic cables. Several cases were considered to determine the effectiveness/ relative efficiencies of either of the methods. Both the methods were compared in regard to the treatment of force and mass distribution of a tethered system and also the stresses, dynamics and kinematics that result. The parameters considered were topological considerations, internal loads / inertial loads, external loads such as cable weight, buoyancy, hydrodynamic inertia forces, and hydrodynamic drag. After each of the parameter was studied, the authors concluded that FEM would provide a closer approximation to the continuum approach if curved elements were used and either FEM or Lumped mass approach would provide equivalent results if straight line elements were used. It was also suggested that if the length of each segment or distance between the nodes was reduced, the inaccuracies from not considering the true mass distribution, incase of the lumped parameter approach, would be greatly reduced.

Zhu and Rahn [10] investigated the dynamic response of a circularly towed cable-body system with fluid drag. The system considered included, about the steady state, a non-linear and linear vibrational equations. The steady state equations were solved

numerically via a shooting technique and the vibrational equations were linearized and discretized using a Galerkin's method. The numerical results obtained indicated that the stable single-valued solutions (Tip radius and verticality) for a given range of angular velocities always existed for low rotational speeds whereas for high rotational speeds with small drag and large end mass multi-valued steady-state solutions were found to exist.

Jones and Krausman [11] studied a tethered aerostat's response to turbulence and other disturbances with the help of a computer program developed for nonlinear dynamic simulation. Dynamic motion of a ballonnet air, tether and six degrees of freedom of the aerostat has been considered for the development in the theoretical model. The simulated computer data has been compared with that of the experimental data obtained from a series of instrumented flights with a 365 tethered aerostat. The aerodynamic forces and moments for the theoretical model have been based on the experimentally determined coefficients of drag using a rotating-arm tank. The tether has been modeled such that it has finite number of straight elastic segments. Consecutive segments of tether were either connected by universal joints or nodes at which the mass of each segment is concentrated. The effect of tension and internal damping has been used in the computation of the drag force. The aerodynamic drag forces on each segment of the tether, cylindrical segment, are proportional to the square of the respective relative velocities. The effect of turbulence has also been considered and for tethered flights above an altitude of 2000 ft, the turbulence has been assumed to be isotropic. When the

experimental data was compared to the simulated data, it was found that there was a reasonable match with certain exceptions. The exceptions were attributed to either the inaccuracies in turbulence model or to the measuring/data transferring procedure. It was also found that the experimental model was highly damped when compared to the simulated model based on the tether tension excursions.

Nakagawa and Obata [12] studied the longitudinal stabilities in an aerial-towed system which consisted of a rigid, symmetric towed body and a long flexible, inextensible/inelastic cable with a circular cross-section. Lagrange's equations, with the approximation of finite degrees of freedom for the cable motion, were used for the derivation of the governing equations of motion for the towed system. The motion of the towed system was categorized into steady-state and perturbed motions based on an initial consideration of the system moving in a steady state configuration. The aerodynamic drag forces used in this work by the author were based under the assumption of cross-flow principle, at sub-critical Reynolds numbers, according to Hoerner [13]. The linearized equations of motion of the system were based on the assumption that the perturbations of motion are small. The stability analysis of the system was evaluated for different cases which include 1) straight cable configuration with two different towed systems a) body and b) sphere; and 2) curved cable configuration with a towed body system. The cable was assumed to have a uniform cross-section along its length and the sphere was assumed to be made up of homogeneous material with only the aerodynamic drag force acting on the sphere. Several diameters of the towed sphere were considered,

for the stability analysis of the towed sphere system, along with evaluation of the size effect on the dynamics of the system. It was found that, for small diameters of the sphere, all vibration modes were split into new modes called “wave-down” and “wave-up” modes out of which some of the wave-down modes become unstable. This unstable motion of the wave-down mode was called as the “cable flutter”. For the towed system case, the aerodynamic effects on the system dynamics have been studied for which the stability derivatives are the most important characteristics in the evaluation of system stability. The “pitching” and “pendulum” modes as identified by the author were influenced by the stability derivatives. In case of the stability analysis of the curved cable configuration, similar results as that of the towed system with straight cable configuration were obtained except for the “bowing” mode which becomes unstable. The unstable motion of this mode was called as the “bowing flutter”.

Etkin [14] developed a mathematical model in order to compute the stability of towed bodies subjected to fluid-dynamic forces, efficiently. The developed model consisted of a cable, flexible and elastic with internal damping, as a means of connecting two bodies (towing body and towed body). When the model developed was applied to a practical application such as the case of a pendant vehicle towed by a short cable attached to an aircraft orbiting at a constant speed, inherent lateral instabilities were found to occur (when cable was attached to the center of gravity of the towed body) for certain ranges of aircraft speeds which were later eliminated by means of proper cable attachment (either above or ahead of the center of gravity of the towed body). The longitudinal instabilities

were not discussed by the author for the example considered, in regard to the cable attachment, as there were no noticeable instabilities.

Pai and Nayfeh [15] developed a full nonlinear cable model, which accounts for the various cables models as special cases, based on energy approach. The model has also taken into account the various factors such as the effect of static and dynamic loads, Poisson's effect on the cross-sectional area, geometric instabilities, compressibility, material non-uniformities and initial sags. Per the authors linear couplings and non-linear couplings, have been observed in the nonlinear equations of motion, as a result of the initial sags and static loads, and due to Poisson's effect and large deflections respectively.

Kanman and Huston [16] developed an algorithm to model the dynamics of both towed and tethered cable systems. The algorithm accounts for both fixed and varying lengths of the tether. Finite number of segments either rigid links or chains were used in the model which were connected by friction less spherical joints. No assumption was made indicating uniform/constant properties of each finite segment of the tether. The mass of each segment has been assumed to be lumped at the end of each link segment. The model was developed to account for tether towed in marine environment (hydrodynamic effects). The external forces such as the drag, buoyancy and weight forces on each and every link are the same for a finite segment with constant length. The procedures developed/used for the theoretical model were coded into algorithms for a

FORTTRAN program called DYNOCABS. The developed software had the capabilities of solving open-loop, closed loop nonlinear dynamic analysis and steady-state open-loop linear analysis. The closed-loop analysis would be of use, if used for testing the towed-body autopilot designs.

Lambert and Nahon [17] conducted a dynamic analysis on a streamlined tethered aerostat held to the ground using a single tether. The tether has been modeled based on a lumped mass approach. Finite difference approach has been used to linearize the system of equations. The stability of several longitudinal and transverse modes has been studied with respect to varying wind speed and length of the tether. The continuous cable has been discretized into smaller elements (straight elastic element) and the forces were subjected to act at the end of each element of the discretized model. It was further mentioned that the visco-elastic properties of the material is the cause of the internal forces acting within each element. The tension caused inside the cable element has been assumed / considered to act along the tangential direction. The external forces acting on any given cable element were due to the aerodynamic drag and the gravity. The lowest frequency modes out of the 33 modes have been studied and the higher frequency modes have been neglected as they were not likely to obtain significant motions in the actual system. The correlation of the behavior at the lower frequency modes were in good agreement with that of the analytical predictions. The stability of the system also improved with increase in wind speed to a certain value after which the stability decreases to reach steady state with the exception of a lateral pendulum mode. The effect

of the length of the tether on all modes of stability has a similar effect of increasing stability with increase in tether length again with the exception of the lateral pendulum mode. The lateral pendulum mode, an exceptional case, has better stability with shorter lengths at high speeds and longer lengths at low speeds.

Williams and Trivailo [18] studied the transitional dynamics of an aerial towed system when the aircraft changes its flight from a straight to a circular path. The dynamics of the system were modeled using a discretized approach. The performance of the system under consideration was evaluated based on two cases 1) Transition of the aircraft with a deployed cable from a straight to a circular path and 2) Deployment of the cable while the aircraft is in a circular path. The study of the flight transition from straight to circular path has been accomplished by means of a relatively simple variation in the tow point velocity. It was found that the end of the cable became slack as a result of a traveling wave along the length of the cable, caused by the transition of the flight from straight to circular path for a known system parameters (aircraft circular path radius and speeds) that would lead to optimal/desired system performance. The second case where the cable was deployed while the aircraft is in a circular path seems to be a better alternative provided the deployment of the cable has been achieved using a smaller rate. Two strategies were considered for the cable deployment rate 1) Heuristic law (in which the rate of deployment is high for most of part of deployment) and 2) Fuzzy logic control law. When the cable is deployed at a larger rate, certain instabilities can be seen. These

instabilities were found to be significantly lowered if the cable deployment rate is proportional to the length of the deployed cable.

Williams and Trivailo[19] studied the equilibrium and stability solutions for a Towed Aerial system attached with a Wind-sock. The equilibrium configurations of the system have been determined based on an inverse approach in combination with the lumped parameter discretization of the cable being considered. In general for long cables the drogue orbit radius is almost close to the center of the circular path taken by the drogue. It was also observed that the drogue orbit radius becomes smaller if the towed body had a higher drag to weight ratio (wind-sock). The approximate value of the coefficient of drag for this closed end wind-sock is approximated to be equivalent to 1.35, by Hoerner [13], based on the projected/frontal area. Based on this observation, the authors suggested that a high drag body/device (wind-sock) should be placed at an optimal position between the two ends of the tether in order to achieve/obtain the lowest orbit radius.

Paul Williams and Pavel Trivailo studied the transient dynamics of a twin aircraft cable system using lumped parameter models for the simplicity and the relative ease of applying the model for later equilibrium analysis and transient dynamic studies. The advantage of the use of two aircraft for the pickup of a single payload is that the components of tension in each of the cable are ideally balanced (nullified) thereby

ensuring that that payload is held at a near stationary position at the center of the circular path. The original concept of the use of twin aircrafts for retrieving a payload was given by Alabrune [21, 22]. The techniques/procedures required for the maneuvering two aircrafts to lift the payload from the ground and for the “tow-in” and “tow-out” maneuvers were discussed by Alabrune [21, 22] and proposed by Wilson [23] respectively.

1.2 ADAMS

Adams is a multi-body dynamics software used to study and analyze the complex behavior of mechanical assemblies. This software allows one to optimize the designs by process called virtual prototyping. All of this can be done without the actual need to built physical prototypes. The core ADAMS package consists of Adams/View, Adams/Solver and Adams/Post-processor. The Adams/View is the module in which the system/prototype can either be imported / designed. Applied forces, motions, stiffness, etc can be given as inputs into the model using this module. Once the model is built, the software checks the system for any modeling errors and then solves the simultaneous system of equations using the Adams/Solver. The results of the solved model, is then presented in the appropriate form such as plots, reports, etc. Extension modules of Adams such as Controls can be used to analyze control systems such as hydraulics, pneumatics

1.3 Scope of Work

The research work mentioned above indicates that equilibrium and stability analysis of the towed cable and aerostat system under consideration have been studied and considered for various configurations and tether models. The tip radius and verticality for a given range of angular velocities have been obtained based on the given motion. The current work involves the use of an available computer package/software to model and obtain the system response for a given range of angular speeds. The obtained simulation results have been benchmarked to the published work in this field [8] to validate the accuracy and appropriateness of the software model. After benchmarking the model was exercised to expose the effects of parameter variations in drag, tether stiffness, damping, combined stiffness and damping, tow radius and end mass. Results included response plots versus speed, the presence or absence of jump phenomena, helical shaped tether path and tether enveloped, including the presence of nodes at high speeds beyond the jump. Since tethers are made of fabric structures and materials that have yet to be tested, an experiment was setup. The experiment was used to correlate the simulation and experimental results for tether like material with unknown co-efficient of drag. The effect of certain parameters on the system under consideration has also been studied based on the simulations and the results have been presented in chapter 4.

CHAPTER 2

FUNDAMENTAL MODEL

A fundamental model has been developed in order to study tether motion using multi-body dynamics simulation software with equations modeling aerodynamic drag forces. The tether is replaced with a multi-link model connected by spherical (ball) joints, without major complexities associated with it. The model under consideration is said to be accurate if either it can be correlated to published results, or by correlating simulation and experimental results. Several researchers [7][8][10][11][12][14] have worked on similar and not-so-similar. The work done by other researchers either involved the development of computer-based simulation and models based on the specific systems under consideration [11][16], or the theoretical evaluation of a given system of governing equations [7][8][10]. The current work involves the use of an existing commercial software package known as ADAMS [24] to automatically formulate the equations of motion and to solve those equations numerically to determine the path taken by the tether for various cases. All equation nonlinearities are accounted for in the software. Inertia forces are automatically generated by the software, along with standard elements such as linear springs and dampers. User-written functions and subroutines are accessible so that complex applied forces such as aerodynamic drag can be incorporated into the model. The equations that are required for this project include input motions and applied

aerodynamic drag forces that act along the entire length of the tether. Aerodynamic drag forces depend on the type of material, cross-sectional area of the element and length of the segment being considered. The model considered here consists of a discretization of the tether into a series of rigid links connected by spherical joints. Simulation results from this model compare favorably to those of other models (see chapter 3).

2.1 Design of Model/System

The Figure 2.1 shows the simple sketch of a tether-mass system. The top of a tether of length “L”, mass “M”, diameter “D” and weight per unit length “W” is attached to the towing link and the bottom is attached with a concentrated end mass also called a “drogue” (optional).

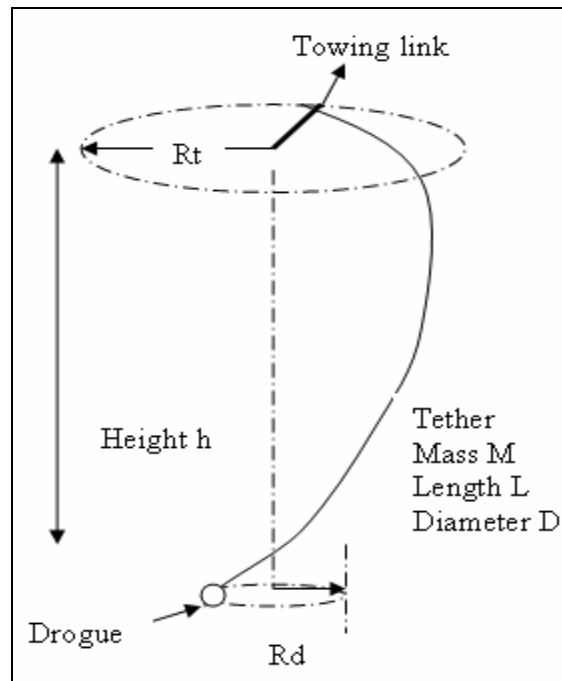


Figure 2.1: Simple Tether Mass System

The towing link is pinned to the ground and rotates about this position at a pre-defined constant speed. The path being taken by the top of the tether attached to a towing link and the mass being towed are represented by the two circles above and below respectively. “Rt” represents the radius of the path taken by the towing member. “Rd” represents the radius of the path taken by the drogue attached at the bottom. The vertical distance between the two ends of the tether is represented by the height h and is termed “Verticality” as pointed out by Zhu [10].

The parameter with the greatest variation in this model is the aerodynamic drag coefficient C_D . The aerodynamic drag forces are calculated for a cylinder by the following formula based on Morison’s equation:

$$F = 0.5 * C * d * (V_{WIND} - V_{CYLINDER})^2$$

Where,

- d – Diameter of the cylinder
- V_{WIND} – Velocity of wind
- $V_{CYLINDER}$ – Velocity of cylinder
- C - Co-efficient of drag
- α – Angle of attack
- λ = $90 - \alpha$

The co-efficient of drag for an inclined cylinder, in the normal and tangential directions below the Reynolds number below the critical number, is given by Hoerner [13].

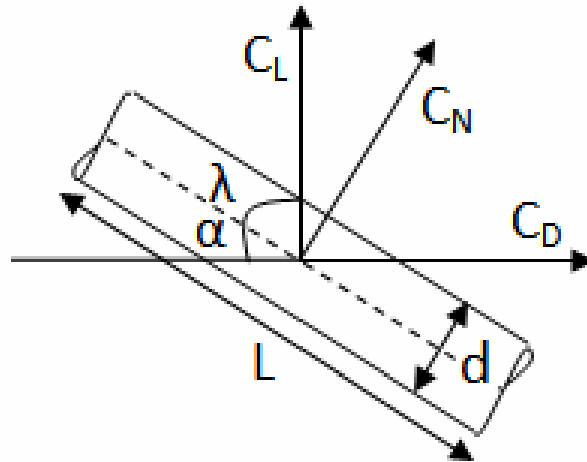


Figure 2.2: Hoerner's Cross-Flow Principle

The Figure 2.2 shows the cross-flow principle and the associated formulae are shown below.

$$C_N = C_{D-BASIC} * (\sin^2 \alpha)$$

$$C_L = C_{D-BASIC} * (\sin(\lambda) * \cos^2(\lambda))$$

$$C_D = C_{D-BASIC} * (\sin^3 \alpha)$$

Where,

$C_{D-BASIC}$ - Coefficient of Drag based on material properties

C_D - Coefficient of Drag

- C_N - Coefficient of drag in the normal direction
 C_L - Coefficient of drag (lift)

The above mentioned formulae were not used; instead a constant value for the coefficient of drag in the normal direction has been used in the simulations. The coefficient of drag(lift) has been neglected (since $\lambda = 0$).

The aerodynamic forces are directly proportional to the square of the relative velocity components of the segment (equation 2.1). The aerodynamic drag forces acting on each segment of the tether can be resolved into two components of force, namely normal force and tangential force. The normal component of the drag force F_N acts in the normal direction (perpendicular to the length of the tether) and the tangential component of the drag force F_T acts in the tangential direction (along the segment of the tether) as shown in the Figure 2.3. These forces can further be resolved and combined along the three dimensional axes system as shown below:

$$F_X = F_{N-X} + F_{T-X} \quad (2.2)$$

$$F_Y = F_{N-Y} + F_{T-Y} \quad (2.3)$$

$$F_Z = F_{N-Z} + F_{T-Z} \quad (2.4)$$

Where,

F_N – Normal component of Drag Force

F_T – Tangential component of Drag Force

F_X – Combined X component of Normal and Tangential drag forces

F_Y – Combined Y component of Normal and Tangential drag forces

F_Z – Combined Z component of Normal and Tangential drag forces

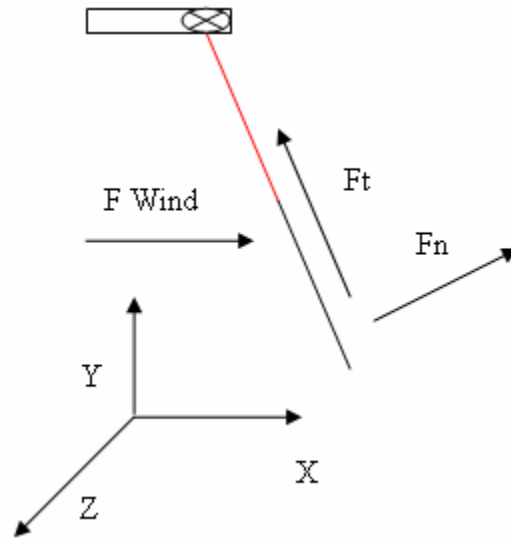


Figure 2.3: Resolution of Forces

Other researchers neglected the tangential component of the drag force, and justified this based on experimental results and the fact that it very small relative to the normal component [10]. This assumption was also used here, although it is by no means necessary. It is by means of the interaction between the various forces acting on the tether system (such as aerodynamic drag forces, inertia force, forces due to gravity and input motions from the towing link) that the overall motion can be calculated, graphed and animated for system analysis.

The model is developed in ADAMS using the basic elements such as links, spherical joints, cylinders and unidirectional applied forces. The advantage of using ADAMS is that it automatically calculates inertial and joints forces. The entire tether has been modeled with finite number of rigid and inelastic elements (cylinders), connected by spherical joints. Hence the tether is broken up into smaller segments to achieve better results as shown in Figure 2.4. The accuracy of the results will depend upon the number of finite links the tether is divided into. The mass moment of inertia of the associated segment of the tether is small and is calculated by ADAMS based on the shape and dimensions of the link. In anticipation of future elastic (spring-mass) modeling of this tether system as shown in Figure 2.5, the drag forces have been transferred to act at the ends of each segment instead of acting at the center of mass. Therefore three forces act at the end of each segment. These are the X, Y, Z components of the drag force acting in the X, Y and Z directions respectively.

At the moment, there is no external cross-wind blowing acting on/against the tether, hence only the absolute velocity will be used for determining the drag forces. When cross-flow is present, the relative velocity of the tether with respect to the cross-wind velocity must be used in the drag force calculation (equation 2.1). The wind force, generated as a result of the angular motion of towing member and acting on the tether is due to the motion of the tether and is always opposite to the direction of motion.

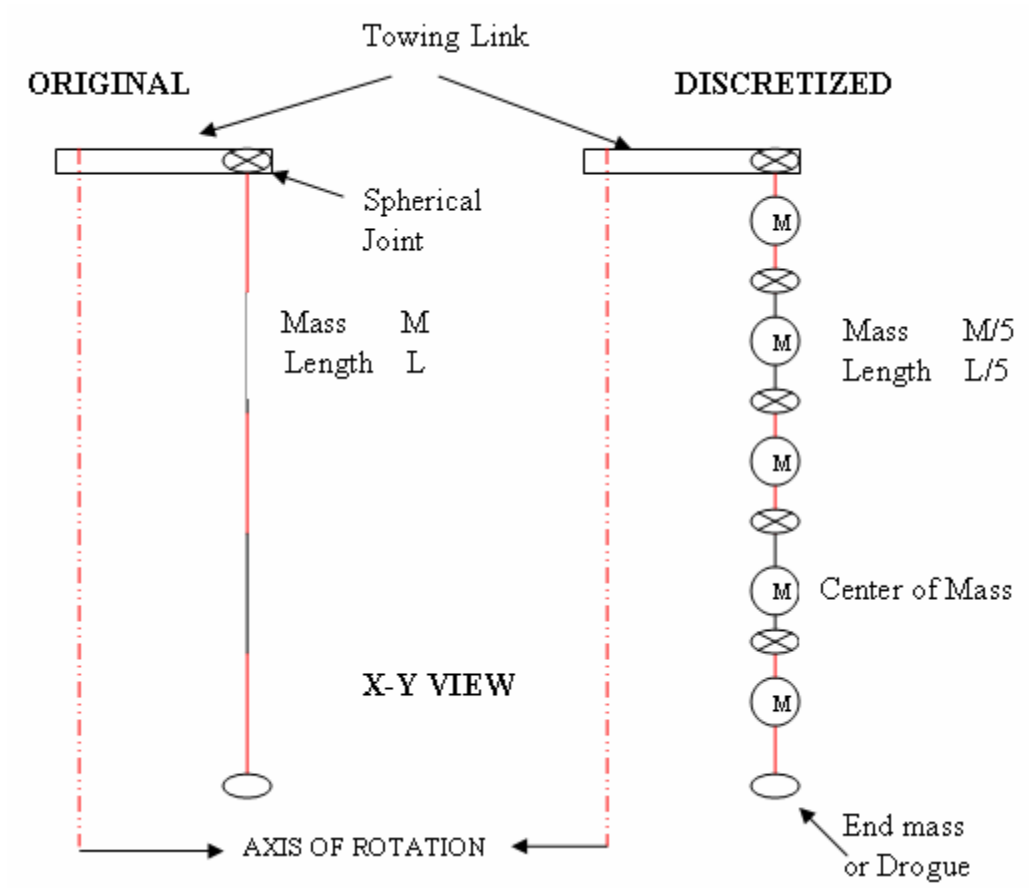


Figure 2.4: Original Model and Discretized Model at Stationary Position

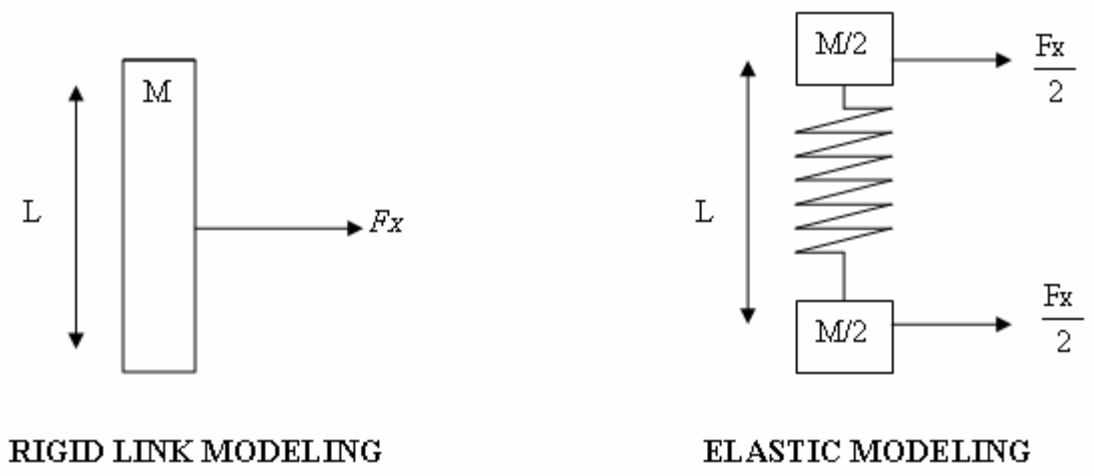


Figure 2.5: Differences between Types of Modeling

The 2-D drawing of the discretized model developed is shown in the Figures 2.6a and b.

The drag forces along the three directions are given by the following equations

$$F_x = -(0.5) \times \text{density} \times c \times A \times V_x^2 \quad (2.5)$$

$$F_y = -(0.5) \times \text{density} \times c \times A \times V_y^2 \quad (2.6)$$

$$F_z = -(0.5) \times \text{density} \times c \times A \times V_z^2 \quad (2.7)$$

Where,

A = Frontal Drag surface area

c = Co-efficient of Drag in the normal direction = 1.2

V = Velocity of the segment

density = Density of air = 43.40277778E-06 Lb-mass/inch³

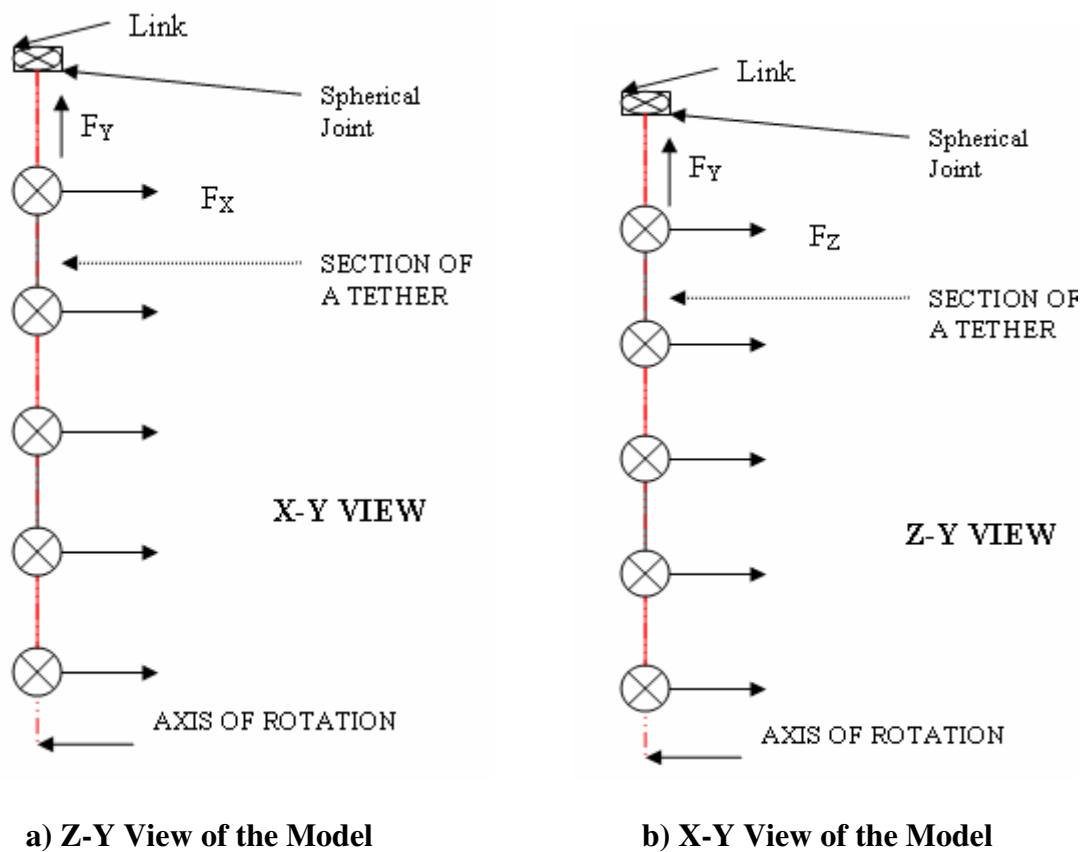


Figure 2.6: Views of the Model

The above formulae will be modified to include the normal and tangential components of force while being fed into ADAMS. It has been assumed that the diameter of the thread (tether) does not deform diametrically in this case and hence

$$D^* \approx d \quad (2.8)$$

Where,

D^* = deformed diameter of the tether

d = diameter of the tether

2.2 Calculations

The factor that has been given utmost importance is the drag forces acting at the ends of each segment. The drag force formulae are fed into the unidirectional force module using the function builder in ADAMS/VIEW. The symbolic form of the drag forces that would be fed into ADAMS is given below

$$F = -(0.5/386) * density * A * c * V^2 \quad \text{Lb-Force} \quad (2.9)$$

Where,

$$A = d * L$$

L = length of the segment (finite element length) = 5.15 inch, [8]

The presence of a factor (1/386) in equation 2.9 is to ensure the resultant force obtained from the equation has a unit in Lb- force. For simplicity, the finite number of links is limited to 5 and hence there would be 5 Parts/segments.

A typical drag force in the X, Y and Z direction that would be fed into the software is shown below for the first segment:

$$\begin{aligned} F_x = & (-0.5*(43.40277778E-06/386)*(0.0185*5.15))* \\ & *(\sqrt{(VX(PART_3.cm))^2 + (VY(PART_3.cm))^2 + (VZ(PART_3.cm))^2} * \\ & *(1.2*VX(PART_3.cm)) \end{aligned} \quad (2.10)$$

$$F_y = (-0.5*(43.40277778E-06/386)*(0.0185*5.15))* \\ *(\sqrt{(VX(PART_3.cm))^2 + (VY(PART_3.cm))^2 + (VZ(PART_3.cm))^2} * \\ *(1.2*VX(PART_3.cm))) \quad (2.11)$$

$$F_z = (-0.5*(43.40277778E-06/386)*(0.0185*5.15))* \\ *(\sqrt{(VX(PART_3.cm))^2 + (VY(PART_3.cm))^2 + (VZ(PART_3.cm))^2} * \\ *(1.2*VZ(PART_3.cm))) \quad (2.12)$$

Where,

VX (PART_3.cm) = X-direction Velocity of the center of mass marker of Part 3

VY (PART_3.cm) = Y-direction Velocity of the center of mass marker of Part 3

VZ (PART_3.cm) = Z-direction Velocity of the center of mass marker of Part 3

“Part 3” represented in the above formula corresponds to the first segment of the discretized tether.

CHAPTER 3

MODELING, SIMULATION AND BENCHMARKING

The chapter explains the assumptions made, modeling procedure and correlation of the data obtained from the model with the data obtained from published work [8].

3.1 Assumptions made in Modeling

- No external cross-wind induced forces are acting on the system
- The system can be modeled by a combination of rigid links and spherical joints, implying that the tether will not stretch significantly.
- Coefficient of Drag forces acting on the tether(cylinder) is based on the cross-flow principle [13]
- Tangential component of the drag force has been neglected

3.2 Modeling

ADAMS/View is the software module that is used to graphically display the motion the tether takes during the course of the analysis for various towing speeds. The shape the tether takes can be verified with experimental data provided the modeling is

sufficiently detailed and the parameter values used in the analytical model match with those in the experiment.

The model developed in ADAMS consists of the following essential components namely

- 1) Tow Link analogous to an aircraft (example)
- 2) Cylindrical shaped links analogous to a tether
- 3) A spherically-shaped link to model the drogue
- 4) Spherical Joints
- 5) Revolute Joint
- 6) Motion Statement at the top of revolute joint
- 7) Drag Forces

Numerical data for this analytical model has been taken from published data used in an experiment [8] so that this model can be compared with that of an existing analytically developed model. The discretized ADAMS model showing all the above mentioned elements is shown in Figure 3.1

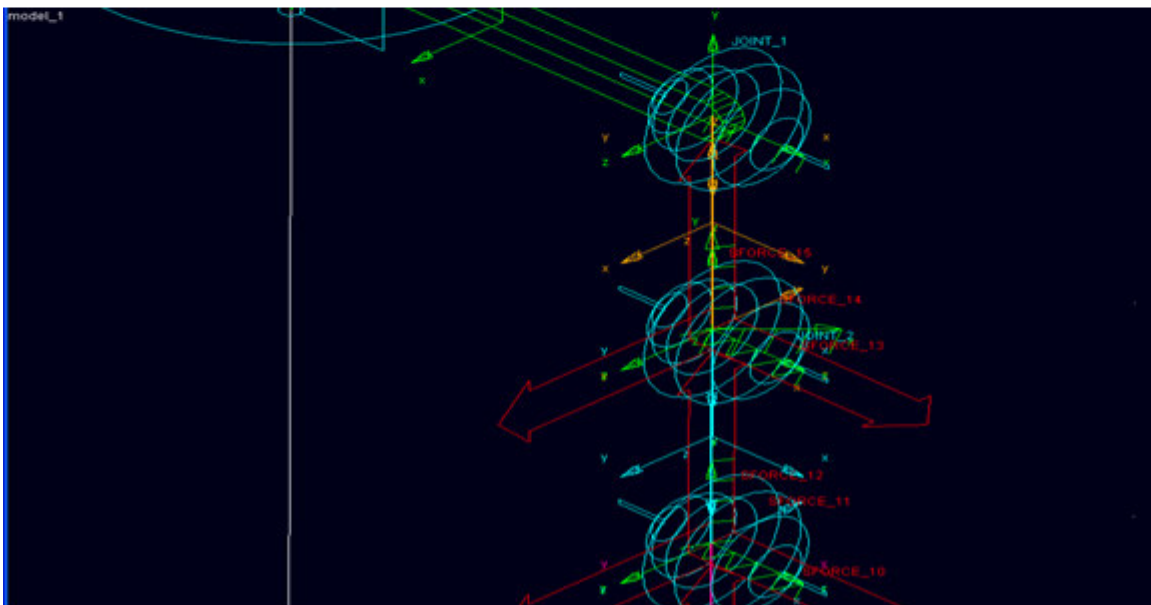
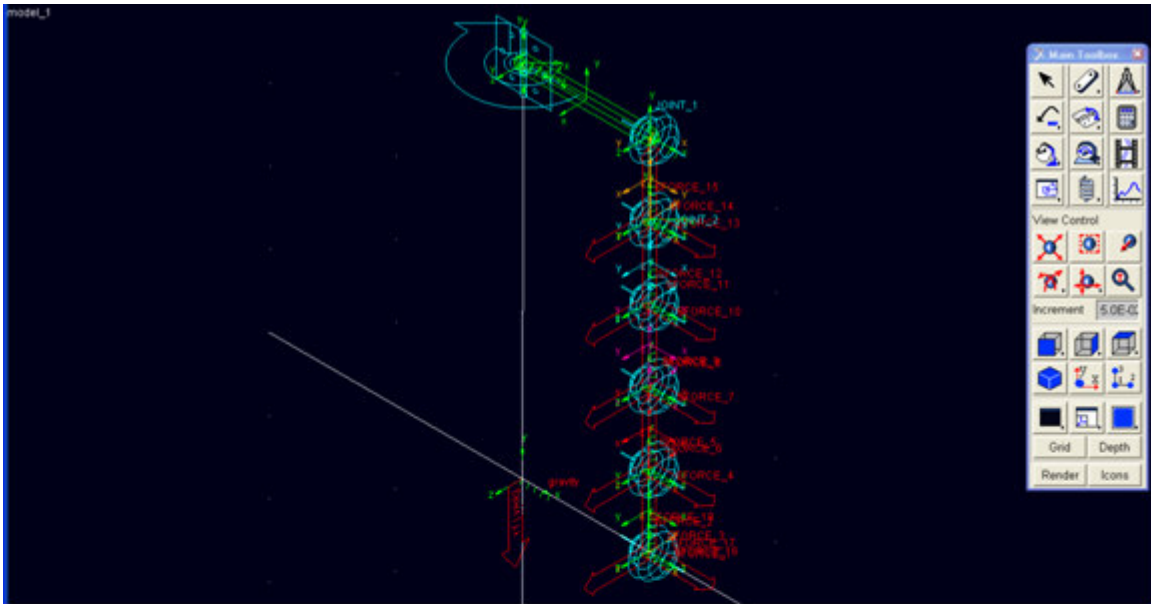


Figure 3.1: Discretized ADAMS Model

3.2.1 Tow Link

The Tow link is the component used for simulating the motion, for example an aircraft moving in a circle. The length of this link is considered to be the tow radius (“Rt”) with which the entire system has been modeled. For practical applications involving delivery or pickup of objects [3][4] using an aircraft, the tow radius depends on the minimum circular path that an aircraft takes. In this case the tow radius would be in order of several 100 ft. Such large amounts of tow radius would be highly difficult to be achieved in a laboratory environment. Hence the values of tow radius chosen for the models are chosen relatively small, to obtain a correlation between the simulation and experimental data. Most existing research work done by authors mentioned in Chapter 1(Past and present research) have non-dimensionalized their work. This work has not been non-dimensionalized as one of the main objectives of this work is to validate the ADAMS model with that existing work. The link is fixed at one end to the ground in ADAMS with a revolute joint. This revolute joint is given a motion statement so that the link rotates about this fixed joint with the chosen angular velocity. The weight and width of the link have no effect on the simulation results and hence are irrelevant.

3.2.2 Cylinder

Cylindrical links are used to represent the tether. The entire length of the tether (L) is equally divided into 5 equal segments. The following data [8], (obtained from the experimental setup) has been used to model the cylindrical segments analogous to the

section of the tether. The mass of each segment depends on the length of the segment being considered and is uniformly distributed.

Length of tether	= 25.75 inch
Radius of tether	= 0.0185 inch
No of elements to divided into	= 5
Weight of the tether	= 9.697020833 E-5 lb
Density of tether	= 1.4009665 Lb-m/(inch ³)

3.2.3 Sphere

A Spherical element has been used to model the light weight drogue attached at the bottom of the tether. This drogue can also be considered as the weight that has to be dropped or picked up at a stationary location on the ground as discussed in [xx]. The following values [8] have been used to model a sphere.

Diameter	= 0.148 inch
Weight	= 9.921 E-05 lb

3.2.4 Spherical Joints

In general, a tether is flexible and bending along the length of the tether is expected. A spherical joint between the smaller segments allows for this bending. These

spherical joints allow only rotational degrees of freedom at the joints which can be considered to account for the flexible nature or any tether.

3.2.5 Revolute Joint

A revolute joint is used to connect the link element to the ground, apart from allowing the required rotatory motion at the joint. The direction of this revolute joint depends on the desired axis of rotation about which the link should rotate. A motion statement is given to this revolute joint to create the required motion about this joint

3.2.6 Motion Statement

A motion statement is a function / formula added to generate the required motion (angular motion) at the relevant joint. A motion statement can be applied to any joint. In this model it has been applied to the revolute joint connected between the ground and one end of the link. This motion provides the required rotating motion (speed) for the link.

A constant value can be used to generate a constant motion. A varying function (like STEP, figure 3.2) is used to create a smooth curve and can also be used to constantly vary the speed based on the parameters used in the function. A varying parameter is used for modeling purposes as it can vary the speed constantly based on the input data and can also help in generating transient and instability state results which will

be discussed later. The motion statement (angular motion of the towing member based on displacement) used for this model is given by the formula

$$\text{STEP}(\text{TIME}, 0, 0, 2000, 15) * \text{TIME}$$

Angular motion based on velocity is given by:

$$\text{STEP}(\text{TIME}, 0, 0, 2000, 15)$$

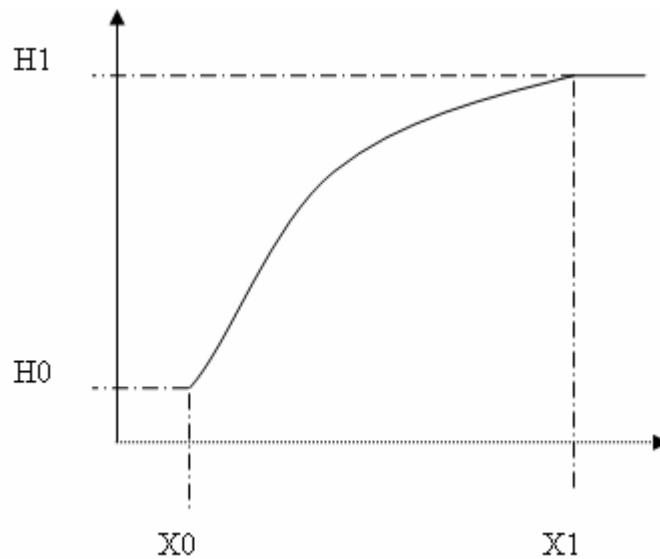


Figure 3.2: Step Function Curve

Step Function

A Step function is used to smooth out the output of any given function such as drag forces and motion statements.

The syntax for a STEP FUNCTION in ADAMS is

$$\text{STEP}(\text{Parameter}, x0, h0, x1, h1)$$

Where,

“Parameter” is the factor associated to the points x0 and x1. In this model the parameter is the time.

3.2.7 Drag Forces

The drag force is susceptible to the uncertainty in the drag coefficient and variations in cross-sectional area of the tether. If these forces are not properly modeled, differences between experiment and simulated solution can be large. The simulation data from this model has been verified with that of published data [8] to ensure that the drag forces are appropriately modeled. The drag forces, in general, would be modeled such that they act at the center of mass of any link. But in this model they are modeled such that they act at the end of the link. The length of each segment is considered to be small and also considering the future discretization of the tether using spring-mass (elastic modeling) as shown in Figure 2.5, the drag forces are modeled to act at the end of each segment. The drag forces are applied at each end of the section along the three-axis X, Y and Z. The forces along X and Z are responsible for the tip radius at the drogue end. The force along Y is responsible for the lift (verticality) of the drogue.

Example of the Drag force in the X-direction, used in this model (incorporating the step function) is

$$F_x = \text{STEP}(\text{time}, 0, 0, 1, 1) * (-0.5 * (43.40277778\text{E-}06 / 386) * (\text{Tether_Length} * \text{Tether_Radius})) * \\ * (\sqrt{(\text{VX}(\text{PART_3.cm}))^2 + (\text{VY}(\text{PART_3.cm}))^2 + (\text{VZ}(\text{PART_3.cm}))^2} * \\ * (1.2 * \text{VX}(\text{PART_3.cm})))$$

The above formula is the normal component of the drag force acting, at the end of the segment, along the X direction. The terms “1.2 * VX (PART_3.cm) is the factor accounting the normal component where 1.2 is the co-efficient of drag in the normal direction. The formula for accounting either the normal or the tangential component of the drag force is the almost the same. Similarly the formula of drag force in the Y and Z directions are given below

$$F_y = \text{STEP}(\text{time}, 0, 0, 1, 1) * (-0.5 * (43.40277778\text{E-}06 / 386) * (\text{Tether_Length} * \text{Tether_Radius})) * \\ * (\sqrt{(\text{VX}(\text{PART_3.cm}))^2 + (\text{VY}(\text{PART_3.cm}))^2 + (\text{VZ}(\text{PART_3.cm}))^2} * \\ * (1.2 * \text{VY}(\text{PART_3.cm})))$$

$$F_z = \text{STEP}(\text{time}, 0, 0, 1, 1) * (-0.5 * (43.40277778\text{E-}06 / 386) * (\text{Tether_Length} * \text{Tether_Radius})) * \\ * (\sqrt{(\text{VX}(\text{PART_3.cm}))^2 + (\text{VY}(\text{PART_3.cm}))^2 + (\text{VZ}(\text{PART_3.cm}))^2} * \\ * (1.2 * \text{VZ}(\text{PART_3.cm})))$$

Different views of the ADAMS model built, at stationary position, are shown in Figure 3.3.

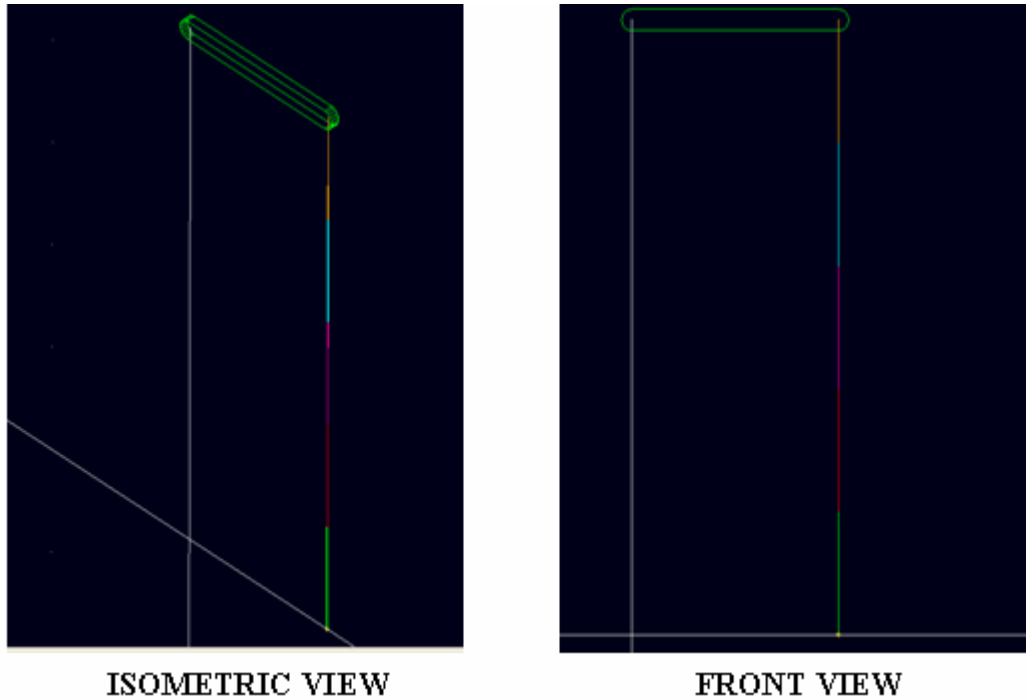


Figure 3.3: System at Stationary Position

3.3 Simulation for Preliminary Model Validation/Correlation

Modeling without validation cannot be used for further analysis of the system, under consideration. In order to validate the ADAMS model, the model has to be compared with that of the data from a similar work. In order to compare the current work with past work, the following data has been obtained from the experimental procedure [8], and will be used for validating the ADAMS model developed.

D = Diameter of the Tether = 0.0185 inch

d = Diameter of the Drogue = 0.148 inch

L = Length of the Tether = 25.75 inch

W = Weight of the Silk Thread = 4.519 E -05 Lb/ft

M = Mass of Drogue = 9.921 E -05 Lb

Rt = Tow radius = 9 inch

In order to validate the accuracy of the ADAMS model, the model has been simulated (based on the data listed above) and outputs have been verified with the model under consideration. The parameters that were compared are the “End Mass (Drogue) Path (Tip) Radius and Verticality”. The dependence of the tip radius (end mass path radius) on the angular velocity of the towing member is discussed in the next section. The results obtained by simulating the ADAMS modeled for different parameters have been discussed in detail in the next chapter.

3.3.1 Tip Radius and Angular Velocity

The radius of the path the drogue follows is known as the tip radius. The tip radius depends on the angular velocity of the towing member, in this model the towing member is the link. ADAMS/VIEW plots the angular velocity of the link and the tip radius with respect to time and later the time factor can be removed to obtain a plot between tip radius and angular velocity. The graph (Figure 3.4) shows the dependence of Tip Radius on the angular velocity without any damping, using a motion statement that defines a slow increase in angular velocity. The motion statement used is given below. From the graph it can be inferred that the tip radius increases steadily with angular

velocity until it reaches a point where the tip radius changes rapidly as a result of instability. After the zone of instability, the tip radius decreases slowly.

$$\text{Motion Statement} = \text{STEP}(\text{time}, 0, 0, 2000, 15) * \text{time}$$

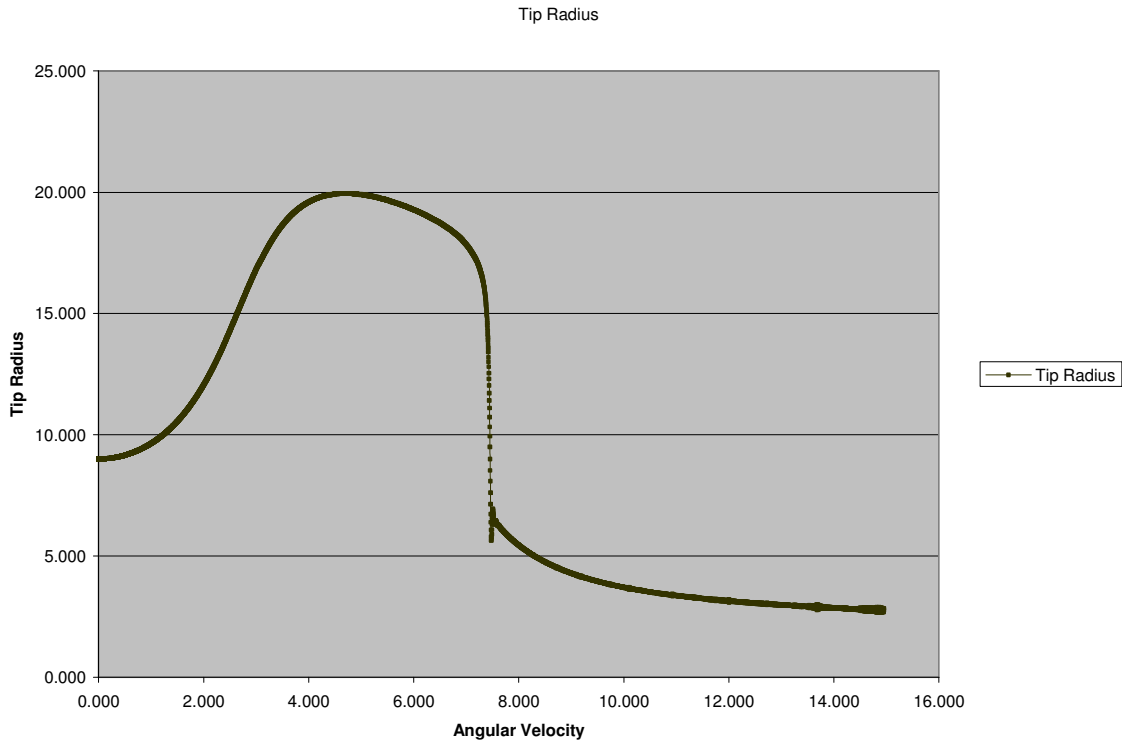


Figure 3.4: Tip Radius Vs Angular Velocity Curve generated by ADAMS

3.3.2 Comparison of the ADAMS Model Response with Published Data

In order to compare the data obtained from published research [8] to that of the data generated using ADAMS, slight change in the motion statement has been made. For this comparison, the ADAMS model has been simulated at a constant angular velocity instead of a uniformly increasing angular velocity. The velocity at which the model has

been simulated is based on the data, mentioned above. The data (Tip Radius and Verticality) obtained has been plotted with respect to angular velocity and the resultant plots have been compared. The simulation data and the published data to which the results have been compared are shown in Tables 3.2 - 3.4 in the Appendix.

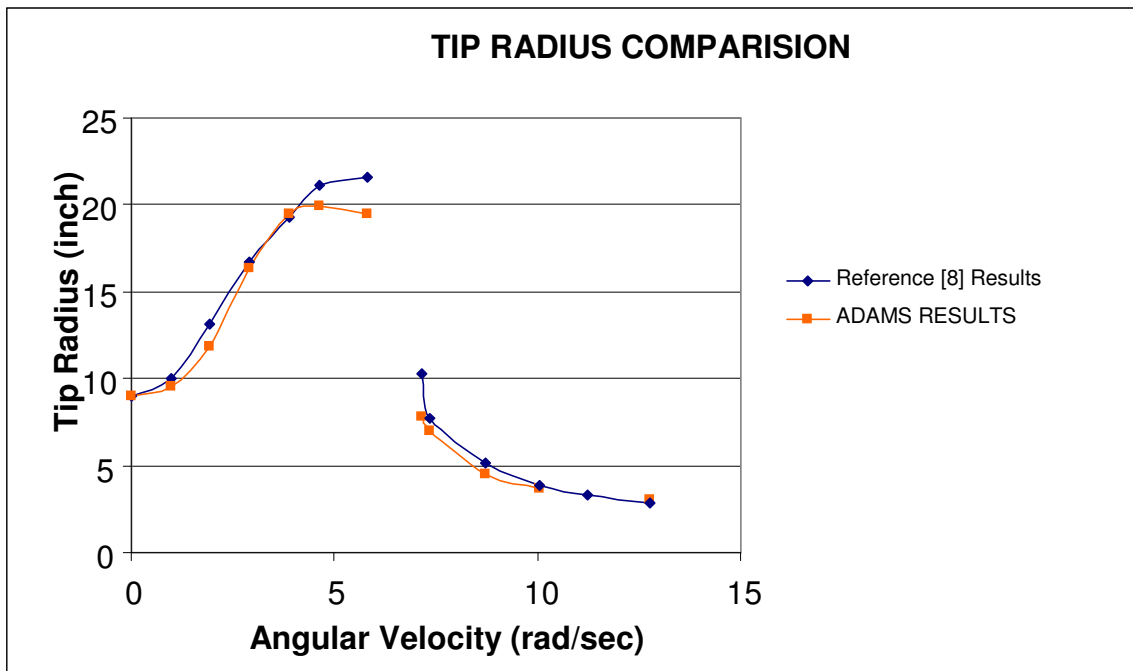


Figure 3.5: Comparison of Tip Radius; ADAMS Data with Published Results

Figure 3.5 shows the plot comparing the Tip radius of the published research [8] and the ADAMS generated simulation data. It can be seen that there is a good agreement between the two sets of data. The tip radius, in general for both curves, increases with increase in angular velocity for the first section of the plot and for the second section of the plot the tip radius decreases with increase in angular velocity.

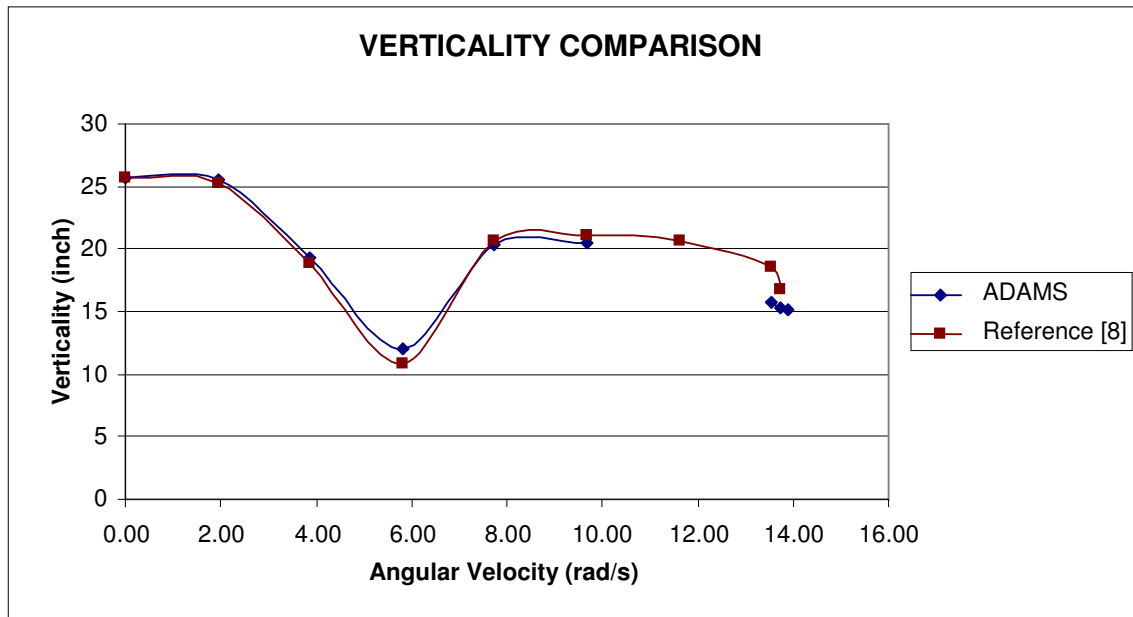
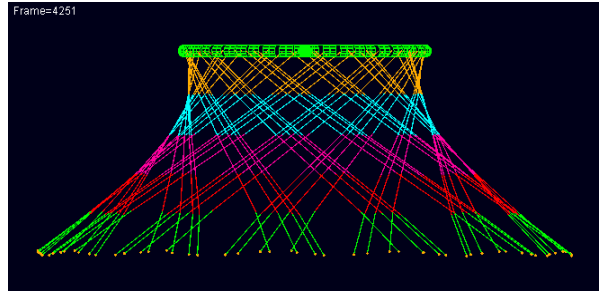


Figure 3.6: Comparison of Verticality; ADAMS Data with Published Results

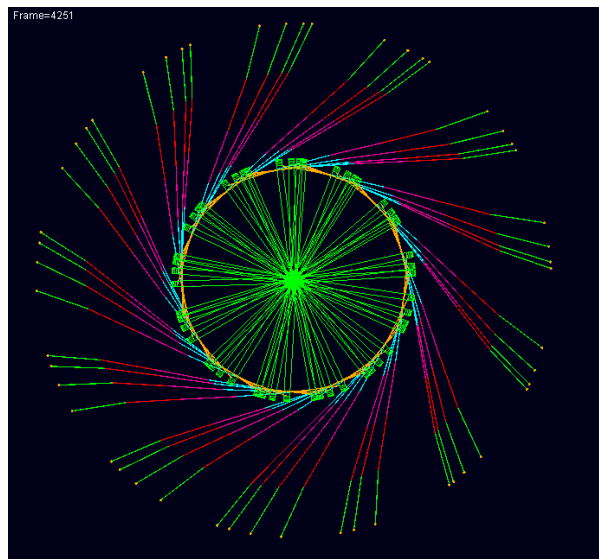
In Figure 3.6 the verticality plot of the two sets of data has been plotted for comparison. The reference position for the verticality measurement, for these curves, is taken at the end of the tow member. The plot indicates that the verticality data of the two plots are in agreement. From the plot it can be inferred that the verticality (elevation from the ground) increases with increase in angular velocity, reaches a highest position, after which the verticality starts to decrease and until a near constant value has been attained. The above graphs (verticality and tip radius) and tables (Appendix-A) clearly indicate that the developed ADAMS model is accurate.

3.4 Superposition in ADAMS Model

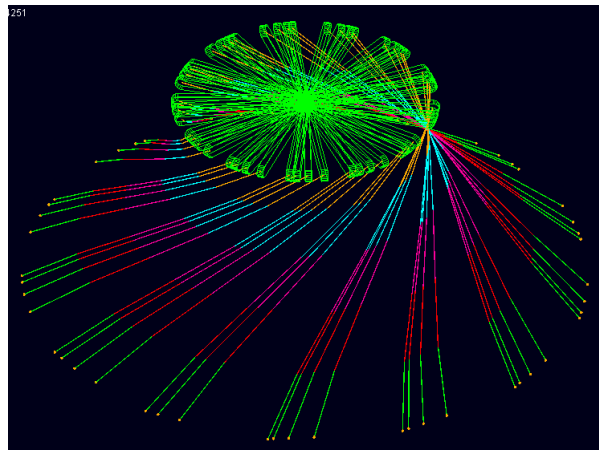
The ADAMS model has been used to obtain the superposition data of the tether for various angular velocities. Superposition data gives an approximate idea about the pattern traced by the tether. The following figures 3.12-3.15, shows the superposition images. The images in figures 3.12 and 3.13 are before the jump (zone on instability) and the two images shown in figures 3.14-3.15 are the superposition images after the jump. One interesting results is the presence of a “node” occurring at speeds after the jump.



a) Front View

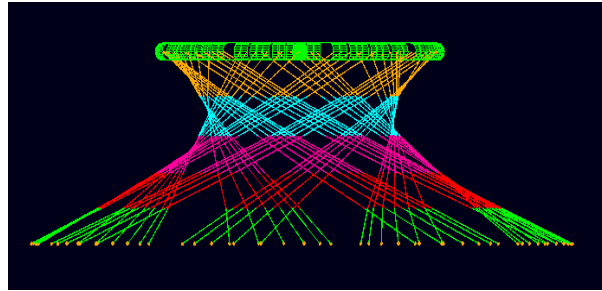


b) Top View

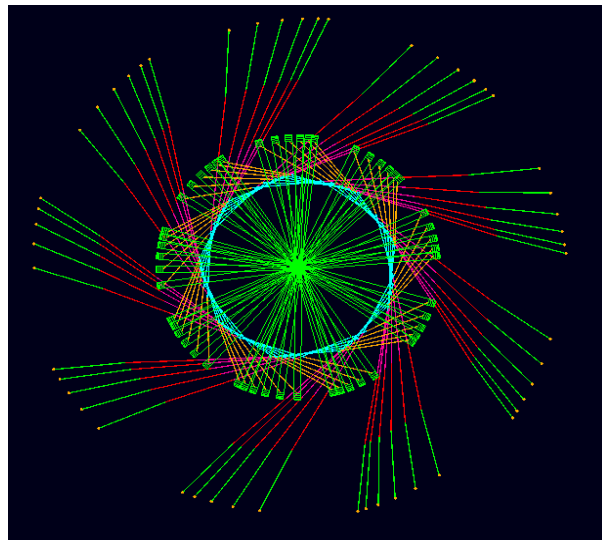


c) Isometric View

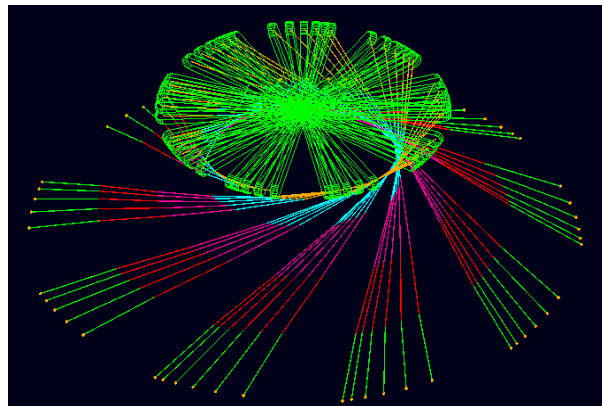
Figure 3.12: Superposition Screen Shot: Angular Velocity 4.82- 4.94rad/s



a) Front View

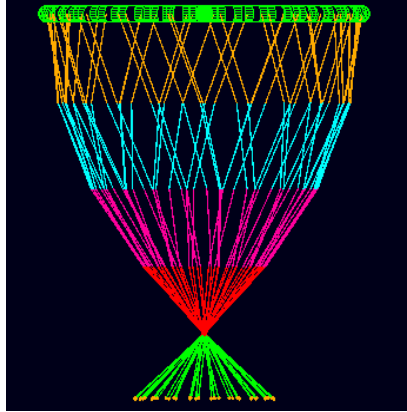


b) Top View

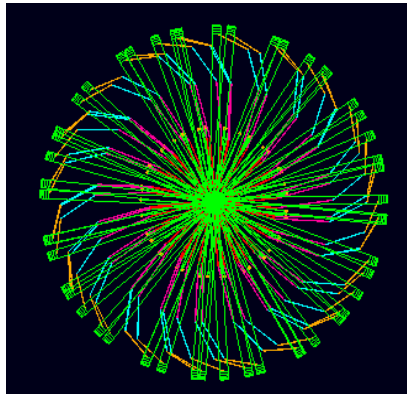


c) Isometric View

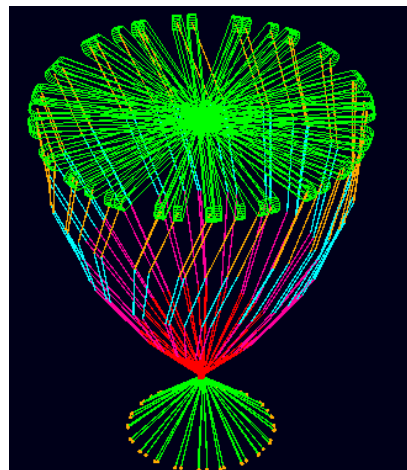
Figure 3.13: Super Position Screen Shot: Angular Velocity 7.03-7.14 rad/s



a) Front View

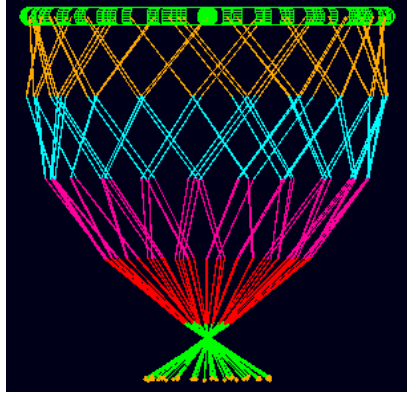


b) Top View

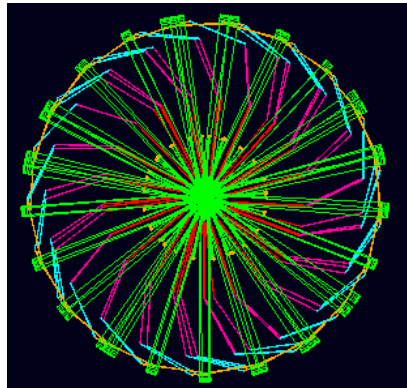


c) Isometric View

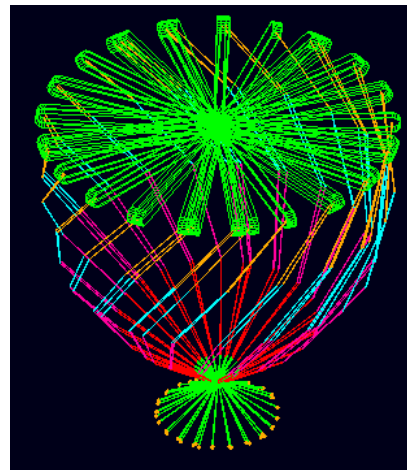
Figure 3.14: Super Position Screen Shot: Angular Velocity 9.42-9.51 rad/s



a) Front View



b) Top View



d) Isometric View

Figure 3.15: Super position Screen shot; Angular Velocity 11.91-12.02 rad/s

CHAPTER 4

NUMERICAL RESULTS

The effects of certain known parameters, on the shape/pattern (Tip Radius and Verticality) exhibited by the tether are discussed in this chapter. In order to study the effect of the parameters, each of these has been modified and in turn the effect of the modification has been evaluated. The following section describes the parameters that would be changed and whose effect on the system will be analyzed.

4.1 Simulation Parameters

Simulations were run to determine the effect of the following parameters on the pattern taken by the tether

- 1) Damping/Stiffness
- 2) Mass of the drogue
- 3) No of Segments
- 4) Tow radius

4.1.1 Damping/Stiffness

Damping is very important in order to damp out most unwanted oscillations. The segments tend to oscillate about the joint connecting one another and hence to reduce the oscillations at the joints bushings (shown in figure) have been used. The stiffness is a material property.

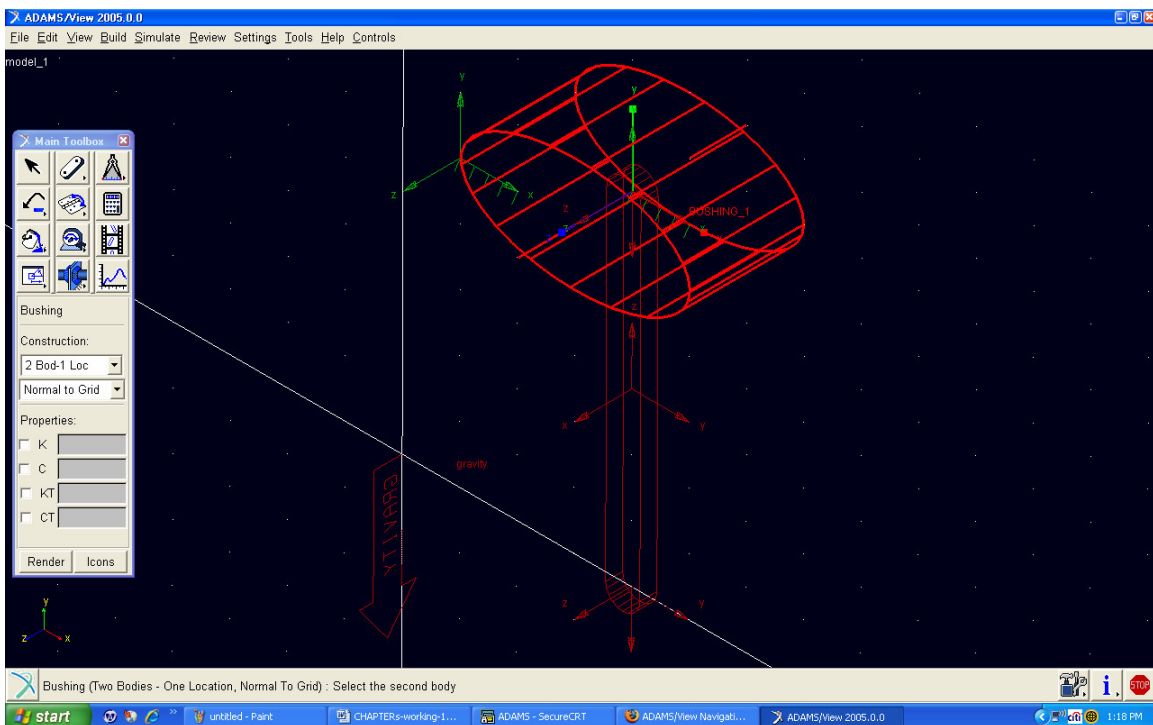


Figure 4.1: Screen-Shot showing Bushing Element

A bushing element [24] applies a linear force/torque that represents the forces/torques acting between two parts over a distance, in directly applying forces to create the appropriate amount of damping and stiffness. This element applies both forces and torques along the three-dimension axis. The amount of damping and stiffness

required in the model can be achieved based on the appropriate input values for the damping and stiffness values in the translational and rotational directions. One can define the forces and torques using six components (F_X , F_Y , F_Z , T_X , T_Y , and T_Z).

$$F_X = K_X * X_x \quad (4.1)$$

$$F_Y = K_Y * Y_y \quad (4.2)$$

$$F_Z = K_Z * Z_z \quad (4.3)$$

$$T_X = R_X * A_x \quad (4.4)$$

$$T_Y = R_Y * A_y \quad (4.5)$$

$$T_Z = R_Z * A_z \quad (4.6)$$

Where,

F_X, F_Y, F_Z – Forces acting along the three dimensional axis X, Y, Z

T_X, T_Y, T_Z – Torques acting along the three dimensional axis X, Y, Z

X_x, Y_y, Z_z – Bushing deformation

A_x, A_y, A_z – Projected small angle of rotational displacement

K_X, K_Y, K_Z – Stiffness along the three dimensional axis X, Y, Z

Different damping and stiffness values, for bushings, have been considered and here we study the affect of damping, stiffness and a combination of both (based on a constant stiffness-damping-ratio). The model has been simulated initially without any

damping medium and later the bushings have been activated to analyze the effect of different damping /stiffness values.

Other Damping Medium

The other damping medium that can be used to add damping to the model is the Frictional Damping, which has not been considered in this work.

4.1.2 Mass of Drogue

The Mass of drogue attached at the bottom of the tether has a major effect on the path the tether takes. The mass of the attached body has been modified and the effect of this modification has been discussed.

4.1.3 No of Segments

The number of links will have an effect on the accuracy of the simulation data generated to a certain extent depending on the length of each segment. The tether, in this model, has been modeled to have 5 segments/links. The reason for discretizing the model to contain the above mentioned number of segments is due to the agreement of the simulation data with published work [8]. The effect of increase in the number of links has not been considered as a result of good correlation between the Adams model and the published data [8].

4.1.4 Tow radius

The distance between the fixed end of the link and the end attached to the tether is known as the tow radius in the model. The tow radius of the system has been modified to study the effect of varying tow radius on the system's output parameters (Tip radius and Verticality), while maintaining the other parameters as a constant.

4.2 Simulation Results

In chapter 3 the accuracy of the simulation model has been validated by comparing the simulation results with that of the published data similar to the current work. Knowing that the model is accurate, the effect of certain parameters listed in section 4.1 such as attached end mass, damping and tow radius on the tip radius and verticality have been discussed in this section. In order to observe response over wide range of speeds on the tip radius and the verticality, a motion statement defining a slowly increasing velocity in time has been created with a step function. As discussed above a step function creates a smooth transition between values which have a large difference/range. The slope of the step function depends on the parameters used (X_0 , X_1 , H_0 , H_1). If the difference between the X_0 and X_1 is large and the difference between the H_0 and H_1 is small then the step function creates a curve with a lower slope. This curve ensures that the rate of increase in the angular speed is small. For most simulations the following step function has been used

```
STEP (TIME, 0, 2000, 0, 15)
```

It is also desired to have an idea about the path in which the “attached mass” travels, when the end of the towing member takes a circular pattern.

4.2.1 Effect of Damping / Stiffness

The effect of damping/stiffness has been studied by varying the “damping/stiffness values” associated with the bushing damping. The tip radius and verticality of the end mass for various cases (varying damping, varying stiffness and varying stiffness and damping) have been determined and plotted as shown in the following sections

4.2.1.1 Effect of Zero Stiffness-Varying Damping

The effect of varying damping based on a constant stiffness in the bushing has been studied in this section. The plots of Tip radius and verticality with respect to Angular velocity have been discussed below

Table 4.1: Damping Values-Zero Stiffness

Zero Stiffness- Varying damping

Series	Damping Values (N-mm-sec/deg)	Stiffness value (N-mm/deg)
Series – 1	0.0000010	0
Series – 2	0.0000050	0
Series – 3	0.0000100	0
Series – 4	0.0000150	0
Series – 5	0.0000200	0
Series – 6	0.0001000	0
Series – 7	0.0002000	0

4.2.1.1.1 Effect of Damping on Verticality

The graphs in **Figure 4.2**, shows the effect of bushing damping on the verticality of the end mass. The plots have been generated using 8 different damping values as shown in the above table.

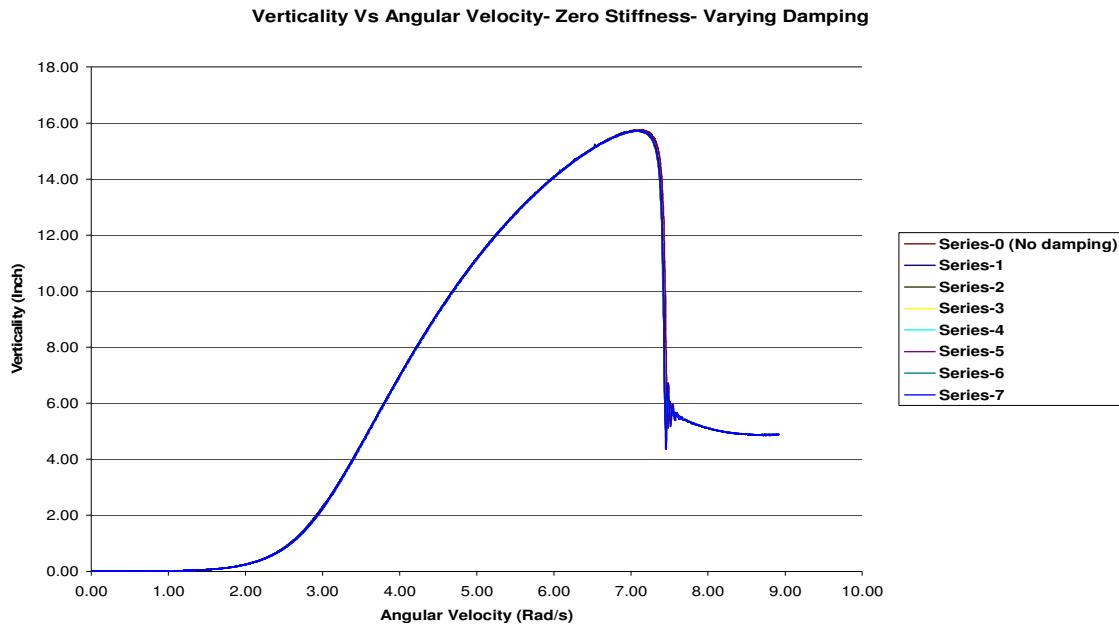


Figure 4.2: Verticality Vs Angular Velocity: Varying Damping-Zero Stiffness

The graph shown in Figure 4.2, shows that the plots for various damping values overlap on each other indicating that the verticality is not affected by the change in the damping values (with zero bushing stiffness) being considered. This indicates that a speed steady-state conditions has been achieved at each speed, where the joint angle is not changing in time hence no damping torques are present to affect the motion.

4.2.1.1.2 Effect of Damping on Tip Radius

The graphs in Figure 4.3, shows the effect of bushing damping on the tip radius of the end mass. The plots have been generated using 8 different damping values as shown in the above table.

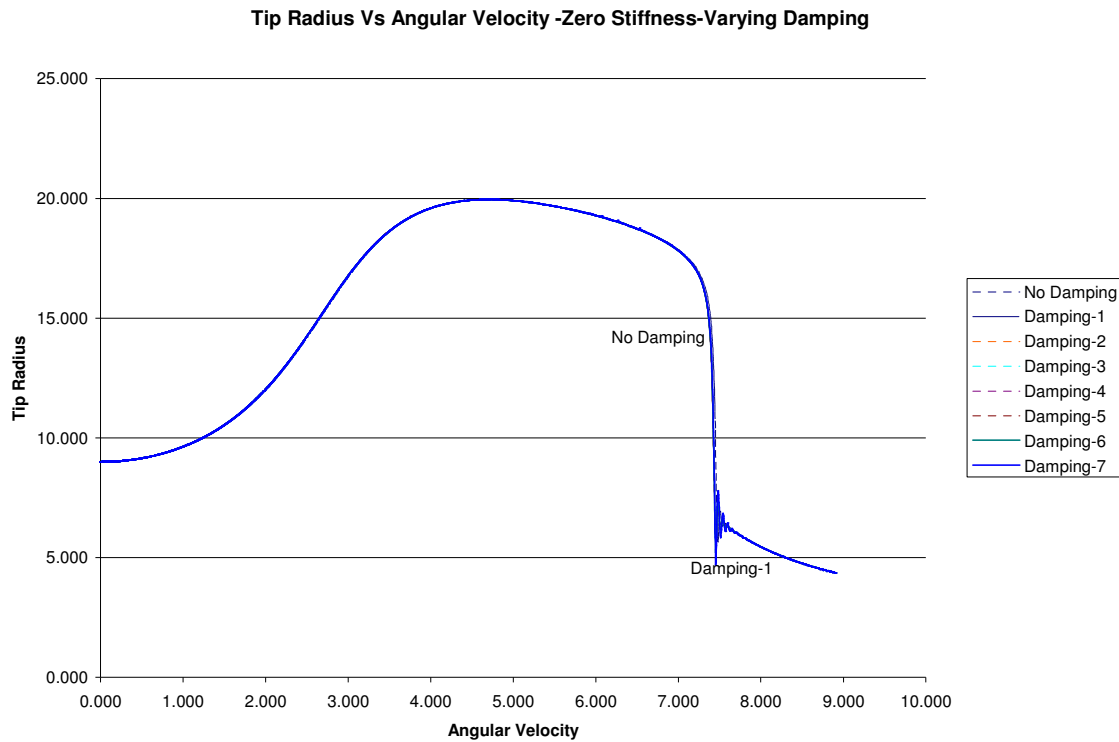


Figure 4.3: Tip Radius Vs Angular Velocity: Varying Damping-Zero Stiffness

The graph shown in Figure 4.3, shows that the plots for various damping values overlap on each other indicating that the tip radius is not affected by the change in the damping values (with zero bushing stiffness) being considered.

4.2.1.2 Effect of Varying Stiffness-Constant Damping

The effect of varying damping based on a constant stiffness in the bushing has been studied in this section. The plots of Tip radius and verticality with respect to Angular velocity have been discussed below.

Table 4.2: Stiffness Values-Constant Damping

Varying Stiffness-Constant Damping

Series	Stiffness Value (N-mm-sec/deg)	Damping Value (N-mm/deg)
Series – 1	0.000001	0.000001
Series – 2	0.000010	0.000001
Series – 3	0.000050	0.000001
Series – 4	0.000080	0.000001
Series – 5	0.000100	0.000001
Series – 6	0.000120	0.000001
Series – 7	0.000500	0.000001

4.2.1.2.1 Effect of Varying Stiffness-Constant Damping on Verticality

The verticality plot versus angular velocity is shown in Figure 4.4. It can be seen from the plot in the below figure, that the curves associated with “Series -1, and 2” overlap on each other. Similar is the case with curves “Stiffness -3 and 7”. For Stiffness curves 4-6, as the stiffness values are increased, the jump phenomenon observed in the respective curves shifts towards higher angular velocities.

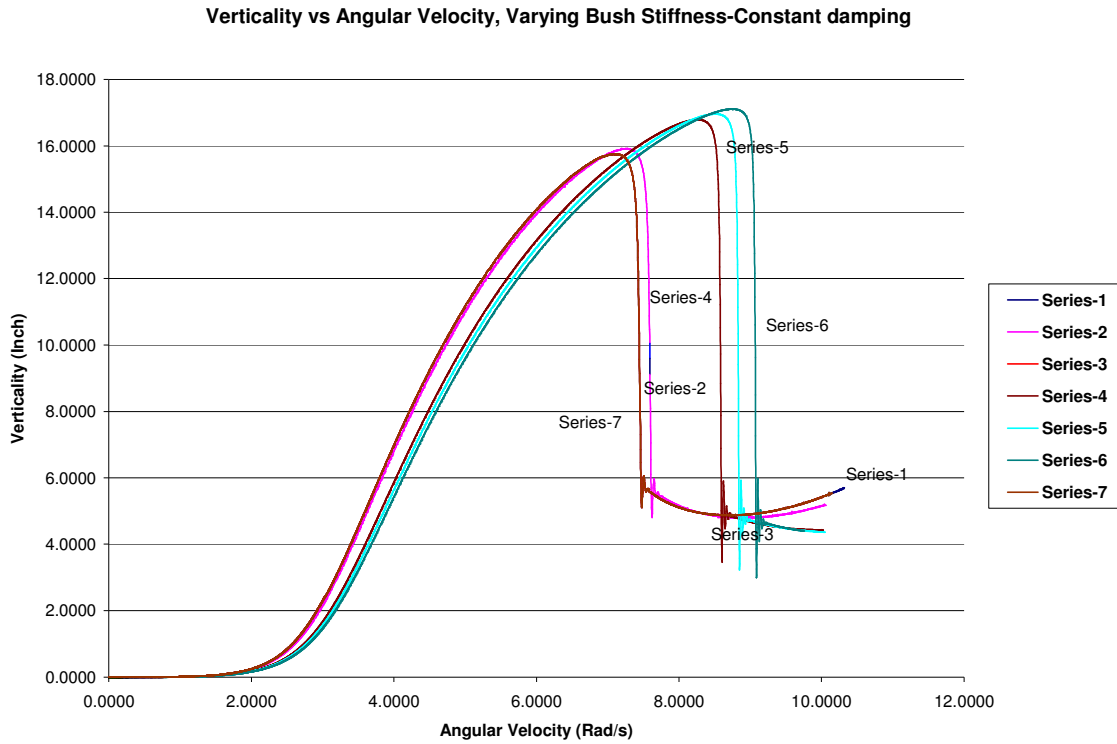


Figure 4.4: Verticality Vs Angular Velocity: Varying Stiffness - Constant Damping

4.2.1.2.2 Effect of Varying Stiffness-Constant Damping on Tip Radius

The plot of tip radius versus angular velocity is shown in Figure 4.5. It can be seen from the plot shown in the below figure, that the curves associated with “Series 1, 3 and 7” overlap on each other. For curves associated with series 4-6, as the stiffness values are increased, the jump phenomenon observed in the respective curves shifts towards higher angular velocities. An exception to this trend can be seen in curve associated with “Series 2 and 3”. It can be expected that in general the jump phenomenon increases with increase in stiffness but for the plot associated with “Series-7”, the jump region (zone of

instability) shifts towards lower angular velocities instead of shifting towards higher angular velocities.

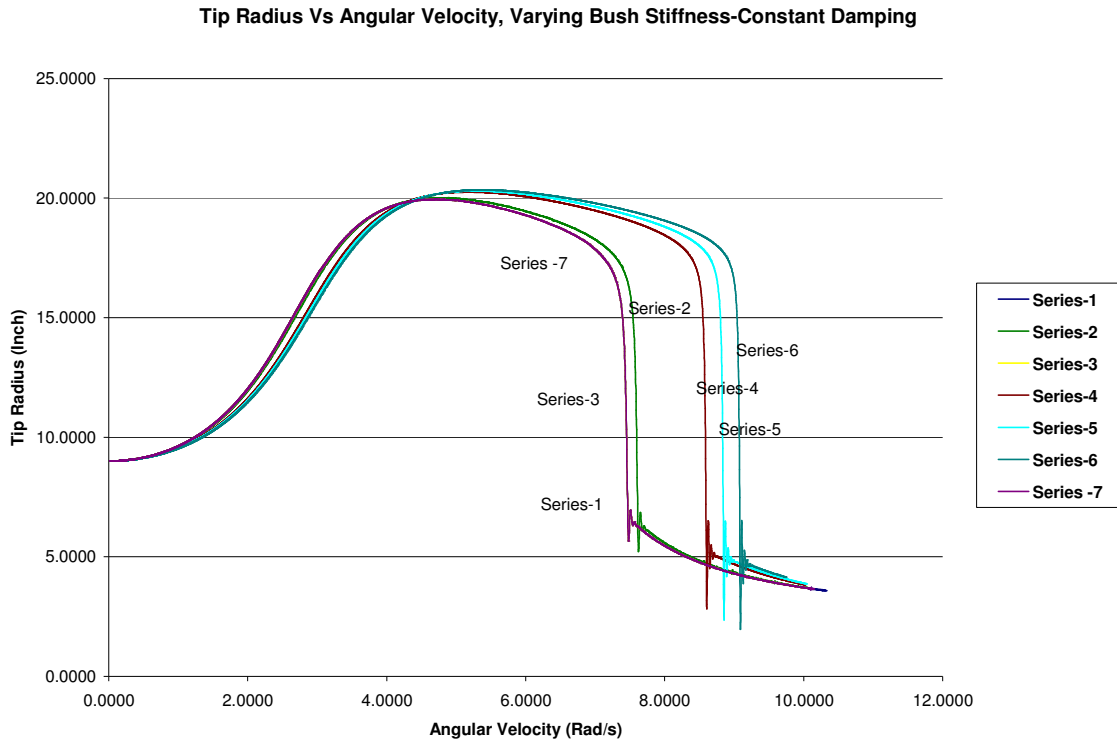


Figure 4.5: Tip Radius Vs Angular Velocity: Varying Stiffness-Constant Damping

4.2.1.3 Effect of Varying Stiffness and Damping

The effect of varying damping and stiffness in the bushing has been studied in this section. The plots of Tip radius and verticality with respect to Angular velocity have been discussed below.

Table 4.3: Damping and Stiffness Values

Varying Stiffness- Varying damping

Series	Damping Value (N-mm-sec/deg)	Stiffness Value (N-mm/deg)
Series – 0	0	0
Series – 1	1.00E-06	1.00E-07
Series – 2	1.00E-05	1.00E-06
Series – 3	1.00E-04	1.00E-05
Series – 4	1.00E-03	1.00E-04
Series – 5	1.00E-02	1.00E-03

4.2.1.3.1 Effect of Damping/Stiffness on Verticality

The graph in Figure 4.6 shows the effect of bushing damping and stiffness on the verticality of the end mass. The plots have been generated using five different damping and stiffness values and have been compared with a “no damping and stiffness” (Series-0) plot as shown in the above table.

In general from any plot (Verticality Vs Angular Velocity) the verticality increases with increase in angular velocity, reaches a highest point after which the verticality rapidly attains a lower value (zone of instability). Further, as the angular velocity increases after the zone of instability (“Jump”), the verticality of the attached masses starts to increase.

It can be inferred from the plot (Figure 4.6) that the verticality, in general, increases with increase in damping and stiffness values. Also, as the damping and stiffness values are increased the zone of instability (“Jump”) is shifted towards higher angular velocities and eventually the zone of instabilities does not exist for curves associated with higher damping and stiffness values (Series -4 and Series-5). Curves associated with “Series-1”, and “Series-0” overlap on each other as the value of damping and stiffness chosen for “Series-1” is almost close to zero (1.0e-005 and 1.0E-006 respectively). Similarly the curves associated with “Series-4” and “Series-5” overlap on each other indicating that the value of damping and stiffness might not have an affect after a certain point.

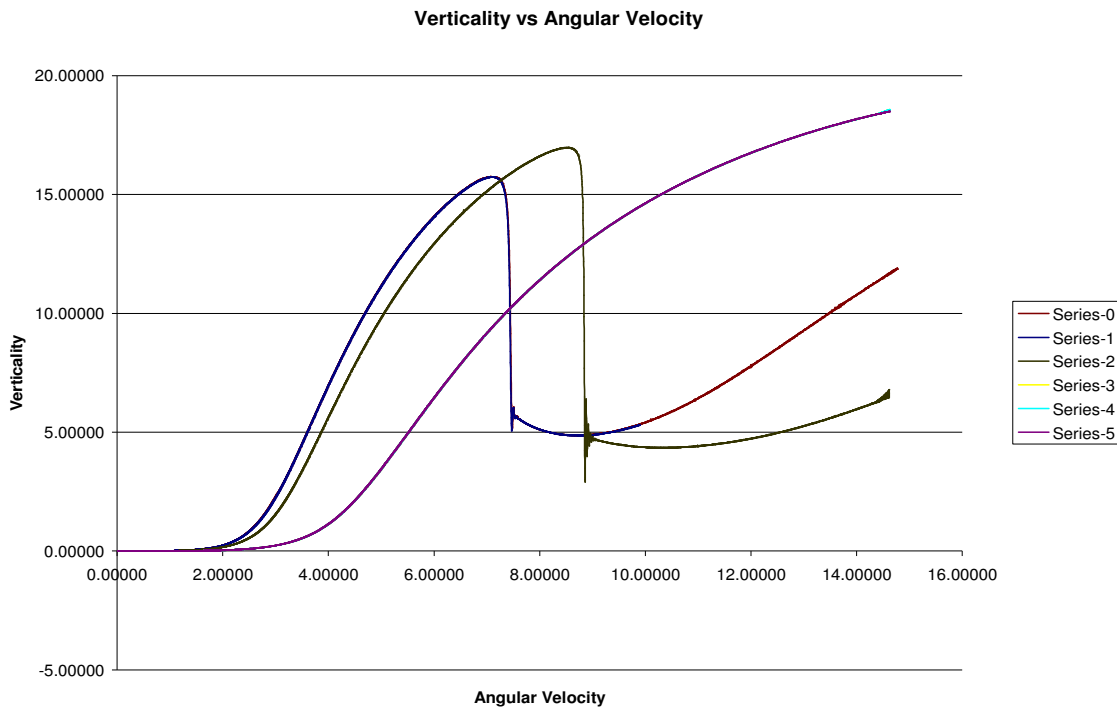


Figure 4.6: Plot of Verticality Vs Angular Velocity: Various Damping and Stiffness Values

4.2.1.3.2 Effect of Damping on the Tip Radius

The Figure 4.7 shows, effect of damping and stiffness on the tip radius of the end mass (drogue or attached mass) for varying angular velocities. The graph has 6 series of damping and stiffness curves which also include a “no damping and stiffness” curve for reference comparison.

Conclusions similar to that of the verticality plots can be made for the tip radius curves. As the damping and stiffness values are increased, in figure 4.8, the zone of instabilities (“Jump”) in the tip radius curve are shifted towards higher angular velocities and eventually the zone of instability cannot be seen for higher damping and stiffness values (Series-3, 4, 5). The rate of increase in tip radius for “Series-3” curve increases steadily with increase in angular velocity whereas for “Series - 4”, and “Series-5” curves the rate of increase in tip radius is very high for lower angular velocities and the rate of increase, decreases with increase in angular velocity and eventually at every high speeds it can be seen that the verticality starts to decrease.

For all the above plotted series, the end-mass follows almost a circular pattern without major deviations as shown in the Figure 4.8 (path taken by end mass-without any damping and stiffness), for angular velocities below 0.225 rad/sec.

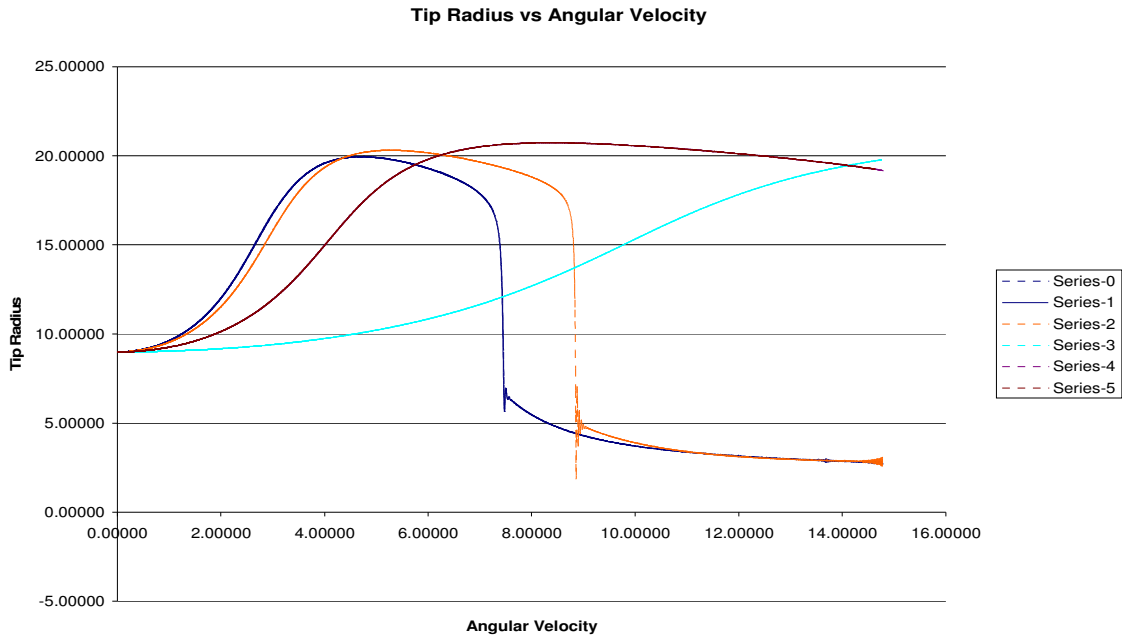
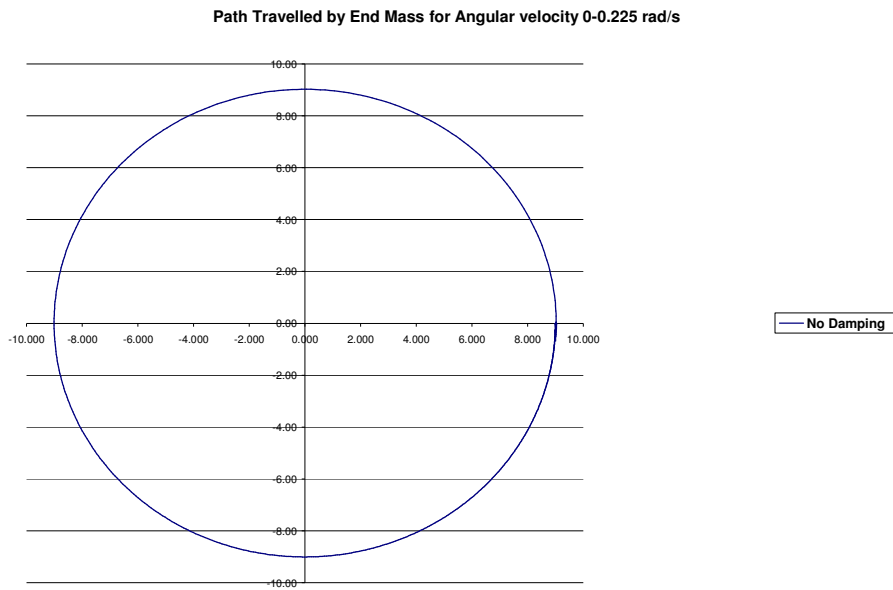
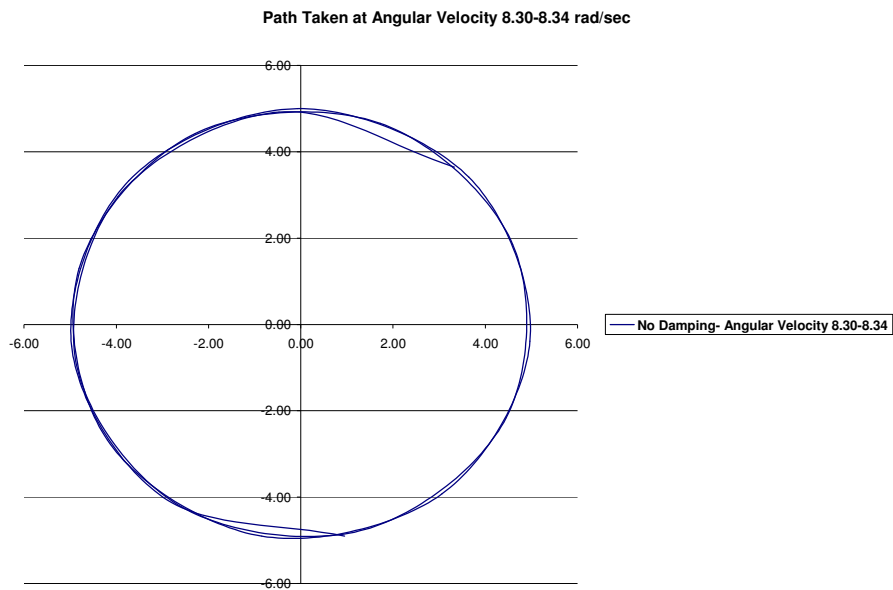


Figure 4.7: Plot of Tip Radius Vs Angular Velocity: Various Damping and Stiffness Values



**Figure 4.8: Path Taken by End Mass: Angular Velocities less than 0.225 rad/s
No Damping and Stiffness**



**Figure 4.9: Path Taken by End Mass: Angular Velocities less than 8.30-8.34 rad/s-
No Damping**

For angular velocities between 8.30 -8.34 rad/ sec, the path traveled by the end mass is shown in Figure 4.9. It can be seen from both the figures that the path traveled is almost a circular pattern and that the center of the circular path followed by the end mass is at the origin.

4.2.2 Effect of End Mass

The mass of the attached “End Mass” has been modified with respect to the other parameters in the system and the effect on the Tip radius and Verticality has been plotted. The reason for considering this type of effect is based on applications such as delivery and pickup of different masses. It should be noted that there is no damping medium

included in this and so stable circular paths need not be achieved for all runs. A factor called “Mass ratio” has been defined as

$$\text{Mass ratio (Mm)} = \frac{\text{mass/ weight of the attached body}}{\text{mass/weight of the tether}}$$

The plots of the tip radius and verticality versus angular velocities, and the path taken by the end mass (attached body or drogue) are shown in the following figures.

4.2.2.1 Effect of End Mass on the Tip Radius

Figure 4.10 shows the plots (Tip radius) for the various mass ratios (Mm). In general the tip radius increases with increase in angular velocity, reaches a maximum value and after which it starts to decrease. The zone of instability occurs for all the mass ratios except for mass ratio equals 0.5. Even after the zone of instability the tip radius decreases. The curves associated with Mass ratios 0.75 and mass ratios 1.1 overlap over each other.

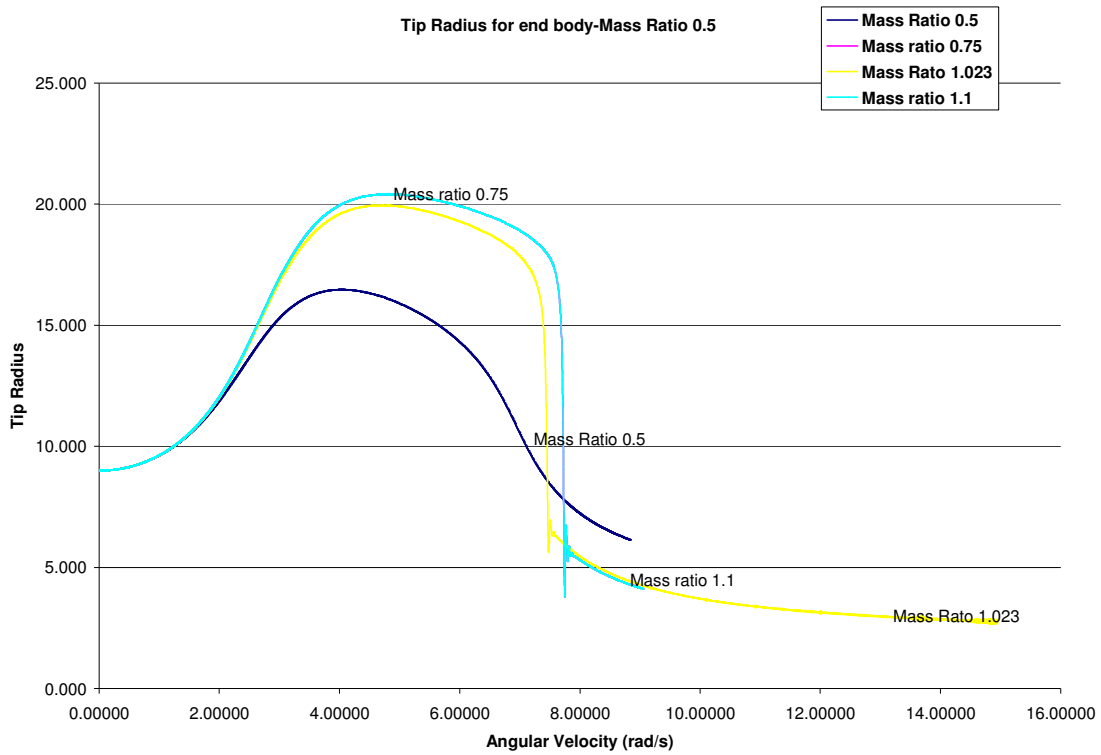


Figure 4.10: Tip Radius Vs Angular Velocity: Effect of Mass Ratio

Figures 4.11-4.18 shows the path taken by the end mass for various mass ratios ranging from 0.5 to 1.1 and for two different ranges of angular speeds. The plot of the “path taken by the end mass” associated with lower speed range (3.0-3.5 rad/s), shows a thicker circular pattern when compared with the higher speed ranges (8.30-8.35rad/s). The reason for this difference can be attributed to the range of speeds considered for the two cases and a small probability that the attached end mass hasn’t reached a stable condition/path at lower speeds. (Note: The scaling on each graph is different, a close look at the numbers in the plot will indicate that the path taken is/or close to a circle)

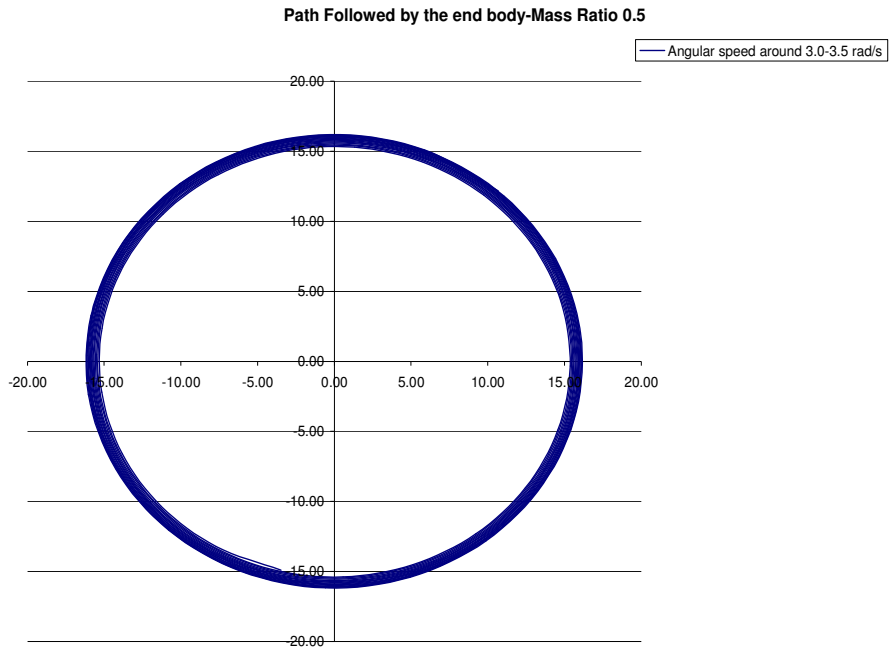


Figure 4.11: Path Taken by End Mass: Mass Ratio - 0.5, Angular Velocity 3.00-3.5
rad/s

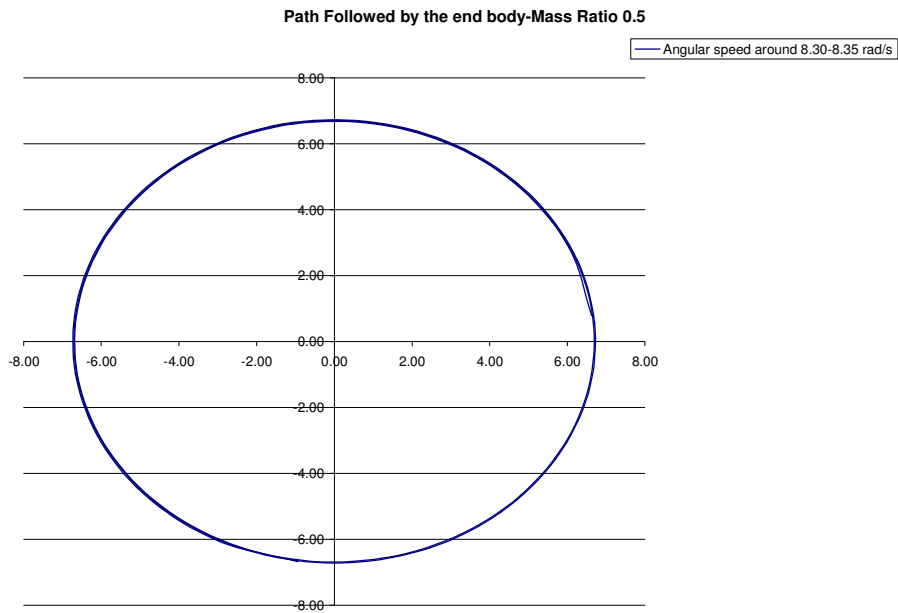
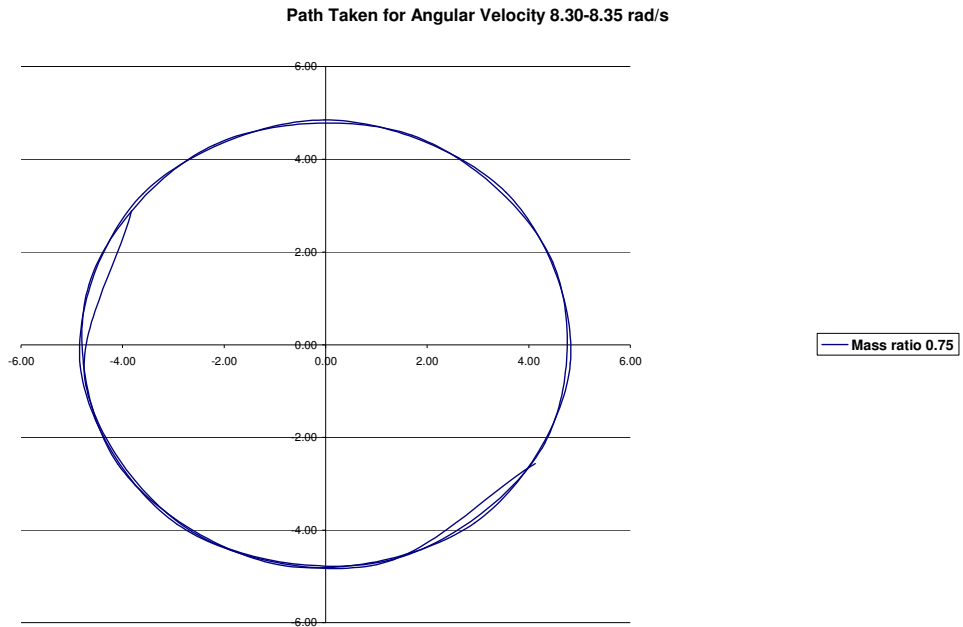
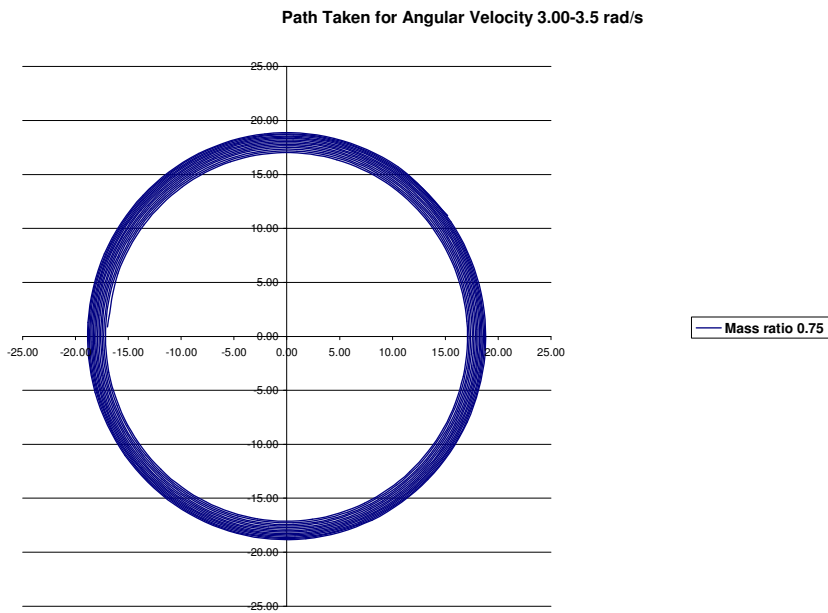


Figure 4.12: Path Taken by End Mass: Mass Ratio - 0.5, Angular Velocity 8.30-8.35
rad/s



**Figure 4.13: Path Taken by End mass: Mass Ratio - 0.75, Angular Velocities 8.3-
8.35 rad/s**



**Figure 4.14: Path Taken by End mass: Mass Ratio - 0.75, Angular Velocities 3.0-3.5
rad/s**

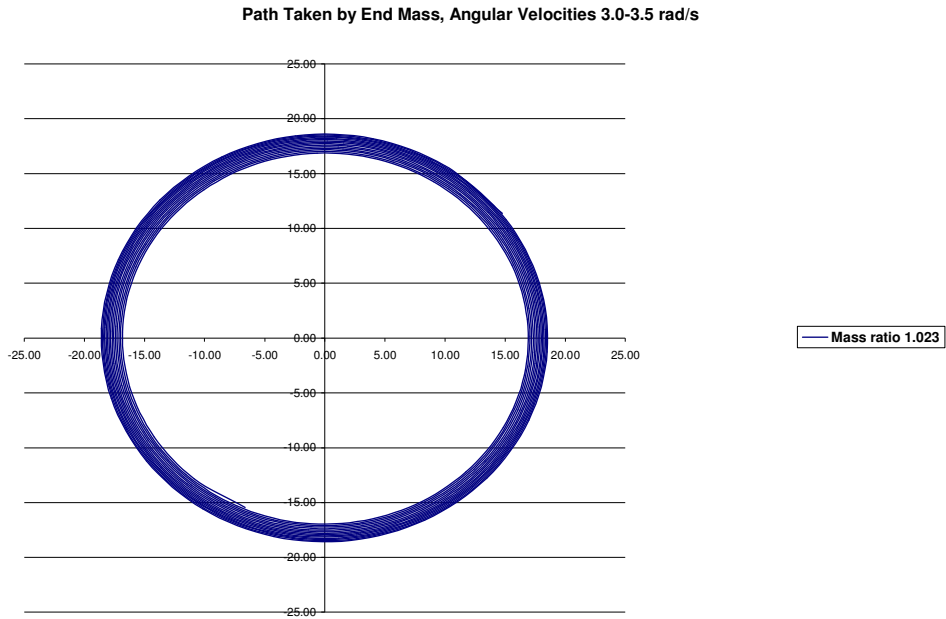


Figure 4.15: Path Taken by End Mass: Mass Ratio - 1.023, Angular Velocities 3.0-3.04 rad/s

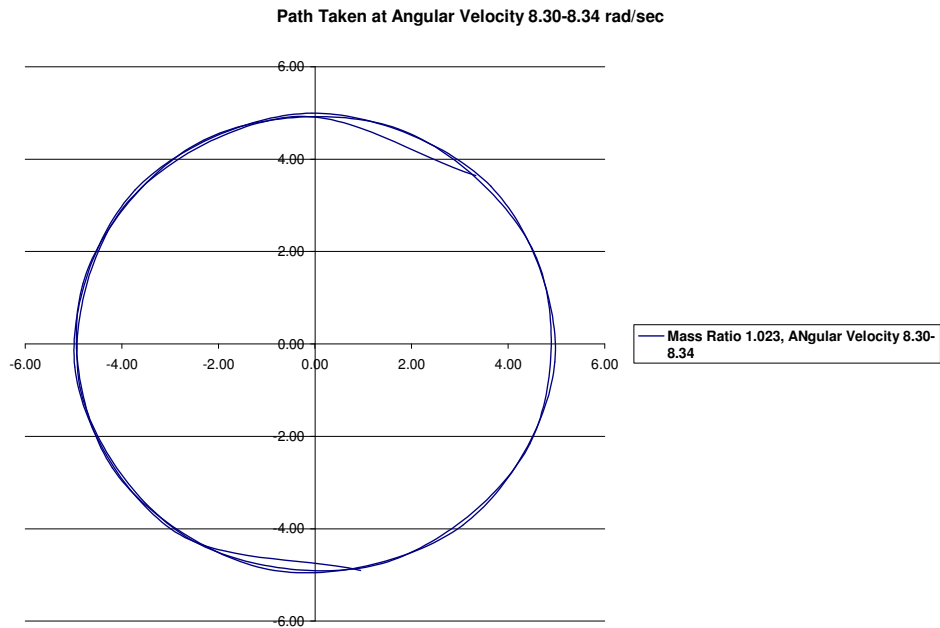
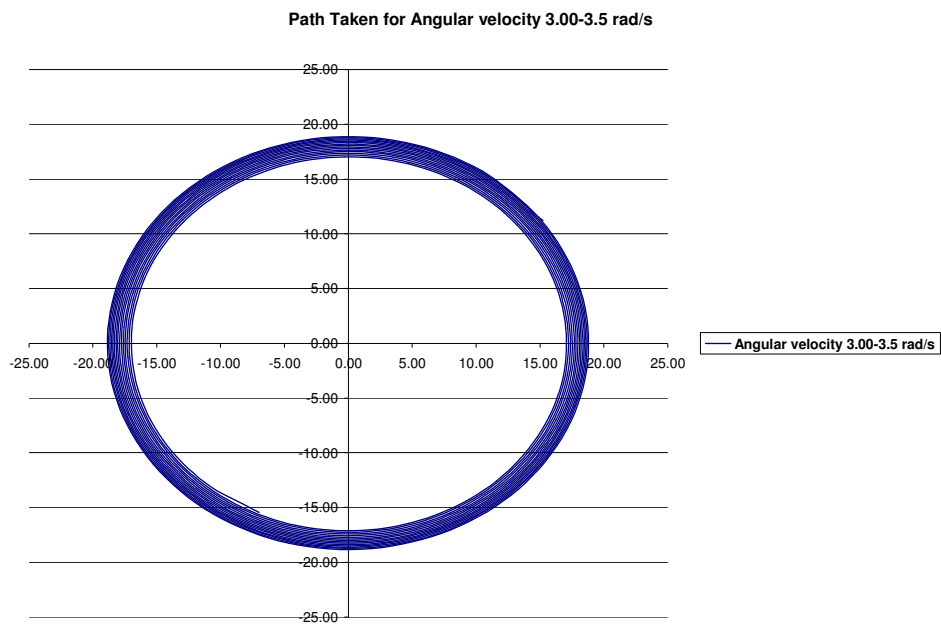


Figure 4.16: Path Taken by End mass, Mass Ratio - 1.023, Angular Velocities 8.3-8.34 rad/s



**Figure 4.17: Path Traveled by End Mass: Mass Ratio - 1.1, Angular Velocity 3.0-3.5
rad/s**

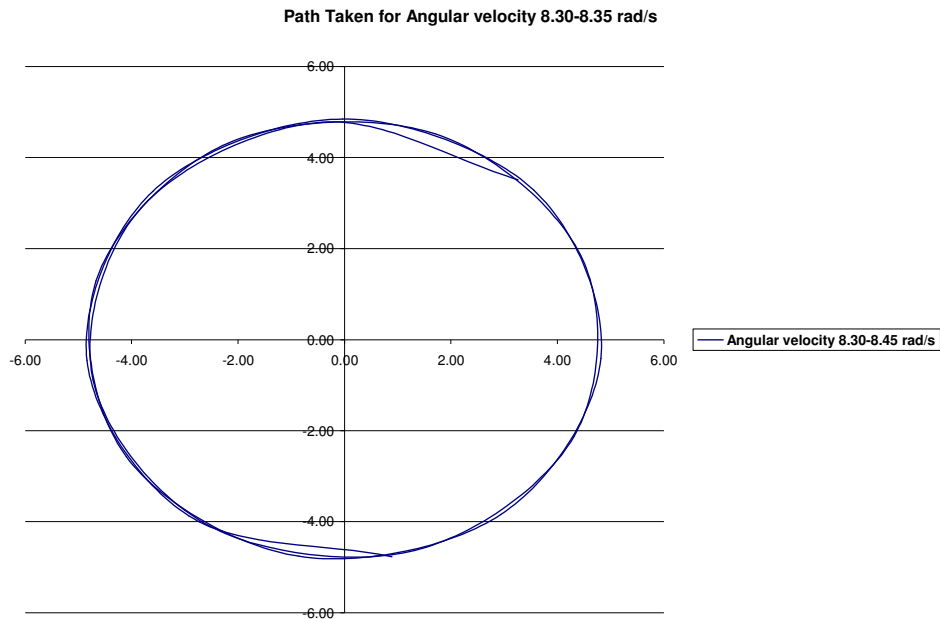


Figure 4.18: Path Traveled by End Mass: Mass Ratio - 1.1, Angular Velocity 8.3-8.45 rad/s

4.2.2.2 Effect of End body Mass on Verticality

The following Figure 4.19 shows the plot of verticality versus angular velocity for varying mass ratios. From the plot it can be seen clearly that the verticality curves for the mass ratios below 1 (in this case two mass ratios 0.5 and 0.75 without any damping medium) nearly overlap on top of each other. For mass ratios (M_m) above 1.0 the verticality increases with angular velocity and also the zone of instability shifts to the right. That means the zone of instability occurs at higher angular velocities. (The comparison has been made based on 2 sets of data for $M_m < 1$ and 2 sets of data $M_m > 1$, for certain $M_m = 1.25$, the simulation could not be run successfully).

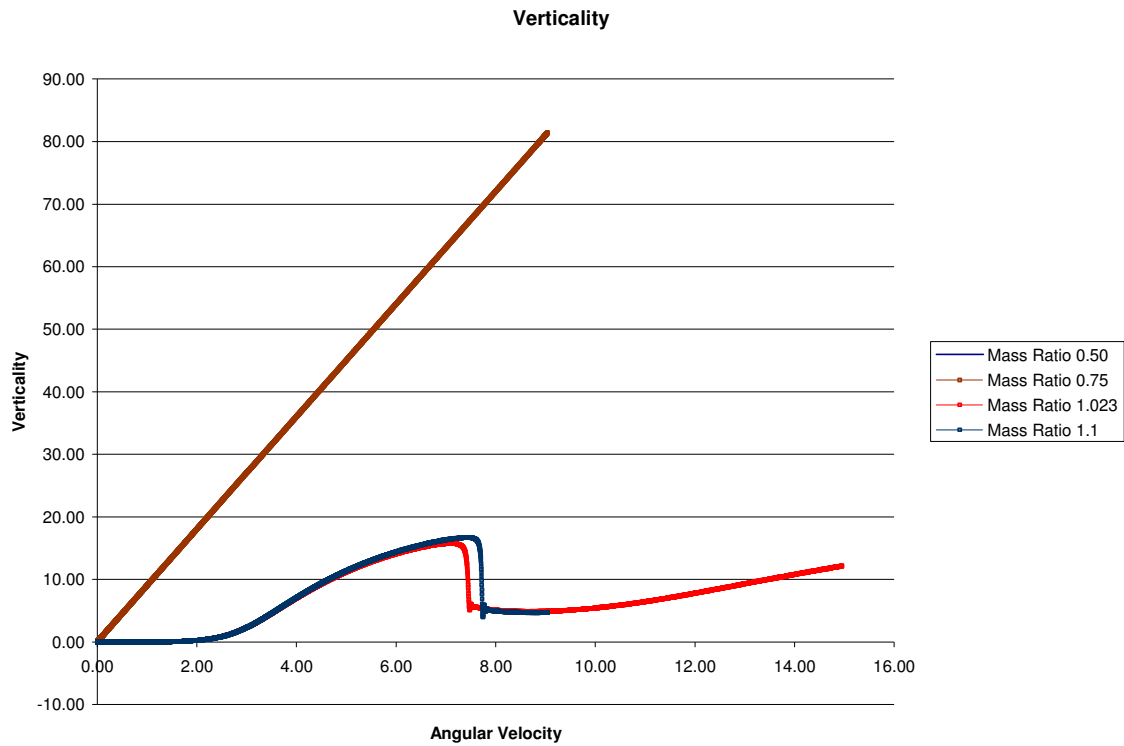


Figure 4.19: Verticality Vs Angular Velocity: Mass Ratio (Mm) from 0.50 – 1.1

4.2.3 Effect of Tow Radius

The length of the tow member has been changed to study the affect of the tow radius on the verticality, tip radius and the path taken by the end body. The plots of tip radius, verticality and the path traveled by the end body for various tow radii are shown in the following Figures 4.20-4.25.

4.2.3.1 Effect of Tow Radius on Verticality

It can be seen from the graph in Figure 4.20 that the verticality increases with increase in angular velocity. An interesting observation is that there are no instabilities in the curves of lower and higher tow radii such as less than 8 inches and greater than 11 inches.

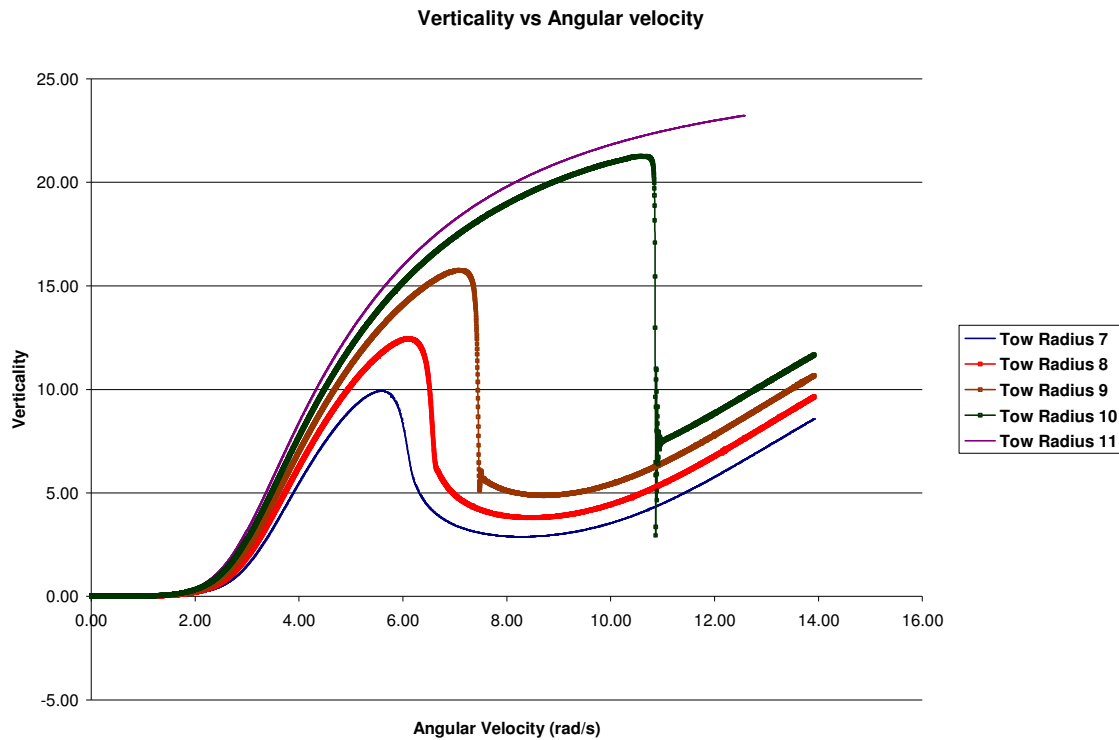


Figure 4.20: Effect of Tow Radius: Verticality Vs Angular Velocity

Also as the tow radius increases, the maximum elevation that the end body will attain before the zone of instability, if any, increases. The zone of instability shifts towards higher angular velocities as the tow radius increases and eventually it disappears at higher tow radii. The shift in the zone of instability is greater when the tow radius

increases from 9 to 10 inches. After the zone of instability, the verticality of all the plots increases with increase in angular velocity, with almost all the curves having the same rate of increase. For the tow radius of 11 inch, no instability zone exists and the verticality keeps increasing with increase in angular velocity. For this curve though the verticality increases, the rate of increase in verticality decreases with increase in angular velocity.

4.2.3.2 Effect of Tow Radius on Tip Radius

Figure 4.21 shows the plot of tip radius versus angular velocity. In general the tip radius of the end mass will increase with increase in angular velocity reaching a largest radius after which the tip radius starts to decrease. The zone of instability occurs while the tip radius is decreasing. The zones of instability are not observed for lower and higher tow radii below 8 and above 11 inches. For tow radius between 8 and 11 inches the zone of instabilities shifts towards higher angular velocities with increase in tow radius.

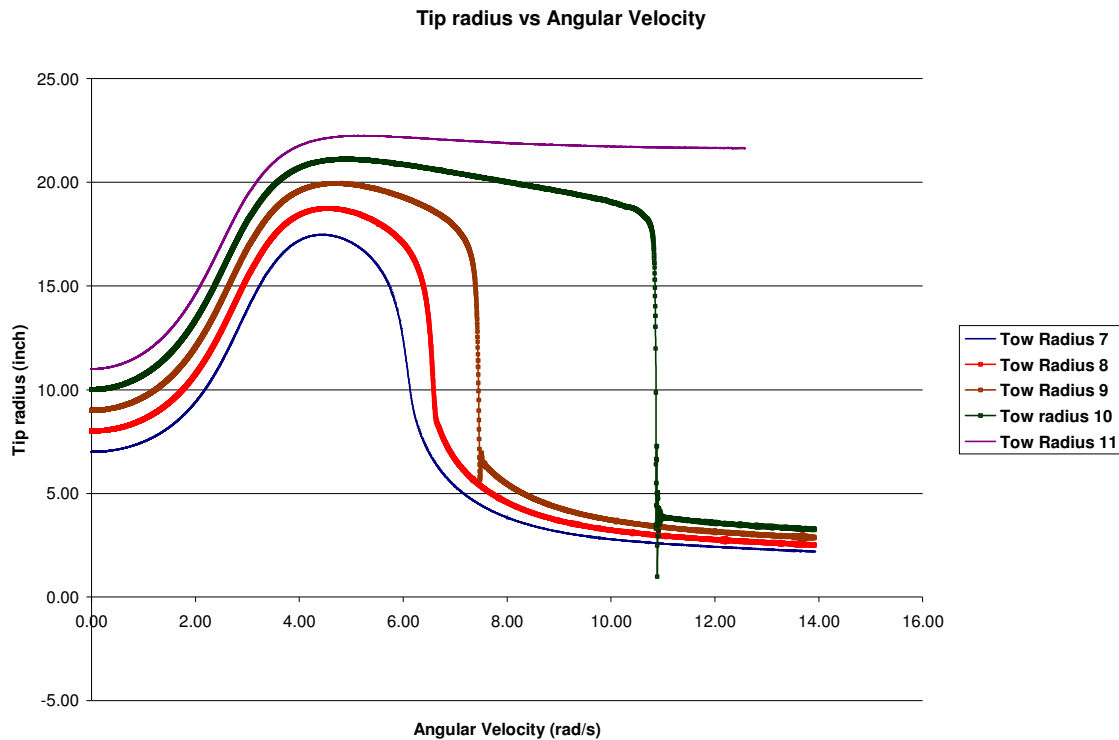
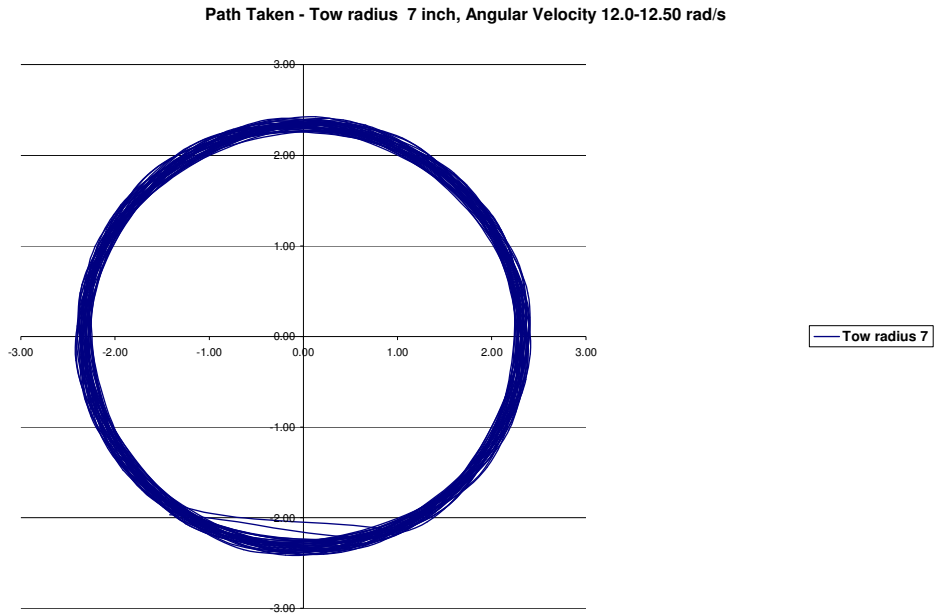
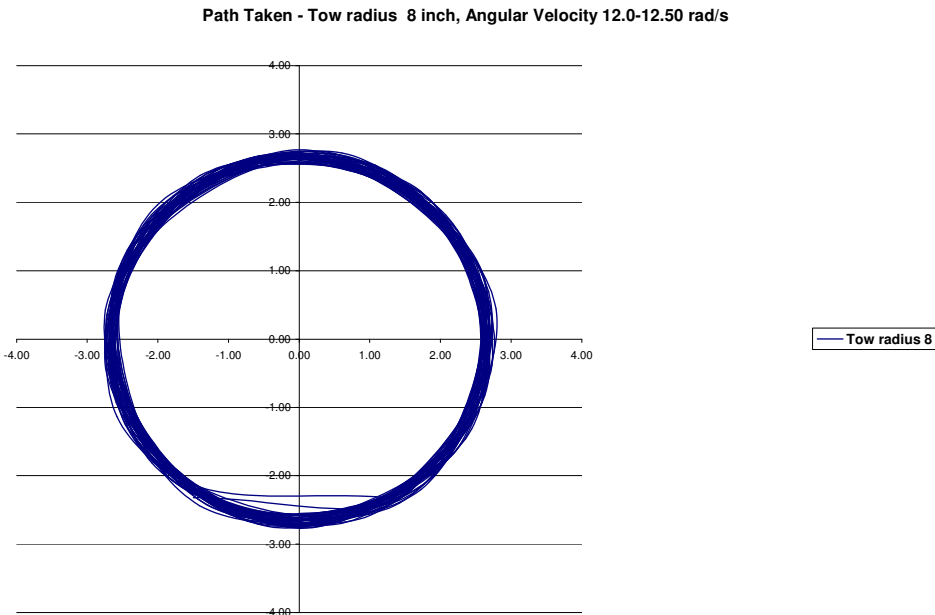


Figure 4.21: Effect of Tow Radius: Tip Radius Vs Angular Velocity

The following Figures 4.22-4.26 shows the path taken by the end body for various tow radii at angular velocities between 12.00-12.50 rad/s. In this case most of the plots seem to be circle without any major complexities. The circles in the plot seems to be thicker, the reason for this is that the range of speeds considered and a small probability that the attached end mass has not reached a stable path (One can never expect the path to be at a constant value without any variations). (Note: The scaling on each graph is different, a close look at the numbers in the plot will indicate that the path taken is/or close to a circle)



**Figure 4.22: Path Traveled by End Mass: Tow Radius- 7 inch,
Angular Velocity 12-12.50 rad/s**



**Figure 4.23: Path Traveled by End Mass: Tow Radius 8 inch,
Angular Velocity 12.0-12.5 rad/s**

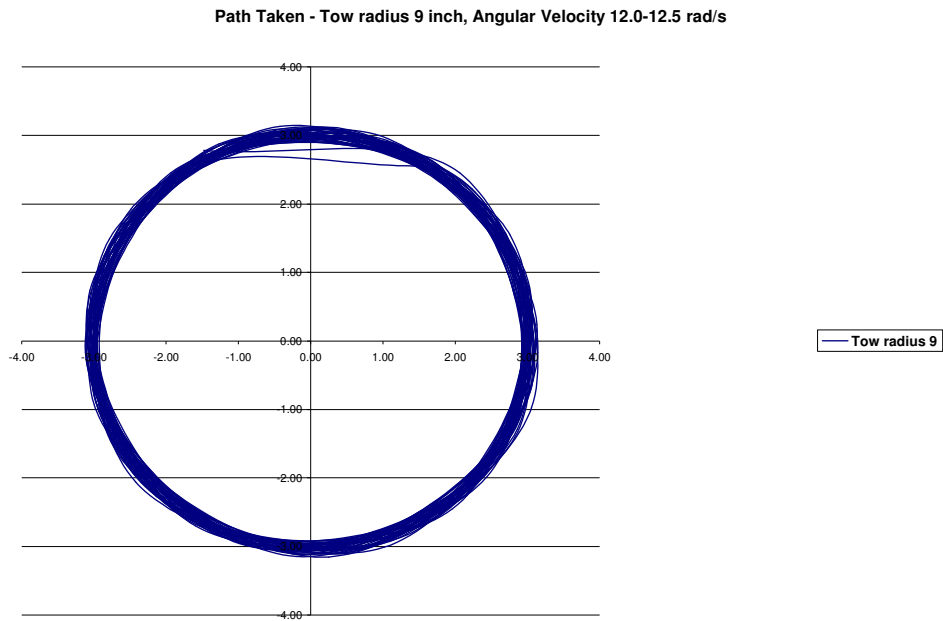


**Figure 4.24: Path Traveled by End Mass: Tow Radius-9 inch,
Angular Velocity 12.0-12.50 rad/s**

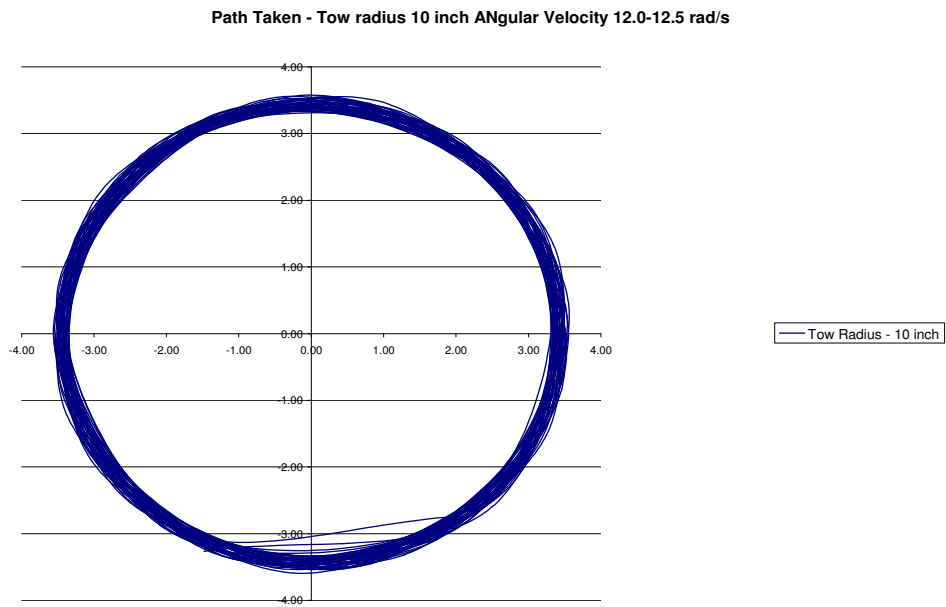


**Figure 4.25: Path Traveled by End Mass: Tow Radius- 10 inch,
Angular Velocity 12.0-12.5 rad/s**

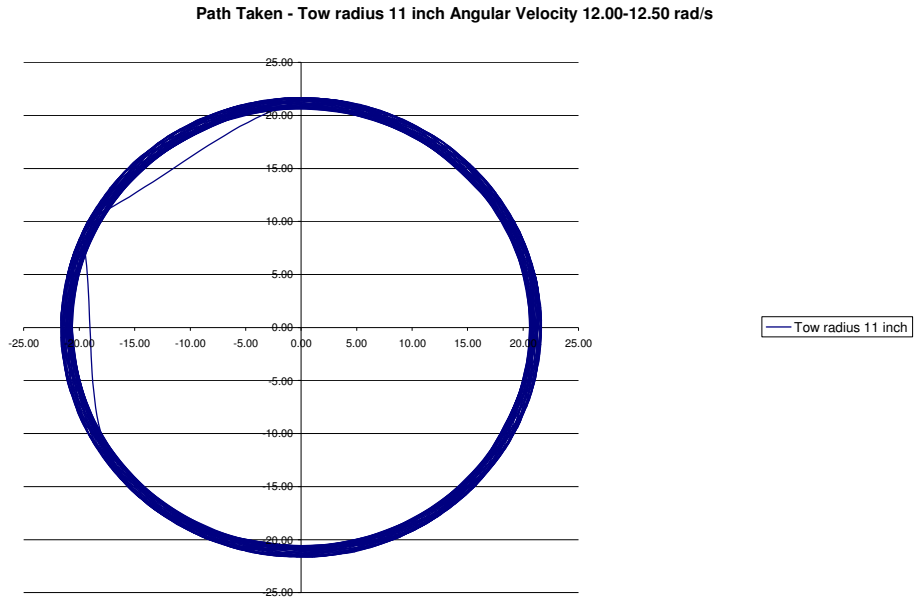


**Figure 4.26: Path Traveled by End Mass: Tow Radius- 11 inch,
Angular Velocity 12.0-12.50 rad/s**

4.2.4 Time Response Plot

The following Figure 4.27 shows a general time response plot (Tip Radius Vs Time) of the Tip radius of the end mass. The plot in the figure indicates the tip radius decreases (no sudden change) with increase in time (no jump).

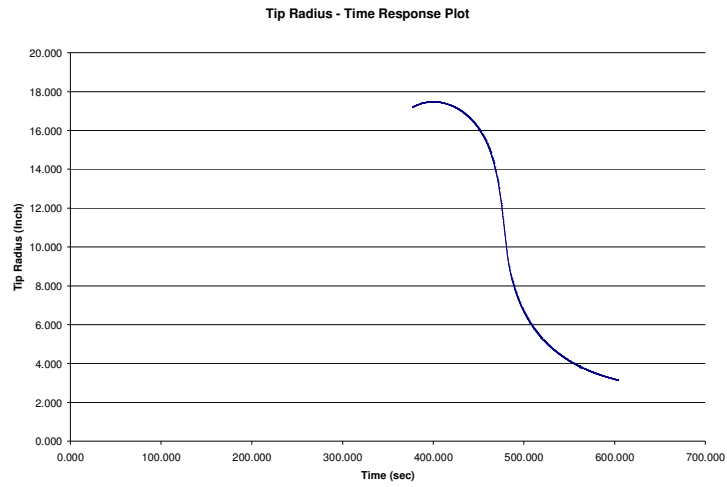


Figure 4.27: Time Response Plot: Tip Radius Vs Time (No Jump)

The following Figure 4.28 gives the time response plot of the X-position of the tip of the end mass associated with the above plot (Figure 4.27).

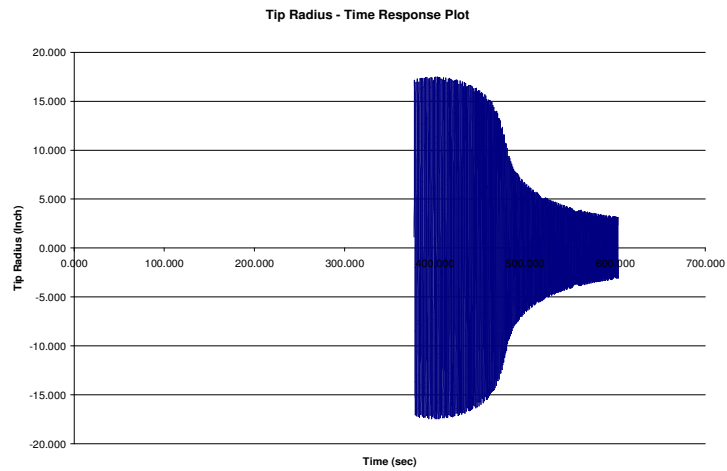


Figure 4.28: Time Response Plot: X-Position Vs Time (No Jump)

Figure 4.29 shows the time response plot (Tip Radius Vs Time) of the Tip radius of the end mass. The plot in the figure indicates the tip radius decreases quickly (sudden change) with increase in time, during the instability zone (“Jump”).

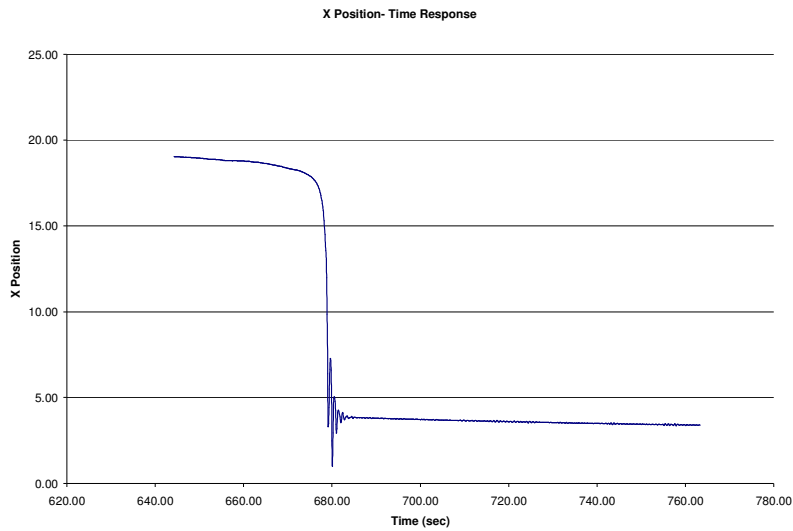


Figure 4.29: Time Response Plot: Tip Radius Vs Time (Jump)

The following Figures 4.30 gives the time response plot of the X-position of the tip of the end mass associated with the above plot (figure 4.29).

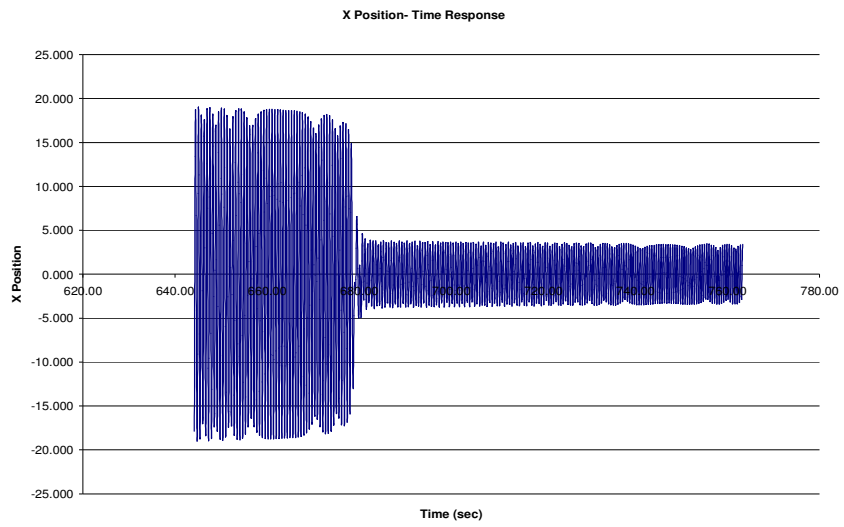


Figure 4.30: Time Response Plot: X Position Vs Time (Jump)

CHAPTER 5

Investigations into an Experimental System for Validation with Application to Realistic Tether Materials

5.1 Experimental Setup

An experimental setup has been constructed to verify the data generated by the ADAMS Model. This setup consists of the following

- 1) Table Top
- 2) DC Motor
- 3) DC Motor Speed Controller
- 4) DC Power Source
- 5) Electrical Wiring
- 6) Aluminum Beam
- 7) Tachometer
- 8) Digital Cameras

5.1.1 Table Top

A wooden table top of approximately 64 inch x 38 inch x 1 inch is used as the supporting member for the entire setup. Holes have been drilled at the center of this table top for attaching the DC motor by means of an aluminum plate and screws. This table is placed at an elevation of approximately 76 inches in order to provide ample clearance for observing the “Verticality” effect and also to accommodate larger tether lengths.

5.1.2 DC Motor



Figure 5.1: DC Motor

The following are some of the properties of the motor

12 Volts DC Permanent Magnet,

Reversible motor with Continuous Duty

Sleeve bearing

470 rpm @ 0.140 amps no load speed.

300 rpm @ 25 oz-in torque 0.650 amps

160 rpm @ 20 oz-in torque 0.850 amps

Dimensions:

Diameter 1-3/8"

Length 2-3/4"

Offset shaft:

Diameter 0.1875"

Length 13/16"

Face mount. Three tapped holes.

5.1.3 DC Motor Speed Controller

A Speed controller is an electrical circuit that has been built (Ramsey DC Motor Speed Controller Kit No.MSC1C) in order to regulate the speed of the motor. The control of the motor speed has been achieved by regulating the resistance, through the controller, in series to the motor. The controller acts as a resistance connected to the motor in series. When the resistance is set to zero or at the lowest level the motor starts running at its full rated rpm and as the resistance is increased slowly, the speed of the motor goes down. The resistance can either be increased or decreased by the turning a resistance knob on the front panel of the speed controller. The speed controller used for this experiment can be seen in the experimental setup in Figures 5.2.



Figure 5.2: DC Motor Speed Controller

5.1.4 Aluminum Beam

This Aluminum beam of approximately one foot in length, analogous to the “Link” member in ADAMS, has been used in this experiment which acts as a towing member. Aluminum has been selected because of its light weight and high strength to weight ratio. Holes have been drilled at the appropriate locations to accommodate varies tow radii. One end of this beam is attached to the shaft of the DC motor with the help of a set screw while the tether is attached to the other end of the beam through one of the holes based on the required tow radius. The image of the beam used along with the tether is shown in Figure 5.3



Figure 5.3: Bottom view of the Setup with Aluminum Beam (Tow Link) and Thread (Tether)

5.1.5 Tachometer

A tachometer is a device that is used to measure the speed of a rotating object. The speed of any object is usually measured using one of the following methods

- a) Contact
- b) Non-Contact

Contact type tachometers usually work on the principle of contact. The tip of the tachometer is brought in contact to that of a rotating member. The rotating member rotates the tachometer tip, which in turn displays the speed of the rotating member. This type of tachometer cannot be used for the current experiment as it is difficult to measure the speed of the motor while the tether is in motion.

Non-contact type tachometer usually works on the principle of reflectivity. A reflecting signal or light is used in determining the speed of angular velocity of any rotating member. A reflective material is attached to the tip of the rotating member to reflect the signal emitted/generated by the tachometer. The reflected signal is in turn read by the tachometer which finally displays the speed of the rotating member. This type of tachometer is suitable for the current project as it might not obstruct the smooth operation of the tether system. The image of a non-contact type tachometer used along with a motor and dc motor speed controller is shown in Figure 5.4

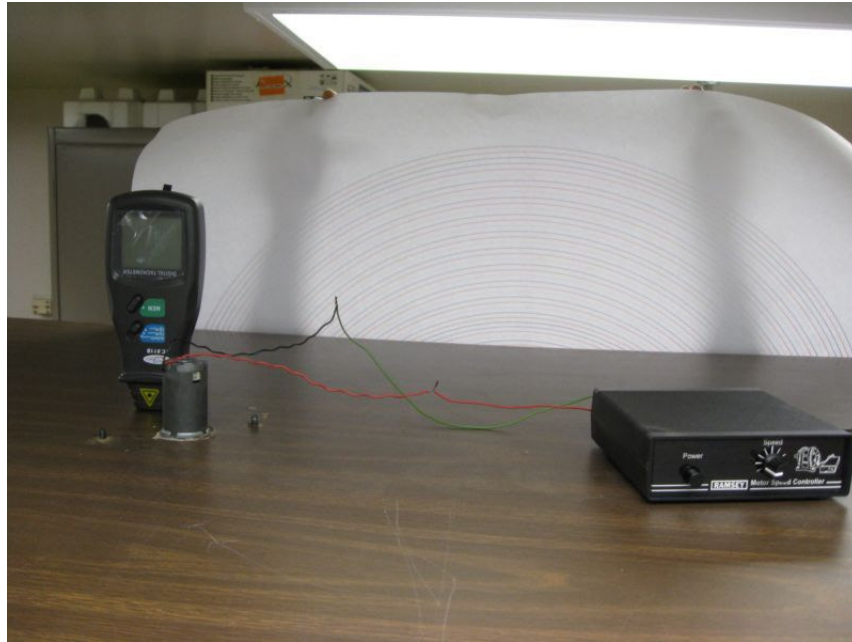


Figure 5.4: DC Motor, Speed Controller and Tachometer

The specifications of the non-contact type tachometer used are given below

Display : Large 5 digit 1.22" (31mm)

LCD Rotation speed : Laser Non-contact 2.5-99,999 RPM

Resolution Laser

- 0.1 RPM (2.5 to 999.9 RPM)
- 1 RPM (over 1,000 RPM)

Accuracy : $\pm 0.05\%$ + 1 digit

Memory function : Last, Max, Min values

Update time : 0.8 seconds (over 60 rpm)

Detection Distance : 2-20" (50 -500mm)

Operating Temperature: 32-122°F (0-50°C)

5.1.6 Digital Cameras

Two digital cameras were used to determine the approximate position (tip radius) and also the verticality of the lower end of the tether. The two cameras have been operated simultaneously so that the tip radius and verticality can be determined at the appropriate speed. A measuring chart has been used as reference for measurement purposes. The measuring chart and the cameras are on either side as illustrated

5.1.7 Tether

A synthetic thread (Spider wire manufactured by Berkeley analogous to a tether) has been used for experimental purposes. One end of the thread with the required length is attached to the aluminum beam. In this experiment a drogue has not been attached at the bottom end of the tether. The diameter of the thread being considered is very important. It is required to have a smaller diameter so that the aerodynamic drag is minimal. The diameter of the thread being considered is so small which cannot be determined using calipers. This can be determined by two methods

- a) Weight Method
- b) Using Microscope

5.1.7.1 Weight method

If the density of the material of the thread is known then computing the diameter becomes simple. The weight of a known length of thread is measured using

a micro-scale. Once the weight has been determined, it is simple to calculate the weight per unit length of the material and later the diameter can be calculated by the following formula

$$\text{Weight} = \text{mass} * (\text{Pi}) * (\text{radius})^2 * \text{Length}$$

From which radius can be determined.

5.1.7.2 Microscopic Method

A microscope of the required magnification can be used to determine the diameter of the thread. The measurement scale on a microscope is placed perpendicular to the axis of the thread. The scale of the microscope is placed such that it is at one end of the thread (tether). This position is located and set as a reference point. The table on which the thread specimen is placed is moved in the y-direction perpendicular to the axis of the thread. The amount by which the table is moved gives a display of the diameter of the thread. This procedure is repeated several times in order to get the average diameter.

The first step in of the experimental procedure is to determine certain properties of the material being used for the tether such as the diameter and any other properties that are required for the ADAMS model verification. The material being used as the tether has been pre-twisted and consists of three to four individual strands. Because of the twist and the combination of the two strands, there is always a possibility that the diameter is not as predicted based on weight and so is the case with the density. Hence the diameter of the

tether has been determined using a microscope. The snapshot of two threads, used in the experiments, from the microscope is shown in Figures 5.5-5.6

The properties of the material (Spider Wire) used (given and calculated) are listed below

Weight of the material (for 3 yards in length)	= 0.1341 gm
Diameter of the thread/tether	= 9.429134E-003 inch
Density of the material (based on calculated diameter)	= 0.392017E-02 Lb/inch ³
Length of the tether	= 58 inch

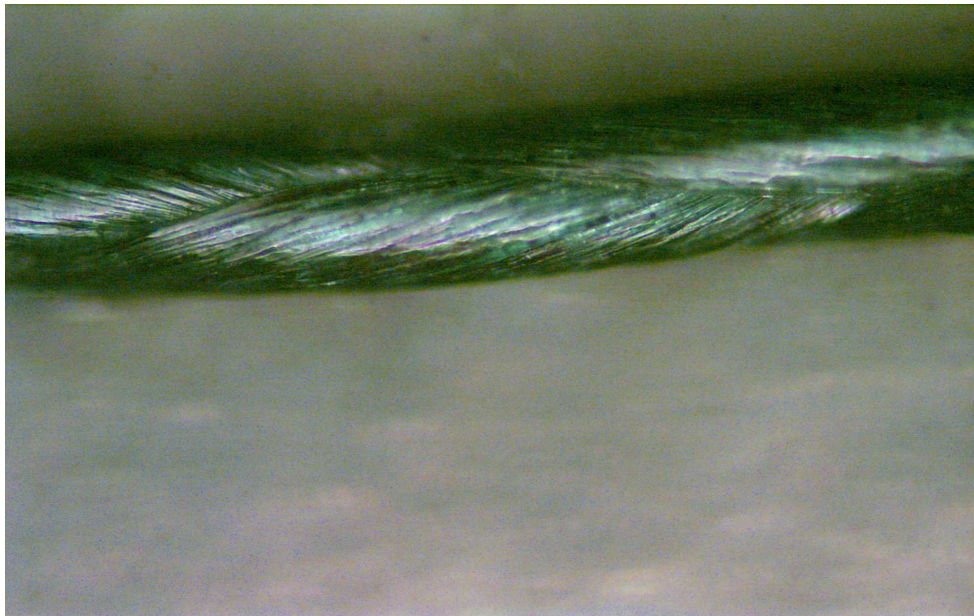


Figure 5.5: Snapshot-1 of a Multi-Strand Braided Material (Spider Wire-fishing line) using a Microscope

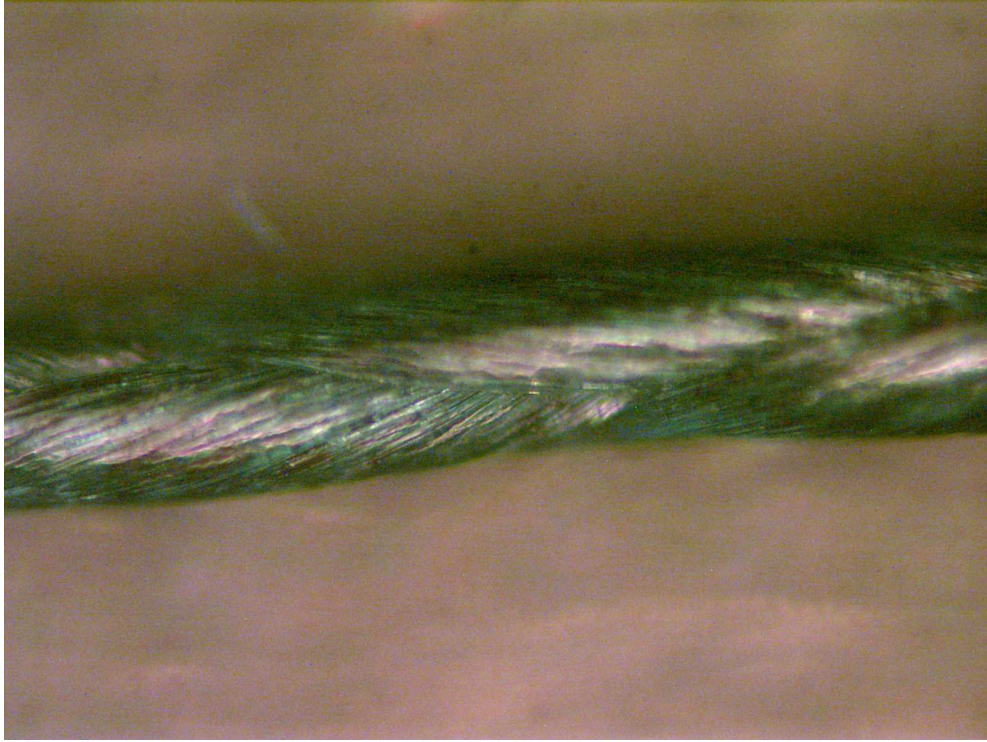


Figure 5.6: Snapshot-1 of a Multi-Strand Braided Material (Spider Wire-fishing line) using a Microscope

Figures 5.7-5.8 shows the front and bottom view of the experimental setup of the system. A measuring chart, can be seen in figure 5.6, is used to measure the verticality of the tip of the tether.



Figure 5.7: Experimental Setup- Front View

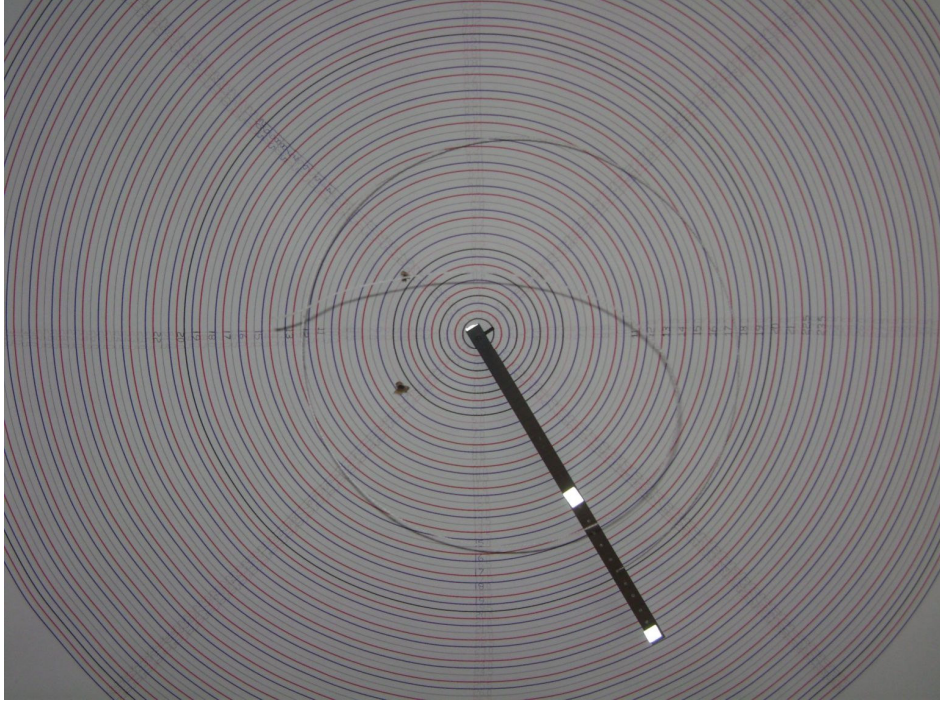


Figure 5.8: Experimental Setup Bottom View

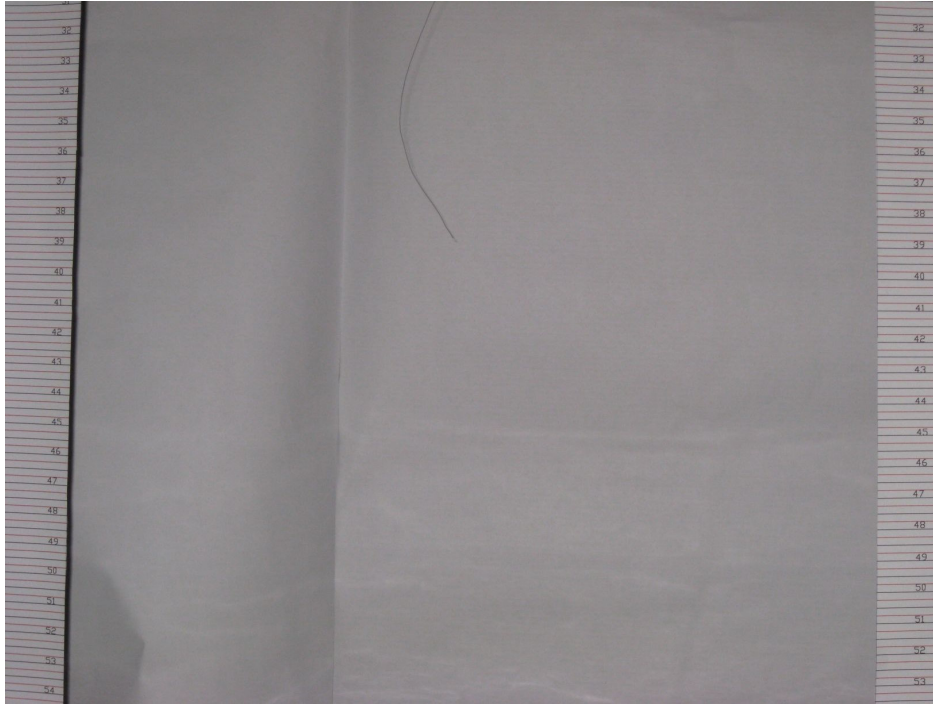


Figure 5.9: Snap Shot to Measure Elevation of the End of the Tether

5.2 Operation Procedure and Measurements

Once the system has been setup, the DC Source is switched on with the DC Speed Controller. A knob on the controller is turned in clockwise direction to decrease the resistance offered by the controller. As the resistance decreases the current passing to the motor increases and the motor starts rotating similar to the link element in ADAMS. It should be noted that in order to achieve a desired speed a certain amount of time is required as the motor needs to overcome initial static friction and inertia to achieve desired speed. Hence certain amount of time has been allocated to achieve a steady state speed. The speed of the motor has been measured using the digital tachometer. For a given controller setting, speed fluctuates by ± 5 rpm.

A constant speed on the motor could never be attained and this is due to the type of motor and speed controller being used (A high precision motor and speed controller should part of the equipment is accurate data is required). After the speed has been measured and found to be almost a constant, the measurements are taken. For measuring the verticality, as mentioned earlier a measuring chart has been used. Two measuring charts were left hanging along the center of the table as shown in the Figure 5.7 and the camera is placed on the opposite end so that the tether is between the measuring chart and the camera. After the desired speed has been attained, the camera is placed in the plane containing the tip of the tether end and as close to the tether and several images are taken to get the trace of the tip so that the average verticality of the tip and also the front view pattern of the tip end can be determined using a computer. The images captured, as shown in Figures [5.8, 5.9], have the tip of the tether, and the reference measuring chart from which approximate (not accurate) readings can be taken. This procedure is repeated for each and every speed. The measured values are later plotted to determine a pattern for the verticality of the tether tip which is later compared with the ADAMS MODEL verticality pattern. The tip radius of the end of the tether/thread cannot be determined based on the current experimental setup because of the limitations (distance between the tip end, the reference scale is larger – the projection of the tip end onto the reference scale will not be accurate) in the experimental procedure for measuring tip radius listed below. A snap shot (bottom view) of the system is shown in Figure 5.10. This snapshot gives an idea about the shape of the tether for given angular velocity of the towing link (aluminum beam).

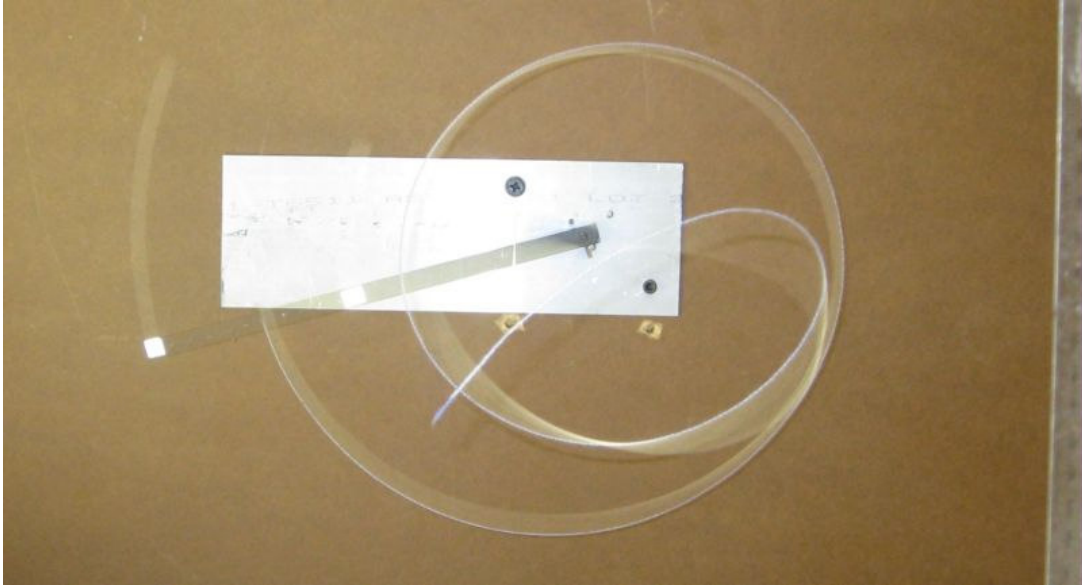


Figure 5.10: Bottom View of the System; Shape of the Tether

5.3 Limitations in Experimental Validation Procedure

There are certain limitations in the experimental model. The following are some of the limitations

- The measurements have to be made in the plane containing the tip of the tether and the camera.
- The tether tip and the reference scale should be as close as possible. If the distance is large, the readings taken will not be accurate. The Tip radius data could not be obtained.
- The measurement procedure followed gives only a rough estimate and need not produce accurate values because of the afore-mentioned limitations.
- The diameter of the tether measured using the microscope need not be an accurate value because of the wavy nature of the tether as a result of the twist. In order to get an accurate measure, several readings have been taken at both the crests and the trough and an average value has been used.
- Stiffness of the material being used could not be determined
- The co-efficient of drag for the material being considered is not known as the material is hairy in nature, strands are twisted and the diameter is not constant. In the subsequent sections, in attempting to correlate between the Adams model and the experimental data, various coefficients of drag were selected to determine an approximate range of the drag coefficient based on experimental results

Hence exact modeling of the physical system in ADAMS cannot be achieved.

5.4 ADAMS Modeling Based on Experimental Setup

It should be noted that the ADAMS simulation runs so far are based on values taken from published data [8]. In order to verify the appropriateness of the drag force equations and the feasibility of the ADAMS model, minor modifications to the existing ADAMS model are required. These modifications are minor in terms of the dimensions of the thread being used, properties in terms of density of the material/thread and also the removal of the drogue from the existing ADAMS model. The Figure 5.11 depicts the ADAMS model of the 58 inch tether, used in the physical system. The modeling of this system consisting of 29 links is similar to that of the previous models.

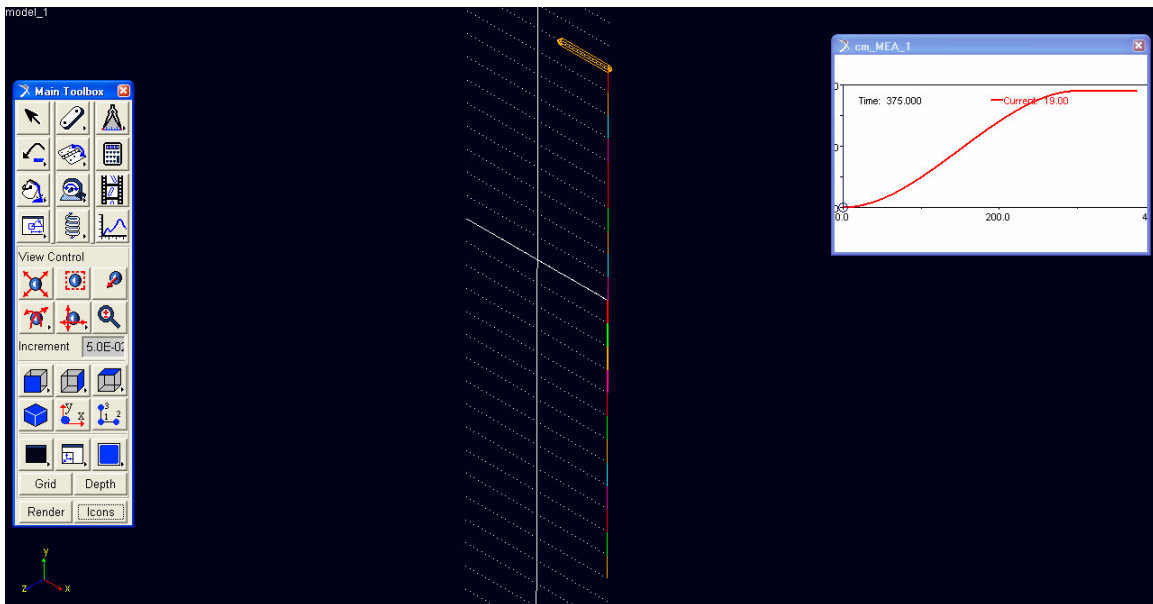


Figure 5.11: ADAMS Model based on the Experimental Setup

The following data has been used to model the physical system in ADAMS.

The properties of the material (Spider Wire) used (given and calculated) are listed below

Weight of the material (for 3 yards in length)	= 0.1341 gm
Diameter of the thread/tether	= 9.429134E-003 inch
Density of the material (based on calculated diameter)	= 0.392017E-02 Lb/inch ³
Length of the tether	= 58 inch

The major difference between the ADAMS model for experimental validation and the ADAMS model for other simulations can be seen in the motion statement. For experimental validation, simulations are run for specific angular speeds using a step function. A step function has been used to ensure that angular velocity of the link increases smoothly. The link is also made to rotate at the given angular velocity for a specific duration, say at least 25 seconds, after the desired angular velocity has been achieved. The stiffness of the material has been calculated and will be applied at the joints if required for fine tuning the ADAMS model. The verticality and the tip radius of the tether end have been plotted for each of the desired angular velocities. The graphs depicting the tip radius and verticality along with the path the tip of the tether follows for a varying angular velocity is shown in the following Figures 5.12-5.14. (Note that scale on these graphs is not uniform in the X and Y direction, hence it is advised to look at the numbers.)

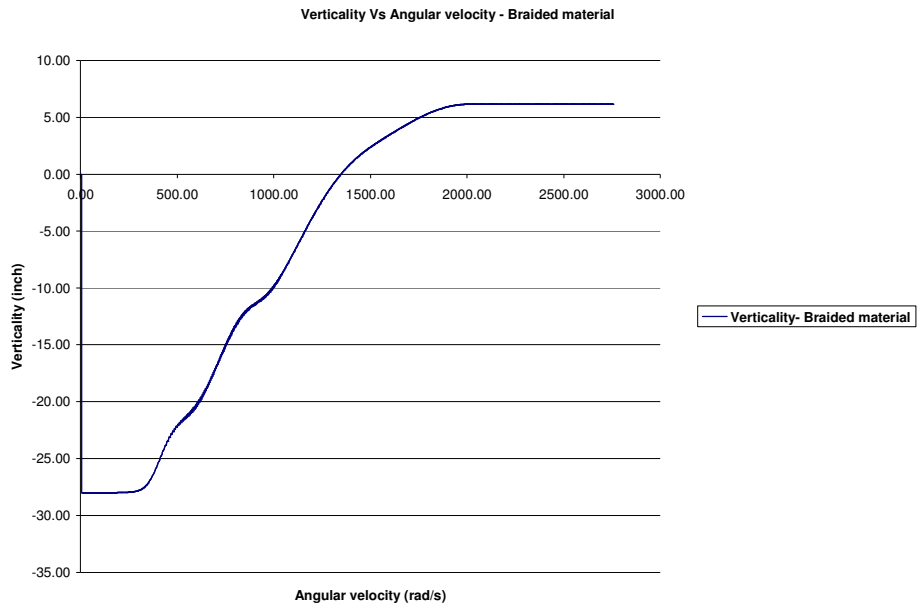


Figure 5.12: Verticality Vs Angular Velocity - ADAMS Model for Experiment

Validation- Varying Speed

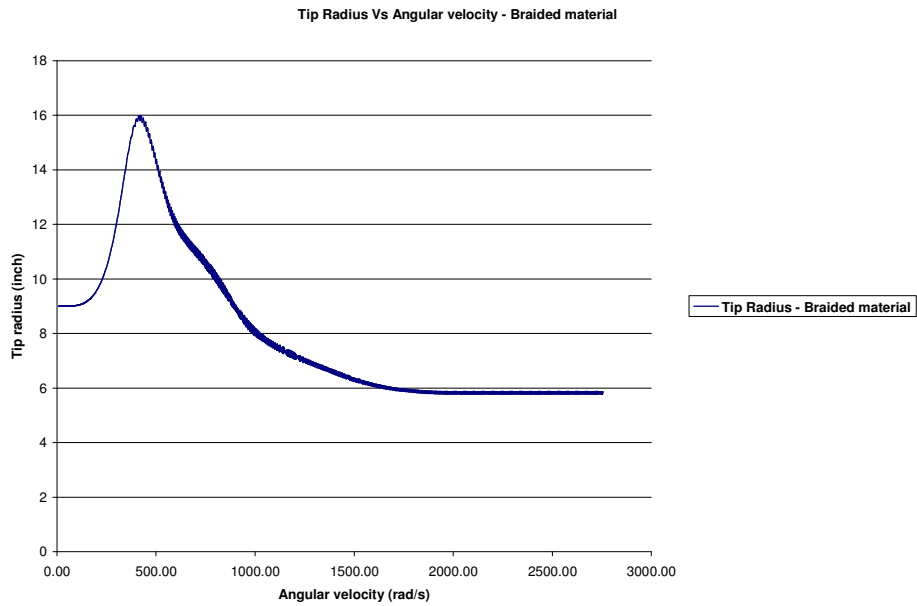


Figure 5.13: Tip Radius Vs Angular Velocity - ADAMS Model- Experimental

Validation-Varying Speed

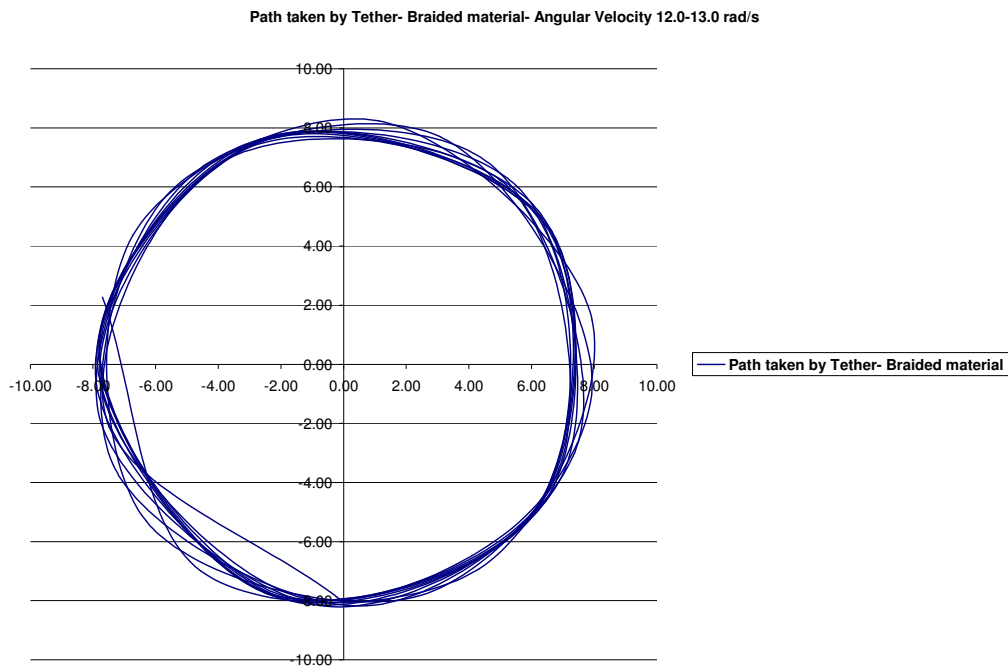


Figure 5.14: Path Taken by Tether- ADAMS Model- Experimental Validation- Varying Speed

5.5 Comparison of ADAMS Simulation with Experimental Data

5.5.1 Correlation Based on Verticality Data Plots

As measurement of verticality cannot be done accurately, the experimental and simulation results have been correlated based on the data obtained as well as the shape of the curve. The graph showing the comparison of the experimental and the simulation data is shown in Figure 5.15.

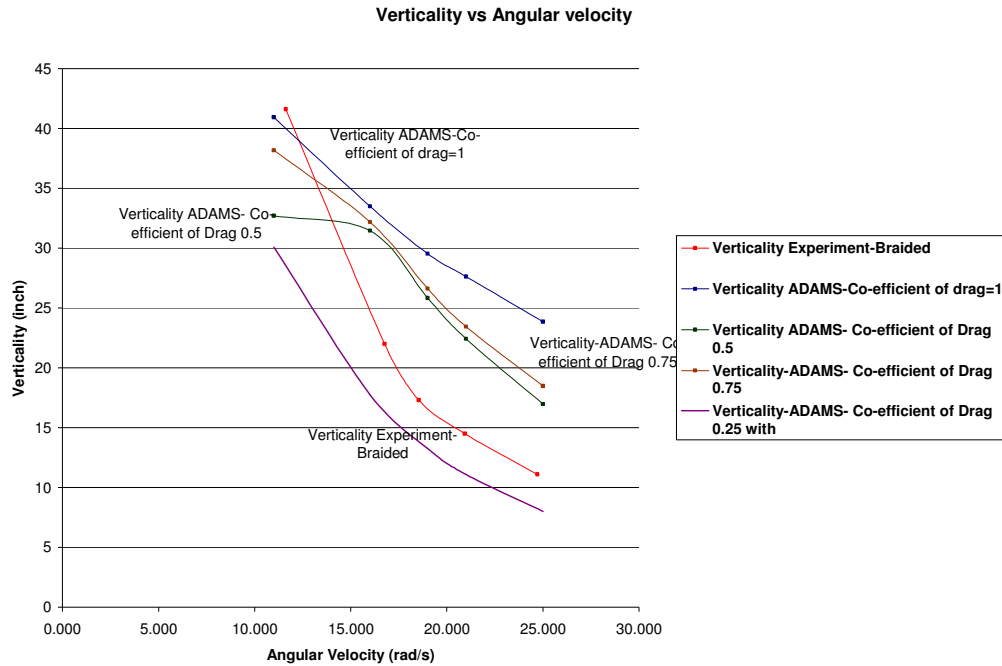


Figure 5.15: Comparison of Experimental and Simulation Data: Verticality Vs Angular Velocity

The above figure shows the verticality data from the experiment, using a tether like material (braided fishing lining), along with the ADAMS simulation data for various co-efficient of drags. As the co-efficient of drag in the experiment is unknown, it becomes difficult to correlate between the ADAMS data and the experimental data. Several simulations were run, with different coefficients of drag values and the various plots were compared to obtain an estimate of the coefficients of drag for the material under consideration. The there is a small amount of bending stiffness present in he material and from that it was conjectured that a small amount of bushing stiffness is required and was added to the simulation. The plot (Figure 5.14) indicates that the tether material has a co-efficient of drag in the range of 0.25 (with stiffness) to 0.50. It can be

seen from the graph that error between the curves “Experiment-Unknown Co-efficient” and the “Co-efficient of Drag = 0.5” is relatively large when compared to the curves “Experiment-Unknown Co-efficient” and the “Co-efficient of Drag = 0.25 with stiffness”. Simulations for the coefficients of drag in the range of 0.25 to 0.50 have not been performed because of instabilities in the verticality curve at higher angular velocities. It can be inferred that the coefficient of drag in the range of 0.25 to 0.50 and close to 0.25 (approximately) gives a realistic match between the experimental results and the ADAMS simulation data, as the error between the two curves is small and both the curves seem to have the same slope. There seems to be an offset between the curves and this is because of the unknown co-efficient of drag. Also as mentioned above the measuring procedure that was employed to get the data is not highly accurate and only provides a rough estimate. It should also be noted that no damping has been considered most of the time while running the ADAMS simulations whereas there is a possibility of certain amount of damping to be present in the experiment. As a result of several factors including damping, an exact match between the experimental data and the ADAMS data was not obtained.

From Figure 5.15 can be inferred that the elevation of the tip of the tether increases (the elevation has been considered from the top end of the tether attached to the towing link) with increase in angular velocity for both the experimental data and the ADAMS data. When the towing member is at a stationary position, the elevation of the tip end of the tether is equivalent to the length of the tether and as the angular velocity of

the towing member increases, the tip of the tether rises from its current position increasing the elevation (verticality) of the tether end.

5.5.1.1 Effect of Co-Efficient of Drag on Verticality (ADAMS Results)

The graph in Figure 5.15 also shows the effect of changing co-efficient of drag on the verticality of the lower tip end of the tether. From the plot it can be inferred that as the co-efficient of drag increases the verticality of the lower tip end of the tether material, based on ADAMS simulations, decreases for a given angular velocity.

5.5.2 Correlation Based on Snap Shots and Superposition Pattern for Verticality

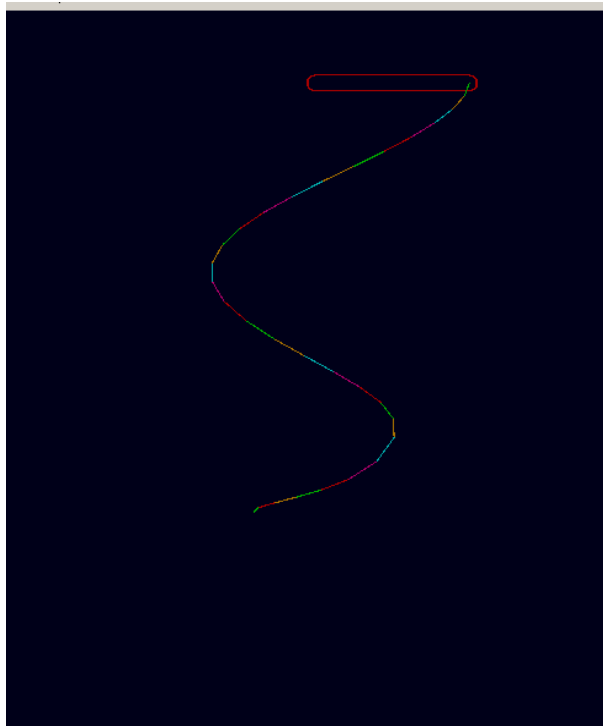


Figure 5.16 Snap Shot of ADAMS Model- Experimentation Model

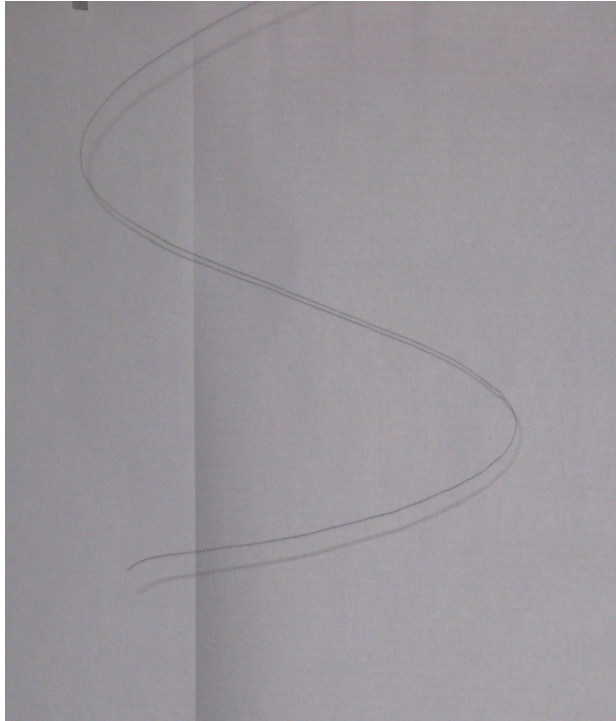


Figure 5.17: Snap Shot of Experimental Model

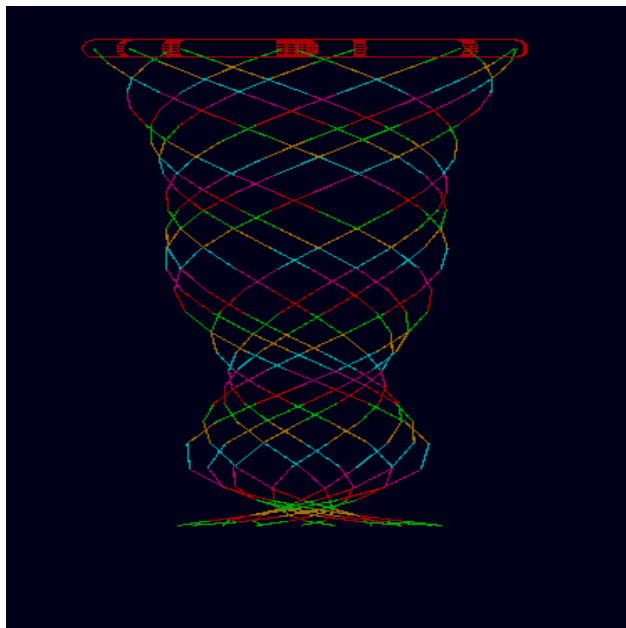


Figure 5.18: Super Position Screen Shot: ADAMS Model based on Experimentation

From Figures 5.16-5.17, it can be seen that the pattern taken by the tether in the experiment and in the simulation is almost the same for a given angular velocity of approximately 24 rad/s. Hence the experimental pattern of the tether has been validated with the ADAMS model pattern. Figure 5.18 shows the super-position plot of the ADAMS model at a speed of 24rad/s

5.5.3 Correlation Based on Snap Shots and Superposition Pattern for Tip Radius

In order to correlate the pattern (as correlating the numerical data was not feasible) the lower end of the tether takes, the pattern of the curve in ADAMS and the shape of the tether in the experiment have been correlated.

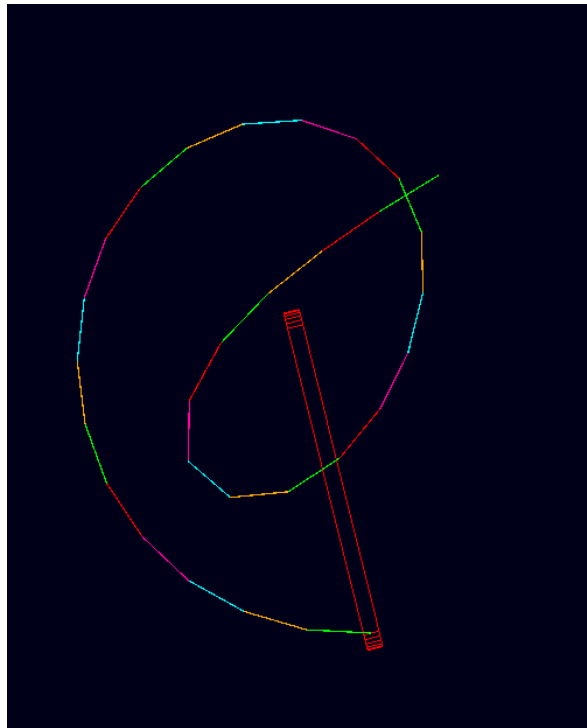


Figure 5.19: Screen Shot of Pattern of the Tether

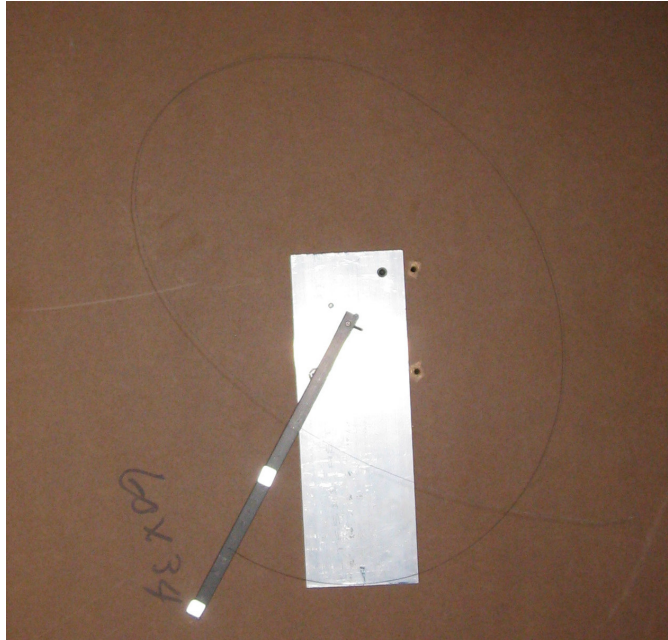


Figure 5.20: Snap Shot of the Experiment: Bottom View

Figure 5.19 shows the ADAMS model screen shot of the bottom view of the tether at approx 24 rad/s angular speed. Figure 5.20 shows the Bottom view of the tether at approximately the same speed rotating in the opposite direction with respect to the simulation screen shot.

It can be inferred from the figures that the path traveled by the tether in the ADAMS model and also in the experiment is the almost the same. A slight bent in the ADAMS model can be seen at the end section of the tip. This might be attributed to the unmodeled bending stiffness of the material. The tether in the physical system has some bending stiffness which has not been represented in the ADAMS model.

CHAPTER 6

CONCLUSIONS

The model has been developed and simulated to obtain a general pattern for tip radius and verticality for varying angular velocities. The preliminary accuracy of the model has been established by correlating the results of the simulation using published data [8]. The model is in excellent agreement (tip radius and verticality) with the published data. Further, the effect of various parameters such as tow radius, mass of the drogue and the damping/stiffness in the bushings on the verticality, tip radius and the path traveled by the end mass has been studied using simulation models and presented. The phenomenon of jump mentioned in existing published work [8], [10] was observed. The effect of all the considered parameters on the tip radius and verticality, in general, has an overall effect that can be seen. As the value of parameters such as bushing damping and stiffness, mass ratio and tow radius are increased, larger amounts of tip radius and verticality can be seen for a certain angular speeds. In general as the tow radius, mass ratio and damping/stiffness values are increased, the tip radius and verticality of the lower end of the tether material increases with increase in angular velocity (prior to the jump) and also the zone of instability shifts towards higher angular velocities. An exception to that general trend mentioned above can be seen in case of Damping/stiffness in the bushings. The zone of instability shifts towards higher angular

velocities and eventually disappears, as the parameter values are increased. Furthermore an experimental model has been constructed to correlate between the ADAMS model and the experiment. As a result of certain limitations in constructing the experimental setup based on existing simulation parameters, a physical system (experimental setup) was constructed and later the ADAMS model replicating the physical system, that was developed, was modeled and the data of the two was compared. The results (pattern of the data) seem to have an agreement and the off-shift in the curves has been attributed to the inaccuracies in the experimental procedure, unknown co-efficient of drag, properties of the material and also on the type of equipment. An approximate value (range) for the coefficient of drag for the material under consideration has been obtained based on trial and error. The superposition screen shots from ADAMS shows the space enveloped by the tether for the range of speed in consideration and also the formation of a node along the length of the tether at higher angular velocities. .

6.1 Future Work

Apart from validating the experimental model with the ADAMS simulation, this work has identified the key factors that would be required for accurate modeling of the system in ADAMS. This work has identified the need for high precision equipment such as DC motors, speed controllers and measuring equipment for effective experimental validation. The future work can include experimentation for determining the effect of various material types including number of filaments and the nature of twist between various filaments (strands), determination of co-efficient of drag for various material

(using wind tunnel tests) on the system response. The existing model (without the towing member) can also be used to develop control system models used for controlling the position of the balloon or aerostat. The software can be used to model and simulate various cases that would be considered in future, without the need to built physical prototypes.

REFERENCES

1. Chilowsky C, "Method and Device for Establishing and Communication Between Aircraft in Full Flight and the Ground", US Patent 1,829,474, Oct 27, 1931
2. Smith B.B., "Method and Apparatus for Cargo Loading and Discharging in Flight", US Patent 2,151,395, Mar 21, 1939
3. Anderson V. R., " Method and Apparatus for Pickup and Delivery by Aircraft in Flight", US Patent 2,295,537, Sept 15, 1942
4. Hitt, R.T., *Jungle Pilot*, Discovery House Publishers, 1997
5. Genin, Joseph., Citron, Stephan J., " Coupling of Longitudinal and Transverse motions of a Flexible Cable in a Uniform Flow Field", *The Journal of the Acoustical Society of America*, pages 438-440, Volume 52, Issue 1,1972
6. Winget, J.M., Huston, R.L., "Cable Dynamics-A Finite Segment Approach", *Computers and Structures*, pages 475-480, Volume 6, 1976.
7. Russell, J.J., Anderson, W.J., "Equilibrium And Stability of a Whirling Rod-mass System", *International journal of non-linear mechanics*, pages 91-101, Volume 12, 1977

8. Russell, J.J., Anderson, W.J., “Equilibrium and Stability of a circularly Towed Cable Subject to Aerodynamic Drag”, *Journal of Aircraft*, pages 680-686, Volume 14, Issue 7, 1977.
9. Leonard J.W., Nath, J. H., “Comparison of finite element and lumped parameter methods for oceanic cables”, *Engineering structures*, pages 153-167, volume 3, Issue 3, 1981
10. Zhu, F., Rahn, C.D., “Stability Analysis of a Circularly Towed Cable-Body System”, *Journal of Sound and Vibration*, pages 435-452, Volume 217, Issue 3, 1988
11. Jones S.P., Krausman, J.A., “Nonlinear Dynamic Simulation of a Tethered Aerostat”, *Journal of Aircraft*, pages 679-686, Volume 19, Issue 8, 1982
12. Nakagawa, N., Obata, A., “Longitudinal Stability Analysis of Aerial Towed Systems”, *Journal of Aircraft*, pages 978-985, Volume 29, Issue 6, 1992
13. Hoerner, S.F., “Fluid Dynamic Drag”, 1965
14. Etkin, B., “ Stability of a Towed Body”, *Journal of Aircraft*, pages 197-205, Volume 35, Issue 2, 1998
15. Pai, P.F., Nayfeh, A. H., “Fully Nonlinear Model of Cables”, *AIAA Journal*, pages 2993-2996, Volume 30, Issue 12, 1992
16. Kamman, J. W., Huston, R. L., “ Modeling of Variable Length Towed and Tethered Cable Systems”, *Journal of Guidance, Control and Dynamics*, pages 602-608, Volume 22, Issue 4, 1999

17. Lambert, C., Nahon, M., “Stability Analysis of a Tethered Aerostat”, *Journal of Aircraft*, pages 705-715, Volume 40, Issue 4, 2003
18. Williams, P., Trivailo, P., “A Study on the Transitional Dynamics of a Towed-Circular Aerial Cable System”, *AIAA Atmospheric Flight Mechanics Conference San Francisco, California*, 15-18 August 2005
19. Williams, P., Trivailo, P., “Stability and Equilibrium of a Circularly-Towed Aerial Cable System with an Attached Wind-Sock”, *AIAA Atmospheric Flight Mechanics Conference San Francisco, California*, 15-18 August 2005
20. Williams, P., Trivailo, P., “Dynamics and Equilibrium of a Twin –Aircraft-Cable System for Payload Retrieval”, *AIAA Atmospheric Flight Mechanics Conference Keystone, Colorado*, 21-24 August 2006
21. Alabrune, F., “Art of Aerial Transportation”, *US Patent*, 2,298,912, Oct 1942
22. Alabrune, F., “Transportation Method”, *US Patent*, 2,373,086, April 1945
23. Wilson, F.M., “Aerial Transport of Payloads with vertical Pickup and Delivery”, *US Patent* 4,416,436 Nov 1983
24. ADAMS Software, www.mscsoftware.com
25. Cotton, R. B., “Aerial Pick-Up and Delivery System”, *US Patent* 3,351,325 Nov 1967

APPENDIX –A

Tables – ADAMS Simulation data and Published data [8]

Table A.1: ADAMS Simulation Data and Published data (experiment) [8]

Dimensional- Reference[8]		ADAMS RESULTS	
Rotational frequency(rad/sec)	Tip Radius(inch)	Rotational Frequency	Tip Radius
0	8.999625	0	9
0.967932438	10.0425	0.967932438	9.595774
1.935864875	13.1325	1.935864875	11.82879
2.903797313	16.7375	2.903797313	16.3878
3.871729751	19.3125	3.871729751	19.45769
4.646075701	21.115	4.646075701	19.95883
5.807594626	21.63	5.807594626	19.44684
7.162700039	10.3	7.162700039	7.833152
7.356286526	7.725	7.356286526	7.001798
8.711391939	5.15	8.711391939	4.531192
10.06649735	3.8625	10.06649735	3.679532
11.22801628	3.3475	11.22801628	
12.77670818	2.8325	12.77670818	3.018009

Table A.2: Published data (experiment) [8] - verticality

Experimental data [8]

Rotational Frequency	Verticality(non- dimensional)	Second		
		Solution(if any)	Verticality (Dimensional)	
0	1		25.75	
0.5	0.98		25.235	
1	0.73		18.7975	
1.5	0.42		10.815	
2	0.8	0.3	20.6	7.725
2.5	0.82		21.115	
3	0.8		20.6	
3.5	0.72		18.54	
3.75	0.65		16.7375	

Table A.3: ADAMS Simulation Data –Verticality

ADAMS RESULTS			
Rotational Frequency (Dimensional) (rad/s)	Verticality (non- dimensional) (inches)	Verticality (Dimensional) (inches)	
0.00	1.00	25.75	
1.94	0.99	25.5384	
3.87	0.75	19.343	
5.81	0.47	12.1	
7.74	0.79	20.388	
9.68	0.80	20.563	
11.62			
13.55	0.61	15.68	
13.75	0.59	15.28	
13.9	0.59	15.19	

APPENDIX-B

ADAMS/SOLVER DATA SET

```
ADAMS/View model name: model_1
!
!----- SYSTEM UNITS -----
!
!
UNITS/FORCE = POUND_FORCE, MASS = POUND_MASS, LENGTH = INCH, TIME =
SECOND
!
!----- PARTS -----
!
!----- Ground -----
!
!
!                                adams_view_name='ground'
PART/1, GROUND
!
!                                adams_view_name='MARKER_3'
MARKER/3, PART = 1, QP = 9, 25.75, 0
!
!                                adams_view_name='MARKER_4'
MARKER/4, PART = 1, QP = 9, 20.6, 0
!
!                                adams_view_name='MARKER_5'
MARKER/5, PART = 1, QP = 9, 15.45, 0
!
!                                adams_view_name='MARKER_6'
MARKER/6, PART = 1, QP = 9, 10.3, 0
!
!                                adams_view_name='MARKER_7'
MARKER/7, PART = 1, QP = 9, 5.15, 0
!
!                                adams_view_name='MARKER_8'
MARKER/8, PART = 1, QP = 9, 0, 0
!
!                                adams_view_name='MARKER_9'
MARKER/9, PART = 1, QP = 0, 25.75, 0
!
!                                adams_view_name='MARKER_30'
MARKER/30, PART = 1, QP = 0, 25.75, 0, REULER = 0, 1.570796327, 0
```

```

!
!
MARKER/50, PART = 1, QP = 9, 0, 0, REULER = 1.570796327, 1.570796327, 0
!
!
MARKER/52, PART = 1, QP = 9, 0, 0
!
!
MARKER/54, PART = 1, QP = 9, 0, 0, REULER = 3.141592654, 1.570796327
, 3.141592654
!
!
MARKER/56, PART = 1, QP = 9, 5.15, 0, REULER = 1.570796327,
1.570796327, 0
!
!
MARKER/58, PART = 1, QP = 9, 5.15, 0
!
!
MARKER/60, PART = 1, QP = 9, 5.15, 0, REULER = 3.141592654, 1.570796327
, 3.141592654
!
!
MARKER/62, PART = 1, QP = 9, 10.3, 0, REULER = 1.570796327,
1.570796327, 0
!
!
MARKER/64, PART = 1, QP = 9, 10.3, 0
!
!
MARKER/66, PART = 1, QP = 9, 10.3, 0, REULER = 3.141592654, 1.570796327
, 3.141592654
!
!
MARKER/68, PART = 1, QP = 9, 15.45, 0, REULER = 1.570796327,
1.570796327, 0
!
!
MARKER/70, PART = 1, QP = 9, 15.45, 0
!
!
MARKER/72, PART = 1, QP = 9, 15.45, 0, REULER = 3.141592654,
1.570796327
, 3.141592654
!
!
MARKER/74, PART = 1, QP = 9, 20.6, 0, REULER = 1.570796327,
1.570796327, 0
!
!
MARKER/76, PART = 1, QP = 9, 20.6, 0
!
!
MARKER/78, PART = 1, QP = 9, 20.6, 0, REULER = 3.141592654, 1.570796327

```

```

, 3.141592654
!
!
adams_view_name='MARKER_79'
MARKER/79, PART = 1, QP = 0, 25.75, 0, REULER = 2.361096869,
0.9530150445
, 4.185955205
!
!
adams_view_name='MARKER_80'
MARKER/80, PART = 1, QP = 9, 20.6, 0, REULER = 2.361096869,
0.9530150445
, 4.185955205
!
!
adams_view_name='MARKER_81'
MARKER/81, PART = 1
!
!
adams_view_name='MARKER_84'
MARKER/84, PART = 1, QP = 9, 0, 0, REULER = 1.570796327, 1.570796327, 0
!
!
adams_view_name='MARKER_86'
MARKER/86, PART = 1, QP = 9, 0, 0
!
!
adams_view_name='MARKER_88'
MARKER/88, PART = 1, QP = 9, 0, 0, REULER = 3.141592654, 1.570796327
, 3.141592654
!
!
adams_view_name='MARKER_89'
MARKER/89, PART = 1, QP = 9, 0, 0, REULER = 1.570796327, 1.570796327, 0
!
!
adams_view_name='MARKER_90'
MARKER/90, PART = 1, QP = 9, 0, 0, REULER = 1.570796327, 1.570796327, 0
!
!----- Part -----
-----
!
!
adams_view_name='PART_2'
PART/2, MASS = 1.106627442, CM = 32, IP = 8.753636861, 8.699018605,
0.0919669325
!
!
adams_view_name='MARKER_10'
MARKER/10, PART = 2, QP = 0, 25.75, 0
!
!
adams_view_name='MARKER_11'
MARKER/11, PART = 2, QP = 9, 25.75, 0
!
!
adams_view_name='MARKER_18'
MARKER/18, PART = 2, QP = 9, 25.75, 0
!
!
adams_view_name='MARKER_31'
MARKER/31, PART = 2, QP = 0, 25.75, 0, REULER = 0, 1.570796327, 0
!
!
adams_view_name='cm'
MARKER/32, PART = 2, QP = 4.5, 25.75, 0, REULER = 4.71238898,
1.570796327
, 1.570796329

```



```

!
!
!           adams_view_name='MARKER_21'
MARKER/21, PART = 4, QP = 9, 20.6, 0
!
!           adams_view_name='MARKER_22'
MARKER/22, PART = 4, QP = 9, 15.45, 0
!
!           adams_view_name='cm'
MARKER/34, PART = 4, QP = 9, 18.025, 0, REULER = 0, 1.570796327, 0
!
!           adams_view_name='MARKER_40'
MARKER/40, PART = 4, QP = 9, 20.6, 0, REULER = 0, 1.570796327, 0
!
!           adams_view_name='MARKER_41'
MARKER/41, PART = 4, QP = 9, 15.45, 0, REULER = 0, 1.570796327, 0
!
!           adams_view_name='MARKER_67'
MARKER/67, PART = 4, QP = 9, 15.45, 0, REULER = 1.570796327,
1.570796327, 0
!
!           adams_view_name='MARKER_69'
MARKER/69, PART = 4, QP = 9, 15.45, 0
!
!           adams_view_name='MARKER_71'
MARKER/71, PART = 4, QP = 9, 15.45, 0, REULER = 3.141592654,
1.570796327
, 3.141592654
!
!           adams_view_name='CYLINDER_3'
GRAPHICS/3, CYLINDER, CM = 13, LENGTH = 5.15, RADIUS = 0.00925
!
!----- Part -----
-----
!
!           adams_view_name='PART_5'
PART/5, MASS = 1.939404167E-005, CM = 35, IP = 8.623104905E-004
, 8.623104905E-004, 1.669089881E-008
!
!           adams_view_name='MARKER_14'
MARKER/14, PART = 5, QP = 9, 15.45, 0, REULER = 0, 1.570796327, 0
!
!           adams_view_name='MARKER_23'
MARKER/23, PART = 5, QP = 9, 15.45, 0
!
!           adams_view_name='MARKER_24'
MARKER/24, PART = 5, QP = 9, 10.3, 0
!
!           adams_view_name='cm'
MARKER/35, PART = 5, QP = 9, 12.875, 0, REULER = 0, 1.570796327, 0
!
!           adams_view_name='MARKER_42'
MARKER/42, PART = 5, QP = 9, 15.45, 0, REULER = 0, 1.570796327, 0
!
!           adams_view_name='MARKER_43'

```

```

MARKER/43, PART = 5, QP = 9, 10.3, 0, REULER = 0, 1.570796327, 0
!
!
!           adams_view_name='MARKER_61'
MARKER/61, PART = 5, QP = 9, 10.3, 0, REULER = 1.570796327,
1.570796327, 0
!
!
!           adams_view_name='MARKER_63'
MARKER/63, PART = 5, QP = 9, 10.3, 0
!
!
!           adams_view_name='MARKER_65'
MARKER/65, PART = 5, QP = 9, 10.3, 0, REULER = 3.141592654, 1.570796327
, 3.141592654
!
!
!           adams_view_name='CYLINDER_4'
GRAPHICS/4, CYLINDER, CM = 14, LENGTH = 5.15, RADIUS = 0.00925
!
!----- Part -----
-----
!
!
!           adams_view_name='PART_6'
PART/6, MASS = 1.939404167E-005, CM = 36, IP = 8.623104905E-004
, 8.623104905E-004, 1.669089881E-008
!
!
!           adams_view_name='MARKER_15'
MARKER/15, PART = 6, QP = 9, 10.3, 0, REULER = 0, 1.570796327, 0
!
!
!           adams_view_name='MARKER_25'
MARKER/25, PART = 6, QP = 9, 10.3, 0
!
!
!           adams_view_name='MARKER_26'
MARKER/26, PART = 6, QP = 9, 5.15, 0
!
!
!           adams_view_name='cm'
MARKER/36, PART = 6, QP = 9, 7.725, 0, REULER = 3.141592654,
1.570796327
, 1.570796327
!
!
!           adams_view_name='MARKER_44'
MARKER/44, PART = 6, QP = 9, 10.3, 0, REULER = 0, 1.570796327, 0
!
!
!           adams_view_name='MARKER_45'
MARKER/45, PART = 6, QP = 9, 5.15, 0, REULER = 0, 1.570796327, 0
!
!
!           adams_view_name='MARKER_55'
MARKER/55, PART = 6, QP = 9, 5.15, 0, REULER = 1.570796327,
1.570796327, 0
!
!
!           adams_view_name='MARKER_57'
MARKER/57, PART = 6, QP = 9, 5.15, 0
!
!
!           adams_view_name='MARKER_59'
MARKER/59, PART = 6, QP = 9, 5.15, 0, REULER = 3.141592654, 1.570796327
, 3.141592654
!
!

```

```

!
!               adams_view_name='CYLINDER_5'
GRAPHICS/5, CYLINDER, CM = 15, LENGTH = 5.15, RADIUS = 0.00925
!
!----- Part -----
-----
!
!               adams_view_name='PART_7'
PART/7, MASS = 1.939404167E-005, CM = 37, IP = 8.623104905E-004
, 8.623104905E-004, 1.669089881E-008
!
!               adams_view_name='MARKER_16'
MARKER/16, PART = 7, QP = 9, 5.15, 0, REULER = 0, 1.570796327, 0
!
!               adams_view_name='MARKER_27'
MARKER/27, PART = 7, QP = 9, 5.15, 0
!
!               adams_view_name='MARKER_28'
MARKER/28, PART = 7, QP = 9, 0, 0
!
!               adams_view_name='cm'
MARKER/37, PART = 7, QP = 9, 2.575, 0, REULER = 0, 1.570796327, 0
!
!               adams_view_name='MARKER_46'
MARKER/46, PART = 7, QP = 9, 5.15, 0, REULER = 0, 1.570796327, 0
!
!               adams_view_name='MARKER_83'
MARKER/83, PART = 7, QP = 9, 0, 0, REULER = 1.570796327, 1.570796327, 0
!
!               adams_view_name='MARKER_85'
MARKER/85, PART = 7, QP = 9, 0, 0
!
!               adams_view_name='MARKER_87'
MARKER/87, PART = 7, QP = 9, 0, 0, REULER = 3.141592654, 1.570796327
, 3.141592654
!
!               adams_view_name='CYLINDER_6'
GRAPHICS/6, CYLINDER, CM = 16, LENGTH = 5.15, RADIUS = 0.00925
!
!----- Part -----
-----
!
!               adams_view_name='PART_8'
PART/8, MASS = 9.921004634E-005, CM = 38, IP = 2.173096855E-007
, 2.173096855E-007, 2.173096855E-007
!
!               adams_view_name='MARKER_17'
MARKER/17, PART = 8, QP = 9, 0, 0
!
!               adams_view_name='MARKER_29'
MARKER/29, PART = 8, QP = 9, 0, 0
!
!               adams_view_name='cm'
MARKER/38, PART = 8, QP = 9, 0, 0, REULER = 1.570796327, 1.570796327, 0
!

```

```

!
!           adams_view_name='MARKER_49'
MARKER/49, PART = 8, QP = 9, 0, 0, REULER = 1.570796327, 1.570796327, 0
!
!           adams_view_name='MARKER_51'
MARKER/51, PART = 8, QP = 9, 0, 0
!
!           adams_view_name='MARKER_53'
MARKER/53, PART = 8, QP = 9, 0, 0, REULER = 3.141592654, 1.570796327
, 3.141592654
!
!           adams_view_name='MARKER_82'
MARKER/82, PART = 8, QP = 9, 0, 0
!
!           adams_view_name='ELLIPSOID_7'
GRAPHICS/7, ELLIPSOID, CM = 17, XSCALE = 0.148, YSCALE = 0.148, ZSCALE
= 0.148
!
!----- DYNAMIC GRAPHICS -----
!
!           adams_view_name='SFORCE_1_force_graphic_1'
GRAPHICS/13, FORCE, ETYPE = SFORCE, EID = 1, EMARKER = 49
!
!           adams_view_name='SFORCE_2_force_graphic_1'
GRAPHICS/14, FORCE, ETYPE = SFORCE, EID = 2, EMARKER = 51
!
!           adams_view_name='SFORCE_3_force_graphic_1'
GRAPHICS/15, FORCE, ETYPE = SFORCE, EID = 3, EMARKER = 53
!
!           adams_view_name='SFORCE_4_force_graphic_1'
GRAPHICS/16, FORCE, ETYPE = SFORCE, EID = 4, EMARKER = 55
!
!           adams_view_name='SFORCE_5_force_graphic_1'
GRAPHICS/17, FORCE, ETYPE = SFORCE, EID = 5, EMARKER = 57
!
!           adams_view_name='SFORCE_6_force_graphic_1'
GRAPHICS/18, FORCE, ETYPE = SFORCE, EID = 6, EMARKER = 59
!
!           adams_view_name='SFORCE_7_force_graphic_1'
GRAPHICS/19, FORCE, ETYPE = SFORCE, EID = 7, EMARKER = 61
!
!           adams_view_name='SFORCE_8_force_graphic_1'
GRAPHICS/20, FORCE, ETYPE = SFORCE, EID = 8, EMARKER = 63
!
!           adams_view_name='SFORCE_9_force_graphic_1'
GRAPHICS/21, FORCE, ETYPE = SFORCE, EID = 9, EMARKER = 65
!
!           adams_view_name='SFORCE_10_force_graphic_1'
GRAPHICS/22, FORCE, ETYPE = SFORCE, EID = 10, EMARKER = 67
!
!           adams_view_name='SFORCE_11_force_graphic_1'
GRAPHICS/23, FORCE, ETYPE = SFORCE, EID = 11, EMARKER = 69
!
!           adams_view_name='SFORCE_12_force_graphic_1'

```

```

GRAPHICS/24, FORCE, ETYPE = SFORCE, EID = 12, EMARKER = 71
!
!           adams_view_name='SFORCE_13_force_graphic_1'
GRAPHICS/25, FORCE, ETYPE = SFORCE, EID = 13, EMARKER = 73
!
!           adams_view_name='SFORCE_14_force_graphic_1'
GRAPHICS/26, FORCE, ETYPE = SFORCE, EID = 14, EMARKER = 75
!
!           adams_view_name='SFORCE_15_force_graphic_1'
GRAPHICS/27, FORCE, ETYPE = SFORCE, EID = 15, EMARKER = 77
!
!           adams_view_name='SFORCE_16_force_graphic_1'
GRAPHICS/28, FORCE, ETYPE = SFORCE, EID = 16, EMARKER = 83
!
!           adams_view_name='SFORCE_17_force_graphic_1'
GRAPHICS/29, FORCE, ETYPE = SFORCE, EID = 17, EMARKER = 85
!
!           adams_view_name='SFORCE_18_force_graphic_1'
GRAPHICS/30, FORCE, ETYPE = SFORCE, EID = 18, EMARKER = 87
!
!----- CONSTRAINTS -----
!-----
!
!           adams_view_name='JOINT_3'
JOINT/3, SPHERICAL, I = 22, J = 23
!
!           adams_view_name='JOINT_4'
JOINT/4, SPHERICAL, I = 24, J = 25
!
!           adams_view_name='JOINT_5'
JOINT/5, SPHERICAL, I = 26, J = 27
!
!           adams_view_name='JOINT_6'
JOINT/6, SPHERICAL, I = 28, J = 29
!
!           adams_view_name='JOINT_7'
JOINT/7, REVOLUTE, I = 30, J = 31
!
!           adams_view_name='JOINT_1'
JOINT/8, SPHERICAL, I = 18, J = 19
!
!           adams_view_name='JOINT_2'
JOINT/9, SPHERICAL, I = 20, J = 21
!
!           adams_view_name='MOTION_1'
MOTION/1, ROTATIONAL, JOINT = 7, FUNCTION = step(time,0,0,2000,15)*time
!
!----- FORCES -----
!-----
!
!           adams_view_name='BUSHING_1'
!BUSHING/1, I = 39, J = 40, C = 1.998551504E-008, 1.998551504E-006
!, 1.998551504E-006, K = 7.994206017E-008, 7.994206017E-006,
7.994206017E-006

```

```

!, CT = 0.01, 0.01, 0.01, KT = 0.1, 0.1, 0.1
!
!
!           adams_view_name='BUSHING_2'
!BUSHING/2, I = 41, J = 42, C = 1.998551504E-008, 1.998551504E-006
!, 1.998551504E-006, K = 7.994206017E-008, 7.994206017E-006,
7.994206017E-006
!, CT = 0.01, 0.01, 0.01, KT = 0.1, 0.1, 0.1
!
!
!           adams_view_name='BUSHING_3'
!BUSHING/3, I = 43, J = 44, C = 1.998551504E-008, 1.998551504E-006
!, 1.998551504E-006, K = 7.994206017E-008, 7.994206017E-006,
7.994206017E-006
!, CT = 0.01, 0.01, 0.01, KT = 0.1, 0.1, 0.1
!
!
!           adams_view_name='BUSHING_4'
!BUSHING/4, I = 45, J = 46, C = 1.998551504E-008, 1.998551504E-006
!, 1.998551504E-006, K = 7.994206017E-008, 7.994206017E-006,
7.994206017E-006
!, CT = 0.01, 0.01, 0.01, KT = 0.1, 0.1, 0.1
!
!
!           adams_view_name='BUSHING_5'
!BUSHING/5, I = 47, J = 48, C = 1.998551504E-008, 1.998551504E-006
!, 1.998551504E-006, K = 7.994206017E-008, 7.994206017E-006,
7.994206017E-006
!, CT = 0.01, 0.01, 0.01, KT = 0.1, 0.1, 0.1
!
!
!           adams_view_name='SFORCE_1'
SFORCE/1, TRANSLATIONAL, I = 49, J = 50, ACTIONONLY, FUNCTION =
, STEP(time, 0.0, 0.0, 1.0, 1.0)*(-0.5*((43.40277778E-
06*0.47*(PI/4)*(0.148**2)))/386))*(sqrt(((VX(38))**2)+((VY(38))**2)+((V
Z(38))**2)))*((1)*VX(38)+ 0.00*VX(38))
!
!
!           adams_view_name='SFORCE_2'
SFORCE/2, TRANSLATIONAL, I = 51, J = 52, ACTIONONLY, FUNCTION =
, STEP(time, 0.0, 0.0, 1.0, 1.0)*(-0.5*((43.40277778E-
06*0.47*(PI/4)*(0.148**2)))/386))*(sqrt(((VX(38))**2)+((VY(38))**2)+((V
Z(38))**2)))*((1)*VZ(38)+ 0.00*VZ(38))
!
!
!           adams_view_name='SFORCE_3'
SFORCE/3, TRANSLATIONAL, I = 53, J = 54, ACTIONONLY, FUNCTION =
, STEP(time, 0.0, 0.0, 1.0, 1.0)*(-0.5*((43.40277778E-
06*0.47*(PI/4)*(0.148**2)))/386))*(sqrt(((VX(38))**2)+((VY(38))**2)+((V
Z(38))**2)))*((1)*VY(38)+ 0.00*VY(38))
!
!
!           adams_view_name='SFORCE_4'
SFORCE/4, TRANSLATIONAL, I = 55, J = 56, ACTIONONLY, FUNCTION =
, STEP(time, 0.0, 0.0, 1.0, 1.0)*(-0.5*(43.40277778E-
06/386)*(2*0.00925*5.15))*(sqrt(((VX(36))**2)+((VY(36))**2)+((VZ(36))**
2)))*(1.2*VX(36)+ 0.00*VX(36))
!
!
!           adams_view_name='SFORCE_5'
SFORCE/5, TRANSLATIONAL, I = 57, J = 58, ACTIONONLY, FUNCTION =

```



```

, STEP(time, 0.0, 0.0, 1.0, 1.0)*(-0.5*(43.40277778E-
06/386)*(2*0.00925*5.15))*(sqrt(((VX(33))**2)+((VY(33))**2)+((VZ(33))**
2)))*(1.2*VZ(33)+ 0.00*VZ(33))
!
!
!           adams_view_name='SFORCE_15'
SFORCE/15, TRANSLATIONAL, I = 77, J = 78, ACTIONONLY, FUNCTION =
, STEP(time, 0.0, 0.0, 1.0, 1.0)*(-0.5*(43.40277778E-
06/386)*(2*0.00925*5.15))*(sqrt(((VX(33))**2)+((VY(33))**2)+((VZ(33))**
2)))*(1.2*VY(33)+ 0.00*VY(33))
!
!
!           adams_view_name='SFORCE_16'
SFORCE/16, TRANSLATIONAL, I = 83, J = 84, ACTIONONLY, FUNCTION =
, STEP(time, 0.0, 0.0, 1.0, 1.0)*(-0.5*(((43.40277778E-
06*1.2*(2*0.00925*5.15)))/386))*(sqrt(((VX(37))**2)+((VY(37))**2)+((VZ(
37))**2)))*((1)*VX(37)+ 0.00*VX(37))
!
!
!           adams_view_name='SFORCE_17'
SFORCE/17, TRANSLATIONAL, I = 85, J = 86, ACTIONONLY, FUNCTION =
, STEP(time, 0.0, 0.0, 1.0, 1.0)*(-0.5*(((43.40277778E-
06*1.2*(2*0.00925*5.15)))/386))*(sqrt(((VX(37))**2)+((VY(37))**2)+((VZ(
37))**2)))*((1)*VZ(37)+ 0.00*VZ(37))
!
!
!           adams_view_name='SFORCE_18'
SFORCE/18, TRANSLATIONAL, I = 87, J = 88, ACTIONONLY, FUNCTION =
, STEP(time, 0.0, 0.0, 1.0, 1.0)*(-0.5*(((43.40277778E-
06*1.2*(2*0.00925*5.15)))/386))*(sqrt(((VX(37))**2)+((VY(37))**2)+((VZ(
37))**2)))*((1)*VY(37)+ 0.00*VY(37))
!
!----- DATA STRUCTURES -----
!-----
!
!           adams_view_name='MARKER_18_MEA_1'
VARIABLE/1, FUNCTION = VM(18,0)
!
!           adams_view_name='MEA_PT2PT_12'
VARIABLE/12, FUNCTION = DX(82,81,0)
!
!           adams_view_name='MEA_PT2PT_13'
VARIABLE/13, FUNCTION = DZ(38,81,0)
!
!           adams_view_name='PART_8_MEA_1'
VARIABLE/14, FUNCTION = DY(38,0,0)
!
!           adams_view_name='MOTION_1_MEA_1'
VARIABLE/15, FUNCTION = WM(31,30)
!
!----- GRAVITATIONAL ACCELERATION -----
!-----
!
ACCGRAV/JGRAV = -386.0885827
!
!----- ANALYSIS SETTINGS -----
!-----
!

```

```
KINEMATICS/ERROR = 1.0E-005, MAXIT = 100
!  
OUTPUT/REQSAVE, GRSAVE  
!  
RESULTS/XRF  
!  
END
```